~~THE~~ RAPID DISCHARGES OF GASES THROUGH ~~BURSTING~~ DISCS ~~VALVES~~ AND SIMILAR PRESSURE RELEASE MECHANISMS

(VOLUME II)

Submitted for the degree of

DOCTOR OF PHILOSOPHY

in

The Faculty of Engineering

of

The University of London

by

George Munday, B.Sc.

Department of Chemical Engineering,

Imperial College, S.W.7.

March 1961

TABLE OF CONTENTS (Volume II)

LIST OF PLATES

LIST OF FIGURES

SECTION B

SECTION C

LIST OF TABLES

APPENDICES TO SECTIONS B & C.

SECTION B SPRING LOAD DIAPHRAGM VALVES

CHAPTER B.I. INTRODUCTION

The pressure release mechanisms discussed in this section are those in which an obstruction is held in the vent by a spring or springs. Conventional steam relief valves fall under this heading but, since they are adequately dealt with in British Standard specifications 1123: 1950, 759: 1955 and 2591:1956, only a brief summary of these specifications will be given.

B.S. 1123: 1950 deals with valves, gauges and other fittings for air receivers and compressed air installations. Part 2 (a) considers the special requirements of safety valves. The main points are:

(a) The valve should be of the direct spring loaded type.

(b) The over pressure should be less than 10% above set blow off pressure. That is, the valve should permit air to escape from the air receiver without increasing the pressure beyond 10% above set blow off pressure when the air compressor is giving full output.

(c) The minimum aggregate area of the orifices (vents) is given by

$$A = \frac{Q}{1{\cdot}2\ P}$$

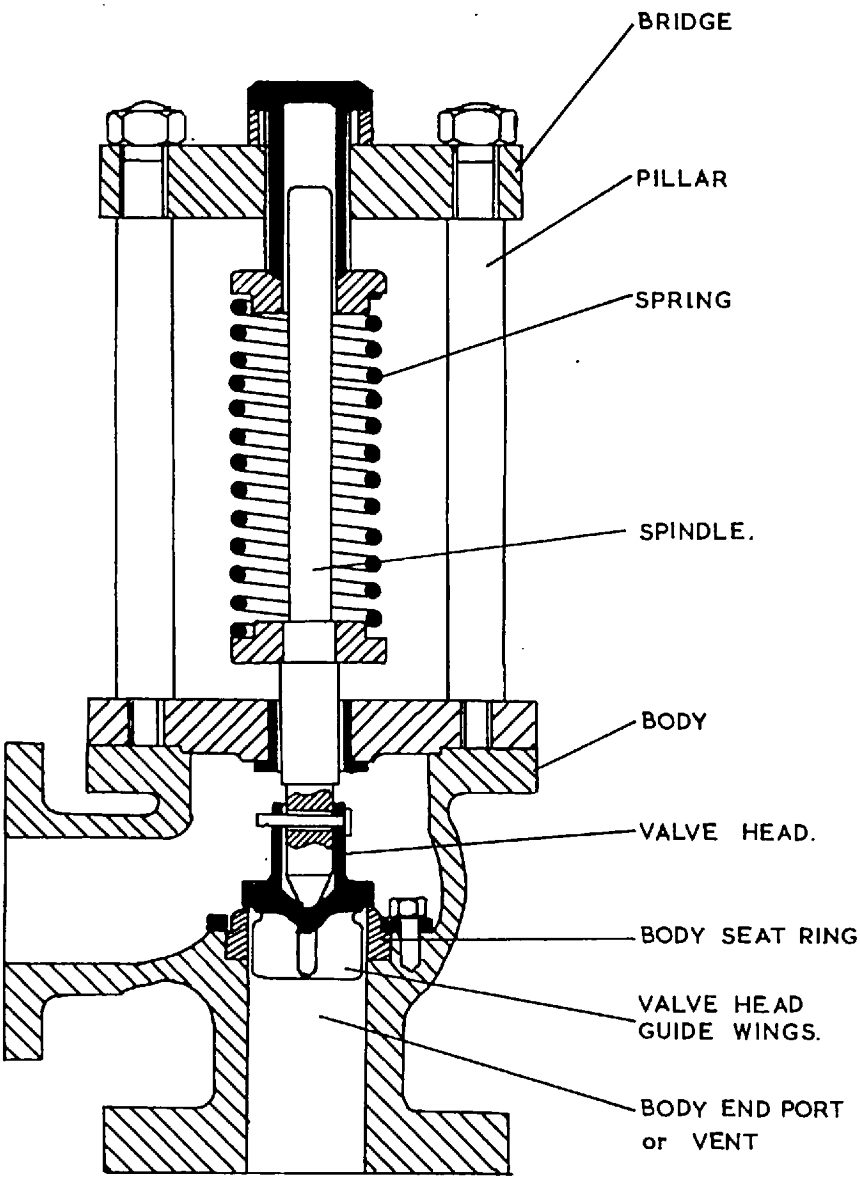

FIG. B.1.1.

Ordinary Safety Valve

B.S. 2591 : 1956. Pt.2.

where A = area in square inches,

Q = full output of compressor in ft^3 free air/min and

P = highest pressure to which the safety valve is to be set to lift in p.s.i. abs.

B.S. 759 : 1955 deals with, amongst other fittings, valves for application to land boilers. Section 3 (a) covers the special requirements of safety valves. Three types of valve are named: the "ordinary lift" valve having a lift of D/24 where D is the diameter of the orifice; the "high lift" valve of lift D/12; and the "full lift" valve in which the lift is such that the area of flow equals the vent area. The minimum venting area is specified in terms of the load of the boiler, the degree of superheat of the steam, the maximum blow off pressure (sometimes termed lift pressure) and the type of valve. Both the over pressure and the pressure drop through the valve are defined and certain mechanical details, testing and identification marks are specified.

B.S. 2591 : 1956, Part 2 is a glossary for safety and relief valves and their parts with illustrations of five types. One of these is shown in Fig. B.I.1 to define the terms used to describe the more important parts.

In this section only full lift safety valves are considered since in these valves maximum discharge is obtained

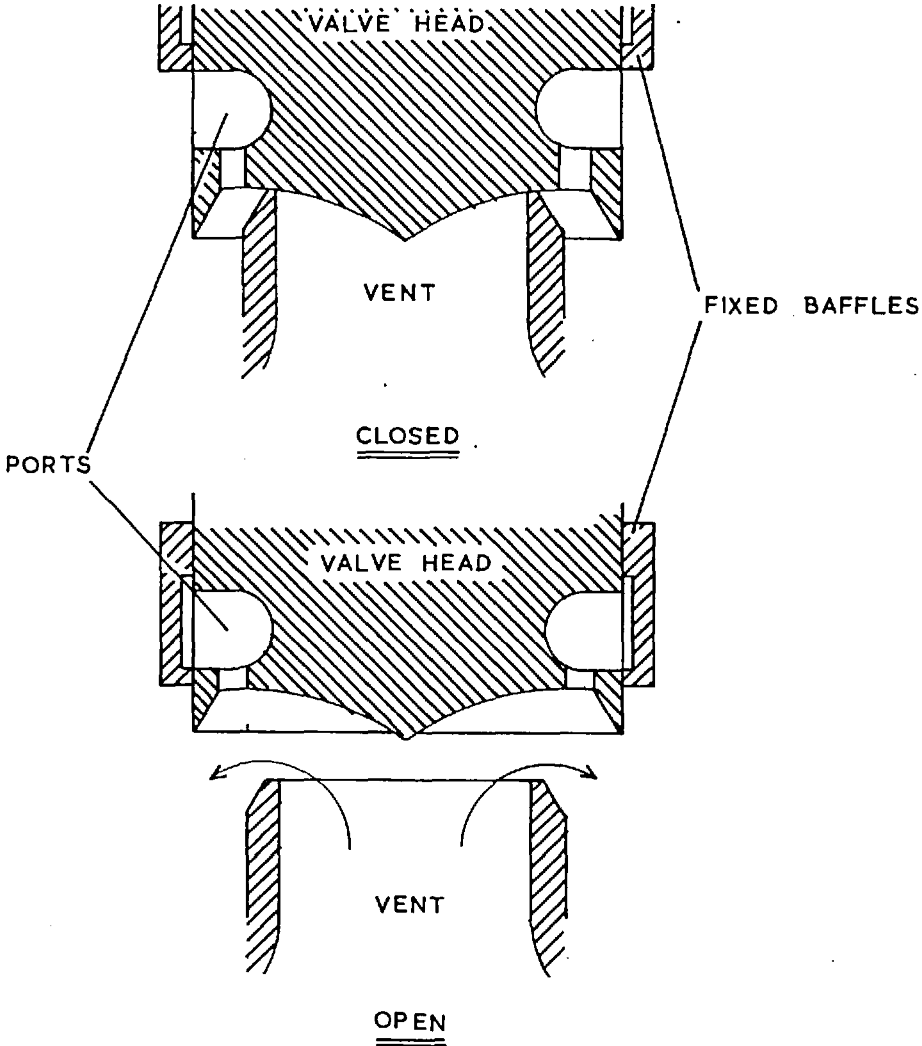

NOZZLE-REACTION SAFETY VALVE.

FIG.B.1.2.

for a given vent area. The ordinary lift and high lift valves are either direct-spring or lever-and-spring loaded and as the valve lifts the reaction from the spring increases and full lift is not possible. Full lift valves are mainly proprietary types and incorporate various devices to increase the thrust exerted on the valve head by the escaping fluid or to reduce the spring reaction as the valve reaches its maximum lift position.

Three methods for increasing the thrust given by S. Elonka (1954) are the huddling chamber, jet flow and nozzle reaction. The last of these three is illustrated in Fig. B.I.2. As the fluid escapes past the valve seating it passes through ports in the valve head. The lift increases and the ports are closed by fixed baffles. The fluid is deflected back towards the vent increasing the thrust on the valve head. These methods are limited in application and in the case of rapid pressure release may reduce the effectiveness of the spring loaded valve.

There are several devices for reducing the spring reaction. Two springs can be employed in a mechanism in which a strong spring holds the valve closed and is released once the valve opens, a second weaker spring returning the valve head when the pressure falls. However, link mechanisms designed to give non linear pressure-displacement loadings on the valve have the widest applications.

In section A the force exerted by the fluid was known and the system of reacting forces had to be determined from the analysis of the stresses and strains in the diaphragm. In this section the reacting forces are known since they are specified by the loading system and the thrust exerted on the valve head must be calculated. The analysis is therefore divided into three parts: the first dealing with the choice of restraining system; the second with the thrust of the gas; and the third with the rate of discharge through these valves. In the concluding chapter of this section the results of this analysis are used to compare two types of spring loaded valve and describe their application to a specific problem.

Finally, to simplify experimental procedure and to allow comparison with bursting disc valves only gaseous discharges are considered.

CHAPTER B.II THE RESTRAINING SYSTEM OF FORCES

Two forms of spring loading will be considered and these will be used in chapter B. IV to analyse the performance of valves relieving pressure in a vessel. Other forms of loading can be analysed in the same manner.

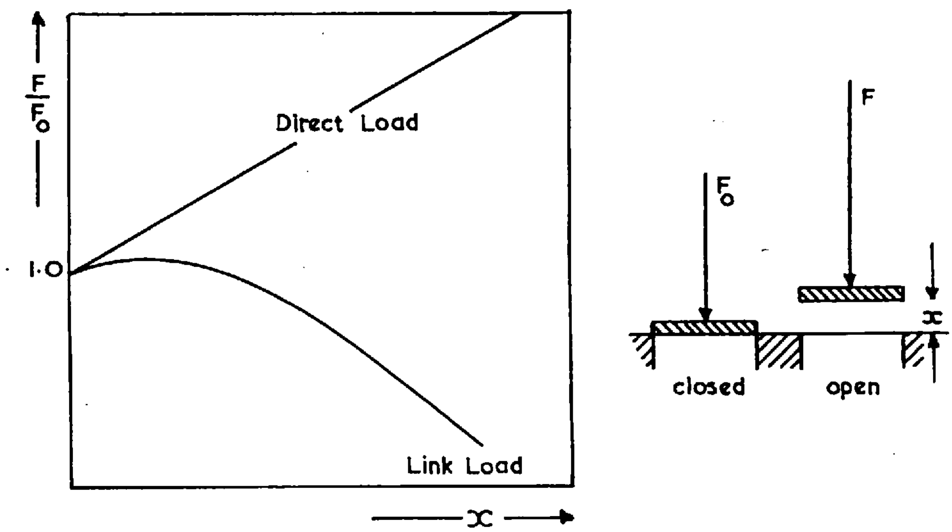

FIG.B.II.I.

Fig. B.II.1

(i) Direct spring load.

The force-displacement relation for a direct spring loaded valve is shown in Fig. B.II.1. As the valve lifts the spring reaction on the valve head increases so that the valve

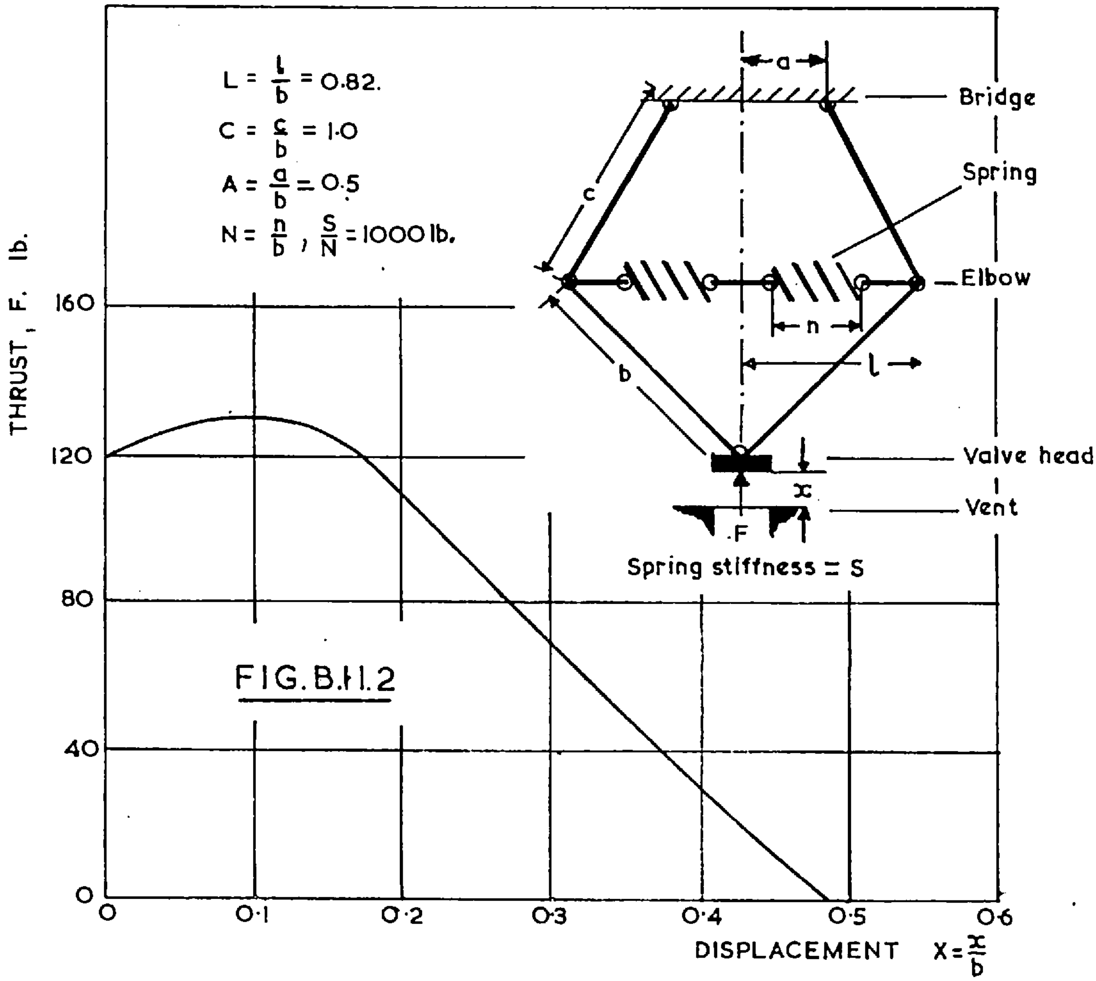
L = l/b = 0.82.
C = c/b = 1.0
A = a/b = 0.5
N = n/b , S/N = 1000 lb.
Bridge
Spring
Elbow
Valve head
Vent
a
c
b
n
l
x
F
Spring stiffness = S
THRUST, F. lb.
160
120
80
40
0
0
0·1
0·2
0·3
0·4
0·5
0·6
DISPLACEMENT X = x/b

FIG. B.11.2

remains open only when the pressure behind the valve is greater than the blow off pressure, P_b.

(ii) Indirect link loading.

As an illustration of this type of loading the link mechanism shown in Fig. B.II.2 has been examined. Four link arms, each made from two links, are fastened at one end to the valve head and at the other to the bridge. The "elbows" of the link arms are attached to a centre ring by four springs. As the valve head rises the elbows are displaced away from the central axis and restrained by the springs. The force on the valve head depends upon the leverage of the system and the extension of the springs.

The force-displacement relation has been determined graphically for one link system and the effect of changing the link lengths obtained by direct calculation. The versatility of this type of loading can be seen in Fig. B.II.3 which shows some of the possible force-displacement relations. The particular configuration used in the final analysis is that shown in Fig. B.II.2 : the link lengths are all equal and the distance between the link arms at the bridge, the length of the spring assembly and the strength of the spring are given by

$$2\Lambda = 1{\cdot}0\ ,$$

$$2L = 1{\cdot}64 \text{ and}$$

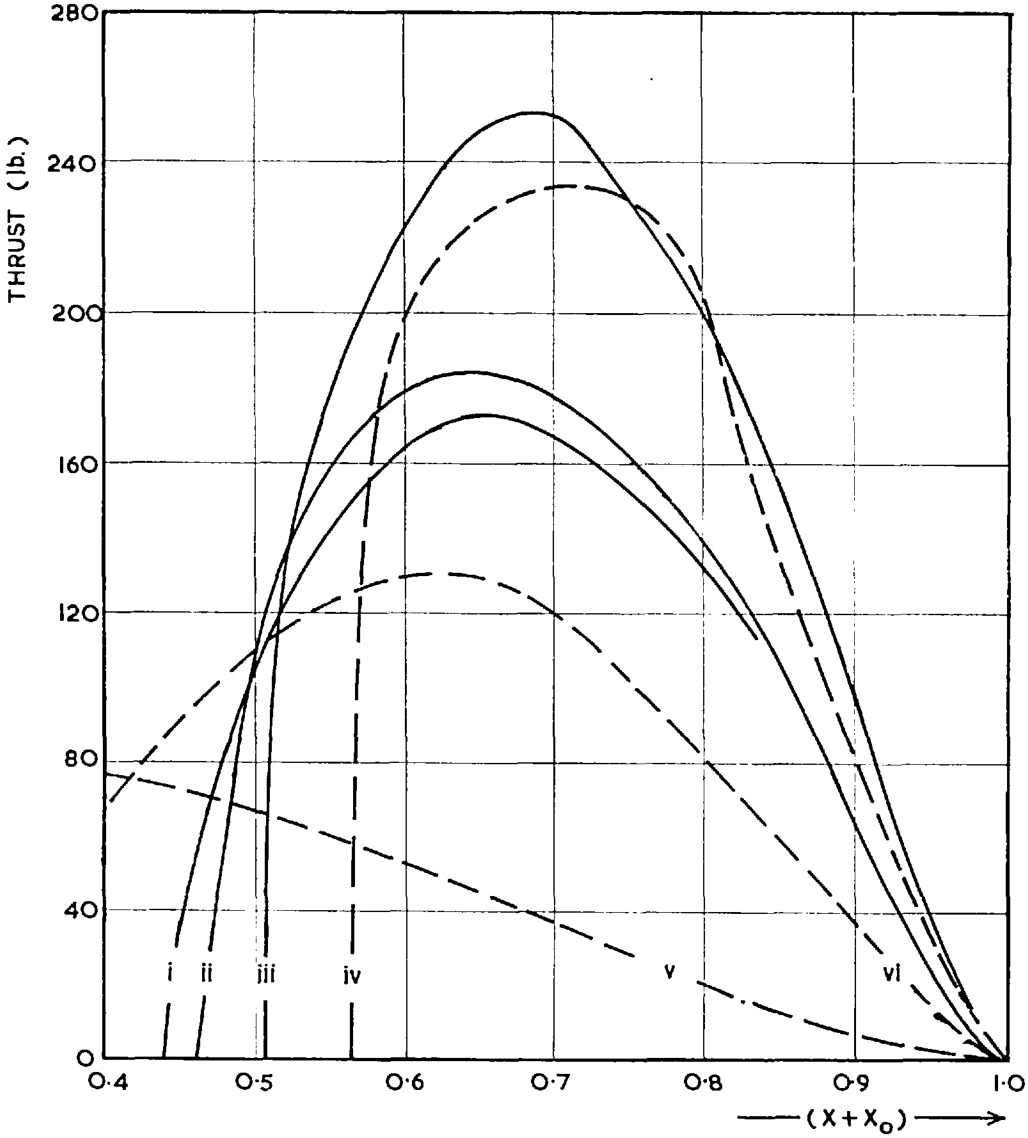

	L	C	A	S/N
i	0·82	0·25	1	1000 lb.
ii	"	1·00	1	"
iii	"	2·00	1	"
iv	"	1·00	2	"
v	"	1·00	0	"
vi	"	1.00	1/2	"

X_0 = arbitrary value of X, fixed by the blow off load. eg, in fig.B.II.2 the blow off load is 120.lb and X_0 = 0·53. (curve vi)

FIG.B.II.3.

$S/N = 1000$ lb. respectively

where S = the spring stiffness in lb.,

N = the spring length and the unit of length is that of one link.

The blow off pressure has been chosen arbitrarilly to give a thrust of 120 lb. so that the force-displacement relation, in future termed the "mechanism-relation", is as shown in Fig. B.II.2 and has a peak load of 130 lb.

CHAPTER B.III. THE FORCE EXERTED BY THE DISCHARGING GAS

B.III.1 Introduction.

By Newton's Law of Motion the thrust exerted by an inviscid fluid will be the sum of the pressure drop across the valve and the rate of change of momentum of the fluid as it impinges on the valve head. The momentum per unit mass is the product of the density of the fluid and the velocity vector. The density and velocity depend upon the state of the gas entering the valve and the velocity depends, as well, upon the shape of the valve which is fixed by the shape of the vent and the shape and position of the valve head.

Hence, any investigation into the forces acting on the valve head must involve the determination of the effects of valve head position and shape and the pressure and temperature of the gas entering the valve. In the case of a viscid fluid skin drag increases the thrust and the size of the valve would have to be included as a variable.

The forces acting on a series of obstructions held at various distances within a vent in a pressure reservoir have been measured. The force exerted on each obstruction has been related to its position in the vent and the pressure in the reservoir but no attempt has been made to examine scale effects. The forces involved in an actual valve will be more complicated and only a preliminary estimate of valve performance is required from these simplified models.

B.III.2 Experimental method and equipment

The equipment described in Chapter A.III, dealing with the measurement of discharge rates through bursting disc valves, was used. The 1" diameter, $\frac{1}{2}$" entry radius valve assembly was adapted to form the vent of the valve. A plate holding an obstruction representing the valve head was fixed to the bursting disc assembly by four pillars. By using a bursting disc in the assembly the pressure was raised and when the disc burst the pressure in the reservoir and the thrust on the obstruction were measured simultaneously. As an additional source of information flash photographs were taken during the discharge and these were initiated electronically by the pressure recording equipment.

(i) Obstructions.

The obstruction represents the valve head in an actual valve and four bodies of revolution were chosen. A flat plate having the same diameter, D, as the vent was taken to approximate most valve heads and a cone of solid angle $\pi/2$ and base diameter D was used for comparison with existing data from experiments carried out in wind tunnels. The two other obstructions were a hemisphere of diameter D and a cusped cone formed by the revolution of a quadrant of a circle of diameter D about a tangent.

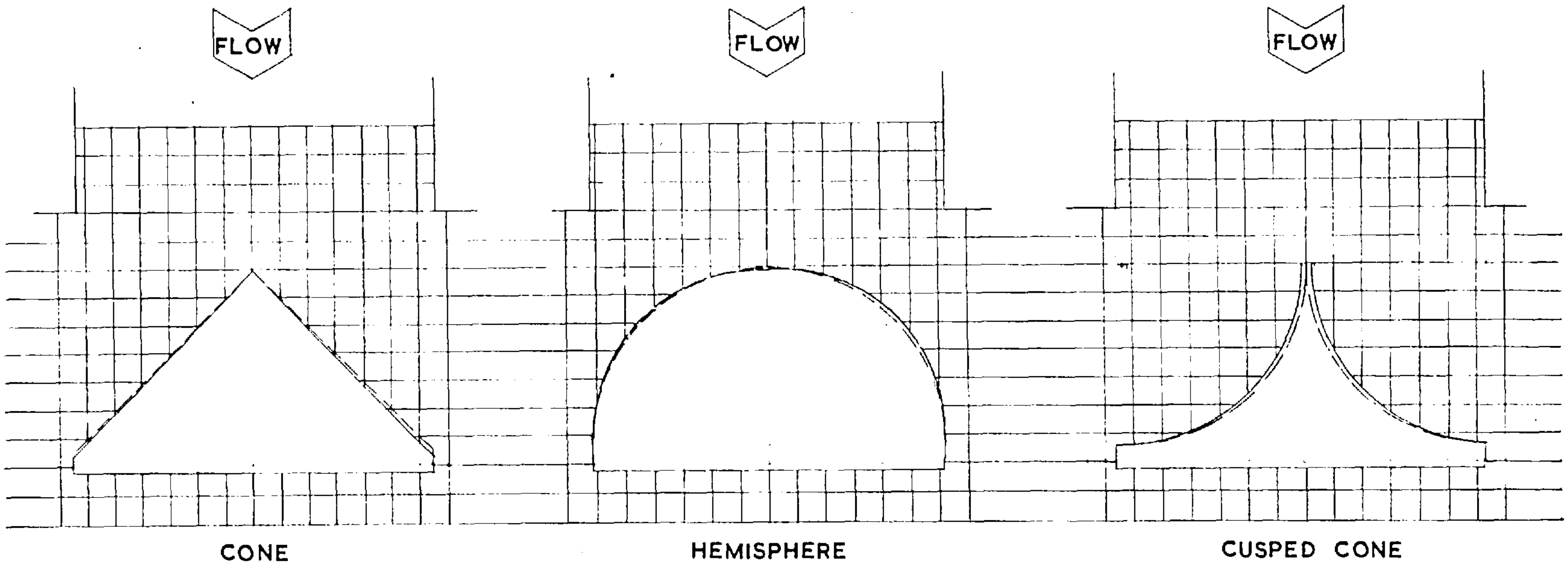

FIG.B.III.1.

—— Measured profile —— — — Theoretical profile

Grid represents 2 mm. devisions.

The measured profiles are indicated in Fig. B.III.1 along with the geometrical shapes assumed in the theoretical analysis.

(ii) Measurement of pressure in the reservoir.

The pressure was measured with the transducer described in Chapter A.III. The pressure variation was recorded by a different method and is described in section (iv) of this Chapter.

(iii) The measurement of thrust on the obstruction.

The requirements of a transducer to measure the thrust are:

(a) the measurement of forces up to 40 lb.wt. such that displacements are sufficiently small not to affect the position of the obstruction,

(b) the dynamic response to be at least as good as that of the pressure transducer, i.e., 2,000 c/sec.;

(c) if possible, a linear pressure output relation; and

(d) a method for accurately adjusting the position of the obstruction in the vent.

As discussed earlier, a number of electronic devices are available for measuring small displacements. An additional method not mentioned is obtained by using the variation in performance of a thermionic valve when its constituent elements are moved with respect to each other. Thus, the valve characteristics of a triode can be altered by moving its anode and small movements can be made to yield considerable changes in its anode resistance. Recent miniturisation techniques have enabled the manufacture of a compact highly sensitive valve transducer and such a device has been used as the basis of an instrument for measuring thrust.

The valve is described in detail in Appendix E and consists of an evacuated glass capsule, supporting the cathode, heater and grid, sealed into a metal cylinder 5 mm. in diameter and 20 mm. long. The anode is attached to a spindle which passes through a diaphragm sealing one end of the cylinder. Displacement of this spindle through a small arc of less than half a degree causes a large change in the valve characteristics and the change in anode resistance bears a linear relation to the extent of the movement. Movement greater than one half degree damages the valve and provision has to be made to prevent excessive deflection.

Electronically, the valve entails a directly heated cathode, a grid and an anode; three terminals and the outer casing provide connections to these elements. The valve requires a power supply for the heater, a potential between the anode and the cathode and, depending upon application, a bias voltage on the grid.

In the present application the change in anode resistance is

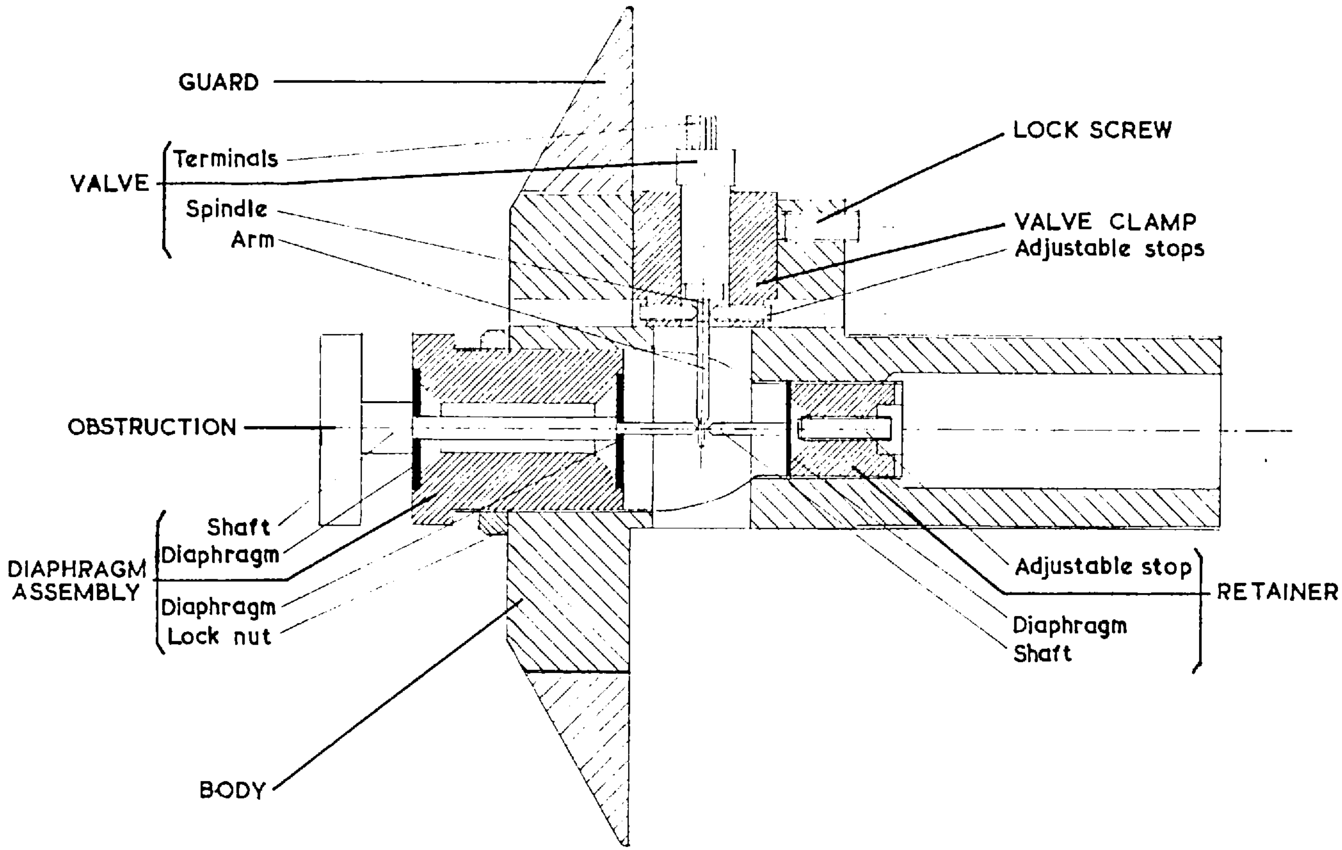

FIG. B.III.2. THRUST TRANSDUCER

FULL SCALE.

measured in a bridge circuit whose arms are such that the grid and cathode can be held at the same potential. To ensure stability, batteries were used to supply the D.C. potential to the bridge and an accumulator was used to supply the heaters.

When designing a clamp to hold the valve the following points should be considered: good electrical and thermal contact with the valve; sufficient heat dissipation to maintain the valve at a reasonable temperature; and ageing of the valve before use.

The valve and its associated circuit translates displacement into a voltage output and a diaphragm is used to relate the thrust on the obstruction to a displacement. The unit shown in Fig. B.III.2 has been designed to meet these mechanical requirements. The thrust from the obstruction is transmitted by a shaft to an arm fixed on the valve spindle and the resistance to displacement is provided by two diaphragms attached to the body of the transducer. The valve is held in a clamp and mounted on the transducer so that the spindle arm is perpendicular to and just touches the end of the shaft. This arm is flatened at the end and held against the end of the shaft by a second diaphragm assembly which incorporates a stop to prevent excessive displacements. The valve clamp also has two

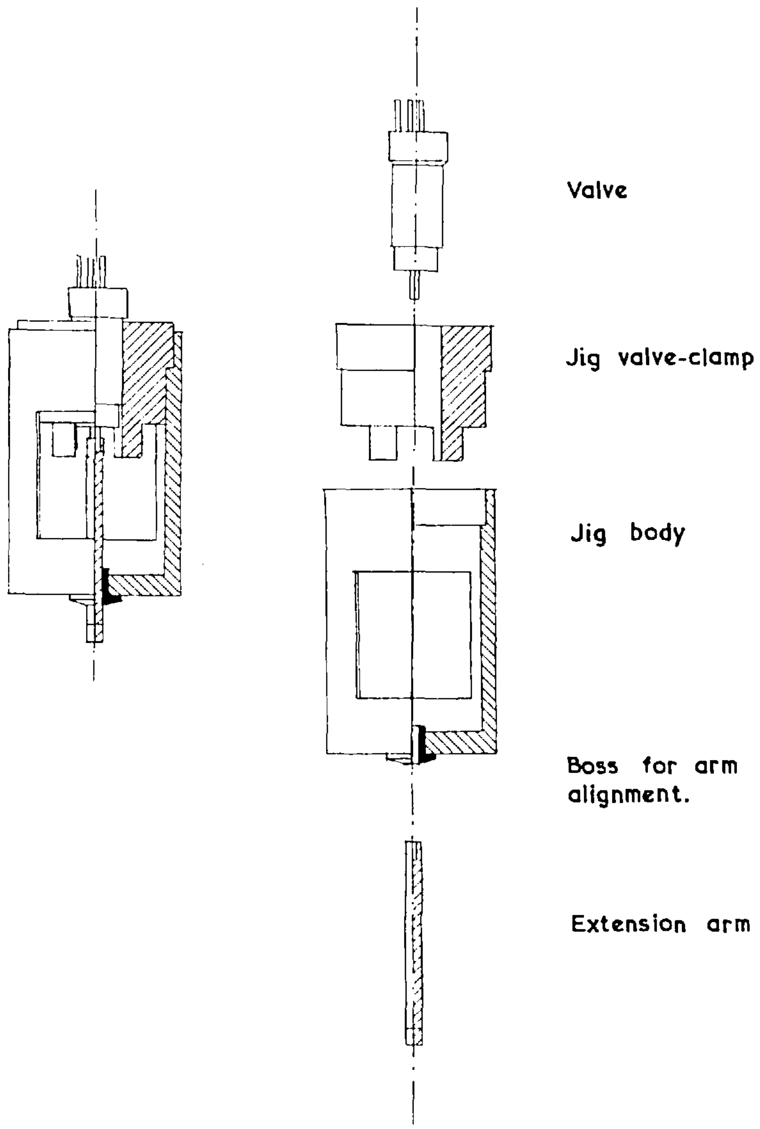

FIG. B.III.3.

ASSEMBLY JIG. (half sections)
Approximately full scale.

adjustable stops and these ensure that the valve spindle cannot be moved through more than the half degree tolerance specified by the manufacturers.

Since the movement of the shaft is of the order of a few thousandths of an inch it was essential to design the transducer so that the constituent parts could be aligned correctly. For this reason the body of the instrument was machined from a single piece of brass and, in turning the holes for the diaphragm assemblies, the unit was held in one position in the lathe chuck for all operations. The hole in the head of the main unit was drilled first and the hole for the other diaphragm unit drilled and threaded through the first aperture. The other units (diaphragm head, the retaining diaphragm and the valve clamp) were machined separately and constructed so that when the complete unit was assembled the two shafts and the extension arm all met at the same point. The units were then locked in position by the diaphragm lock nut and the valve clamp grub screw.

A jig has been constructed to prevent damage to the valve from heat or excessive movement when the extension arm is being soldered to the spindle. It also ensures that the arm is aligned in the axis of the valve. It is shown in Fig. B.III.3 and consists of a replica of the valve clamp and an open cylinder

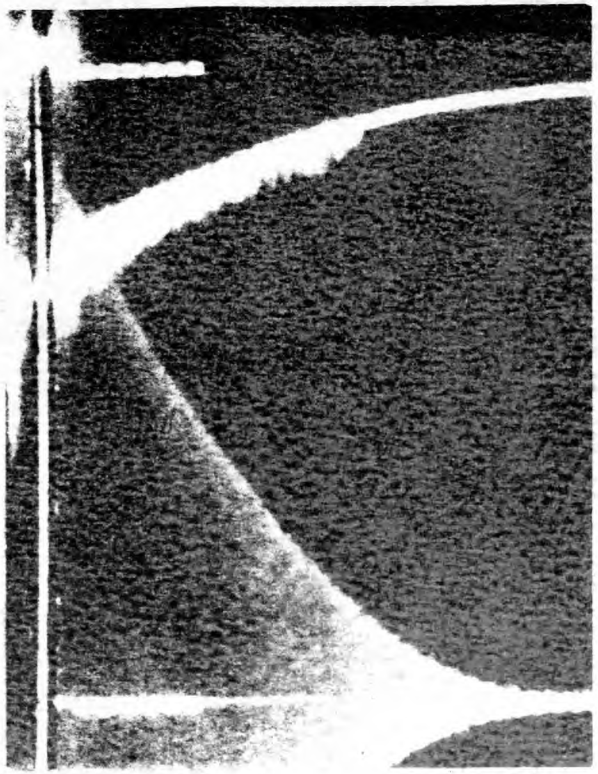

FIG.B.III.4b.

Recording H.I./6/11.10.

Hemisphere

Displacement, $x = 0{\cdot}240$ ins.

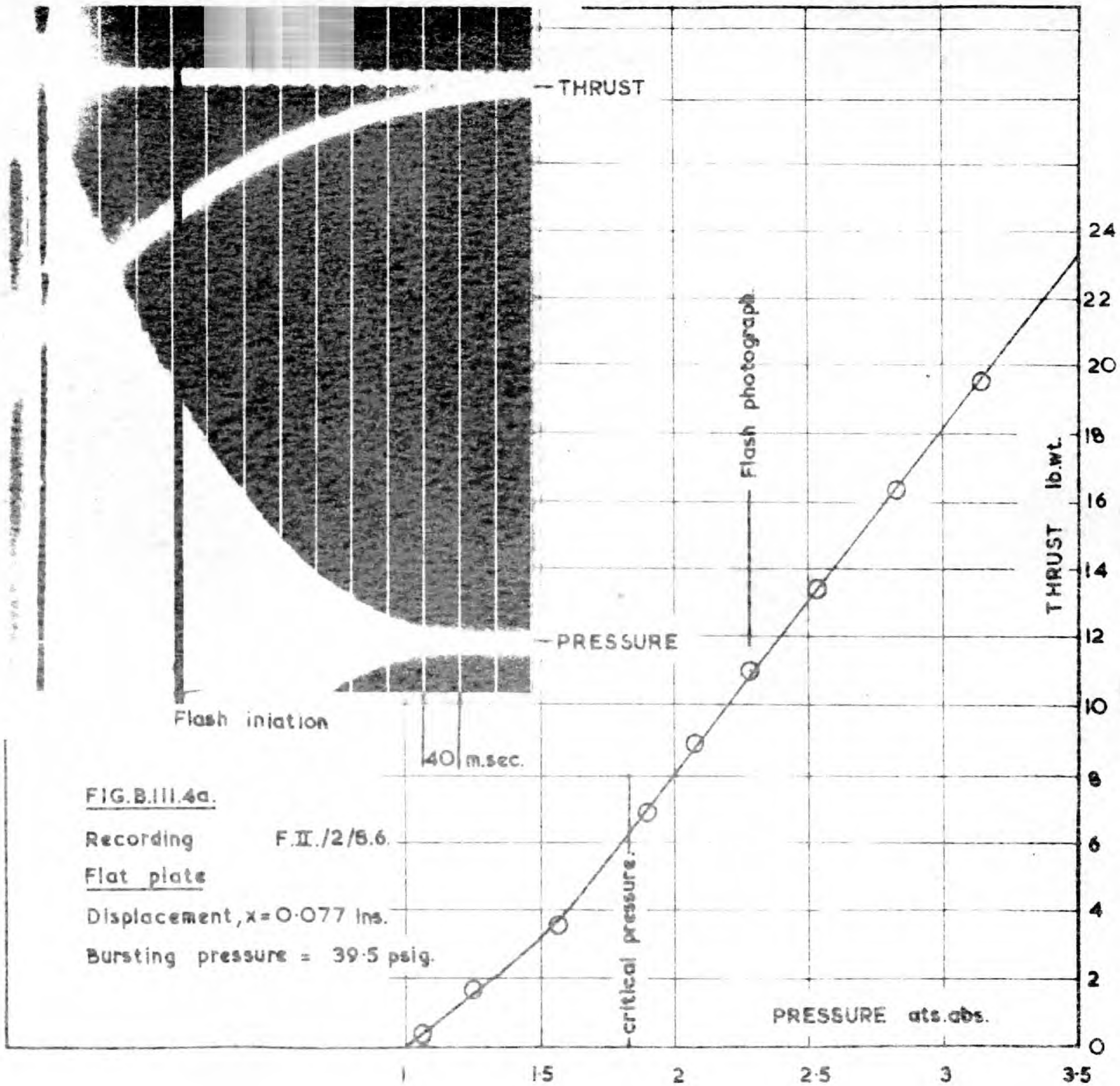

FIG.B.III.4a.

Recording F.II./2/5.6.

Flat plate

Displacement, $x = 0{\cdot}077$ ins.

Bursting pressure = 39·5 psig.

which holds the arm in a boss in one end and has its sides cut away. The clamp exactly fits the cylinder and by bringing the valve and arm together in this jig the two can be soldered together with the minimum distortion.

A number of different arms were tried to keep the dynamic response as high as possible and the calculations dealing with the vibrations of such an arm are given in Appendix E.

The transducer is attached to the bursting disc assembly by a plate mounted on four pillars. It is threaded along its trunk and screwed into a hole in the centre of the plate so that the distance between the obstruction and the vent can be altered by turning the transducer.

(iv) The recording of the pressure in the reservoir and the thrust on the obstruction and the initiation of an electronic flash at preset levels in these parameters.

The outputs from the proximity meter and the resistance bridge were displayed on the two beams of a double beam oscilloscope. The time base was triggered by the signal from the thrust transducer associated with the sudden application of load when the disc bursts. Two typical recordings are shown in Fig. B.III.4 and the two traces can be distinguished as a narrowing band for pressure and a single line for thrust.

To initiate an electronic flash from these measurements a photocell is fitted in the hood which holds the recording camera to the oscilloscope. A thin vertical bar is held between the oscilloscope face and the photocell and when the recording spot passes behind the bar the photocell produces a voltage signal which is amplified and used to operate the flash. By fixing the bar at a particular point in the recording, the flash can be initiated at a fixed time after the disc burst and hence at a fixed pressure or thrust. The pressure at which the flash occurs is recorded by the oscilloscope camera as the pressure at the leading edge of the bar obstructing the photographic image. This is clearly shown in Fig. B.III.4(a).

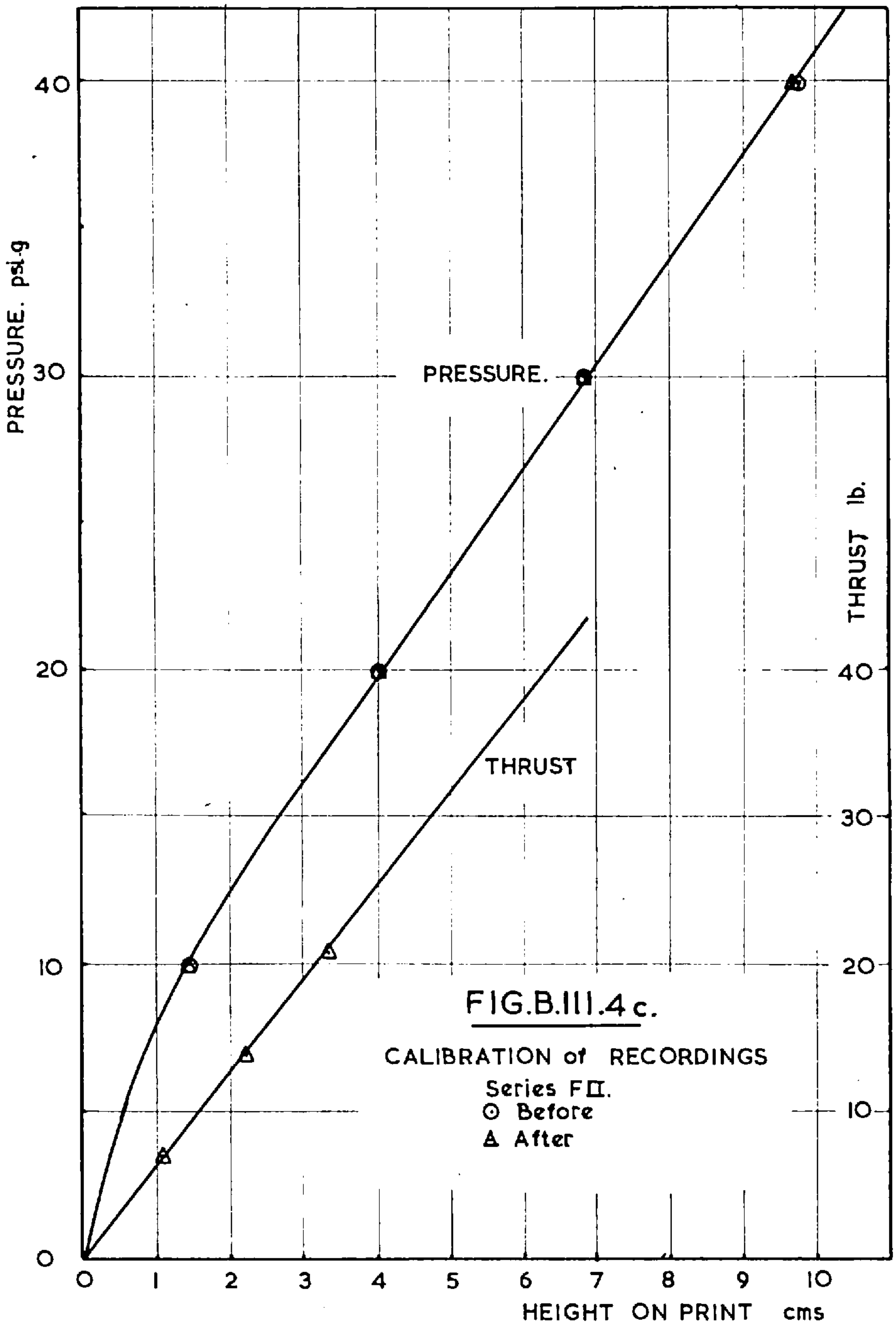

FIG. B.III.4 c.

CALIBRATION of RECORDINGS

B.III.3 Experimental Procedure

The pressure and thrust transducers were not calibrated for each experiment as in Chapter A.III. but before and after each series. Pressure recordings at set levels were made as described in Chapter A.III. and, since they gave identical results at the beginning and the end, they were used to calculate the results in this group.

A similar procedure was adopted for the thrust measurements. The calibration was carried out by placing the appropriate weights on the transducer and photographing the beam position on the oscilloscope. As can be seen from Fig. B.III.4(c) the output is proportional to the thrust.

The bursting disc assembly with a disc of known strength was attached to the reservoir and the thrust transducer attached to the assembly plate. The pressure in the reservoir was increased slowly and, just before the bursting pressure was reached, the recording camera shutter was opened. As soon as the discharge was completed the time axis was calibrated by recording the zero line, intensity modulated at a known frequency. The camera shutter was closed and the next experiment commenced by dismantling the valve assembly, replacing the bursting disc and changing one of the parameters such as the bursting pressure, the position of the obstruction or the time of initiation of the flash.

To minimise the effect of microphonics on the instruments the pressure reservoir was isolated in a separate darkroom and all controls were duplicated. The air supply was connected to the reservoir by a solenoid valve and the beam could be switched off electronically instead of using the camera shutter. Hence, the whole operating sequence could be carried out in the darkroom or from the instruments.

35 mm. H.P.S. film developed in Kodak special developer D.8 was used to record the traces and Process plates cut to fit behind the thrust transducer were used in making the flash shadowgraphs.

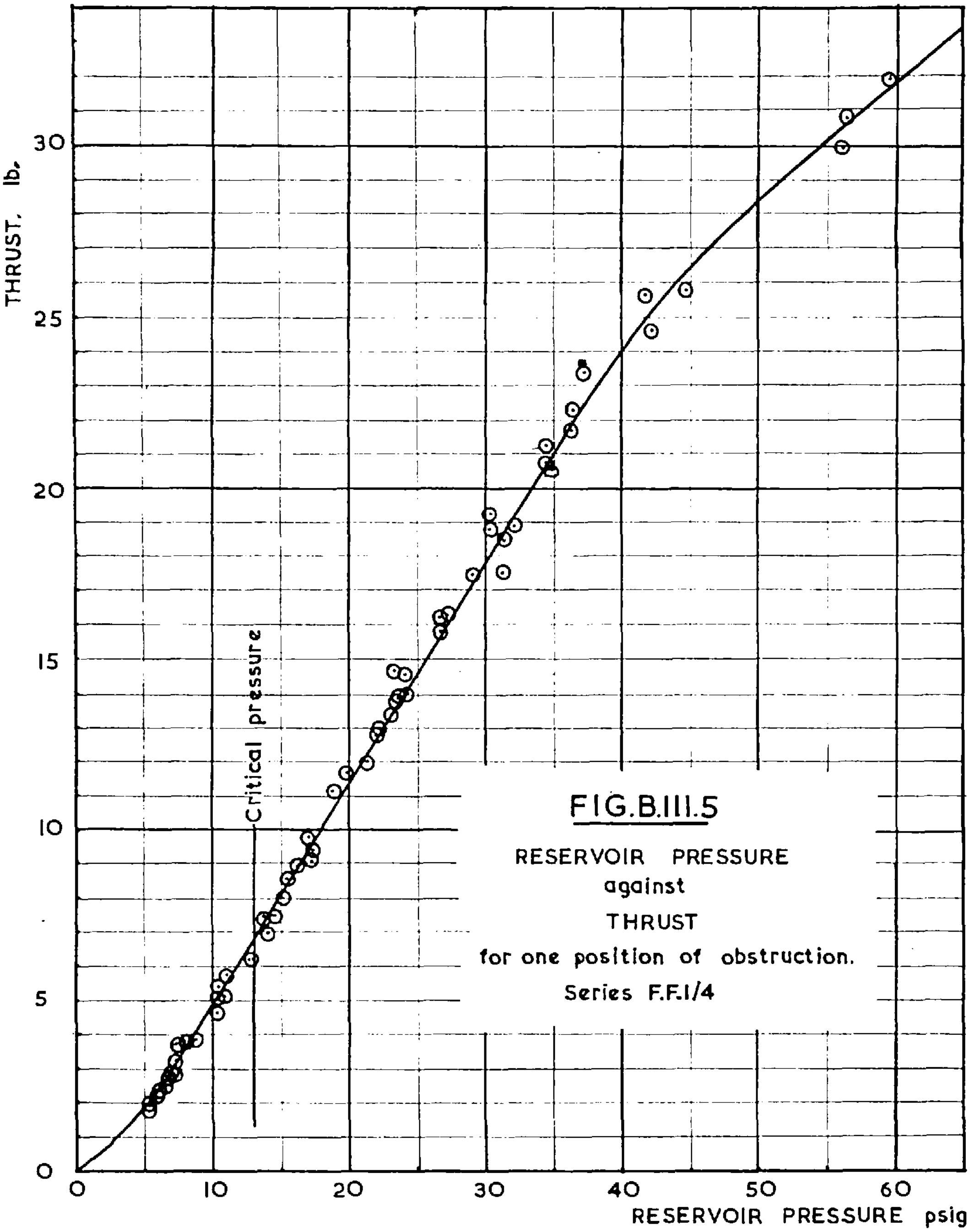
THRUST. lb.
0
5
10
15
20
25
30
Critical pressure
FIG.B.III.5
RESERVOIR PRESSURE
against
THRUST
for one position of obstruction.
Series F.F.1/4
0
10
20
30
40
50
60
RESERVOIR PRESSURE psig

B.III.4 Results

(i) Flat plate.

The experiments are tabulated in Table B.III.1 and it can be seen that they covered a large range of displacements for several bursting pressures and include a group carried out under similar initial conditions. The results from this group indicate good reproducibility and are shown in Fig. B.III.5. as a relation between reservoir pressure and thrust.

Hence, for each displacement of the plate a single curve is obtained and the relation between the two parameters is linear above the critical pressure. Below the critical pressure the reservoir pressure falls more rapidly than the thrust but, since the present investigation is into valves operating under choked conditions, only the supersonic portion of the curve will be considered.

As shown in the discussion, the thrust on the obstruction is directly proportional to the pressure in the reservoir if both these terms are in absolute pressure units. Hence by plotting

$$\left(\frac{\text{Thrust}}{\text{Vent area}} + 1 \right)$$

against (Reservoir gauge pressure + 1), as shown in Fig. B.III.6, a straight line through the origin is obtained. The

RUN NO.			Displacement x ins.	Bursting Pressure psi. g
Series	x' Turns	Film No.		
	½	4·3	0·019	32·9
	1	5·4	0·038	42·8
	1¾	7·5	0·067	38·7
	2	8·6	0·077	39·5
	2½	9·7	0·096	40·3
	3	10·8	0·115	33·6
	3½	11·9	0·135	36·7
F.II	4	12·10	0·154	39·6
	4½	13·11	0·173	35·5
	5½	15·12	0·212	39·6
	6	16·13	0·231	37·3
	7	18·15	0·269	38·0
	7½	19·16	0·288	37·2
	8	20·17	0·308	39·3
	8½	21·18	0·327	36·5
	9	22·19	0·346	40·4

<u>Table B.III.1.(a)</u> Flat plate.

RUN NO.				
Series	x' Turns	Film No.	x ins.	Bursting Pressure psi.g.
F.P.I	3	6	•106	-
	4	7	•144	78•0
	5	8	•183	82•1
	6	9	•221	79•3
	7	10	•260	91•8
F.P.II.	2	28	•077	45•3
	4	29	•154	52•9
	6	30	•231	54•5
	7	31	•269	49•6
F.T.	15	10•8	•577	40
F.T.2.	$4\frac{3}{4}$	4•3	•183	40•8
preliminary		A.1	0•217	42
		A.2	•172	48
		A.3	•122	48
		A.4	•059	50
		A.20	•302	58

Table B.III.1.(b) Flat plate

RUN NO.			Displ- acement x ins.	Burst- ing Pressure psi.g.	Shadowgraph Initiation		
Series	x' Turns	Film No.			Plate no.	Press	P/Pb
	2·4	3	0.154	60.6	I·4	56.2	·941
	5·4	4	"	53.6	I.5	44·7	·871
	7·4	5	"	56.7	I.6	42·4	·801
	10·4	6	"	55·6	I.7	30·2	·639
F.F.I.	12·4	7	"	56·6	I.8	30·2	·629
	15·4	8	"	36·5			
	17·4	9	"	44·7	I.9	19·8	·582
	20·4	10	"	59·7	I.10	17·4	·431
	25·4	12	"	31·3			
	$2\frac{1}{2}$·8	13	·308	44·2	II.1	39·6	·858
	$3\frac{1}{3}$·6	14	·231	48·6	II.2	42·9	·910
	5·4	15	·154	50·6	II.3	40·4	·844
F.F.II.	10·2	16	·077	54·8	II.4	31·3	·663
	$12\frac{1}{2}$·8	18	·308	54·3	II.6	22·3	·536
	$14\frac{1}{4}$·7	19	·269	46·2	II.7	17·9	·536
	$16\frac{2}{3}$·6	20	·231	53·7	II.8	18·1	·479
	25·4	21	·154	51·5	II.9	17·1	·503
	50·2	22	·077	53·5	II.10	14·5	·428

Table B.III.1(c). Flat Plate Shadowgraphs

Series	x' Turns	Film No.	Displacement.	x' Turns	Film No.	Dicplacement
Cone. C.I.	1½	29	.053	2½	31	.091
	2	30	.072	3	32	.111
Cone F.C.I.	6¾	23	.2595	6¾	28	.259
	"	24	"	"	29	"
	"	25	"	"	30	"
	"	26	"	"	31	"
	"	27	"	"	32	"
Cone. F.C.III.	17½	3	.674	17½	8	.674
	10½	4	.404	13½	9	.520
	¾	7	.029	10½	10	.404
Cu.Cone. Cu.I.	½	5	.019	4	12	.154
	1	6	.038	5	14	.192
	2	8	.077	6	16	.231
	3	10	.115	7	18	.269
Cu.Cone. F.Cu.I.	4½	13	.173	4½	18	.173
	"	14	"	"	20	"
	"	15	"	"	21	"
	"	16	"	"	22	"
	"	17	"			
Cu.Cone. F.Cu.II.	13	23	.500	13	28	.500
	6¾	24	.260	8	29	.308
Hemisphere H.I.	5	9	.192	8	15	.308
	6	11	.232	9	17	.346
	7	13	.269	10	19	.374
Hemisphere F.H.II.	11½	2	.443	11½	6	.443
	"	3	"	"	7	"
	"	4	"	"	9	"
	"	5	"	"	10	"
H'sphere F.H.IV.	20	16	.769	15¾	17	.606
	11½	5	.443	6½	6	.250

TABLE B.III.2

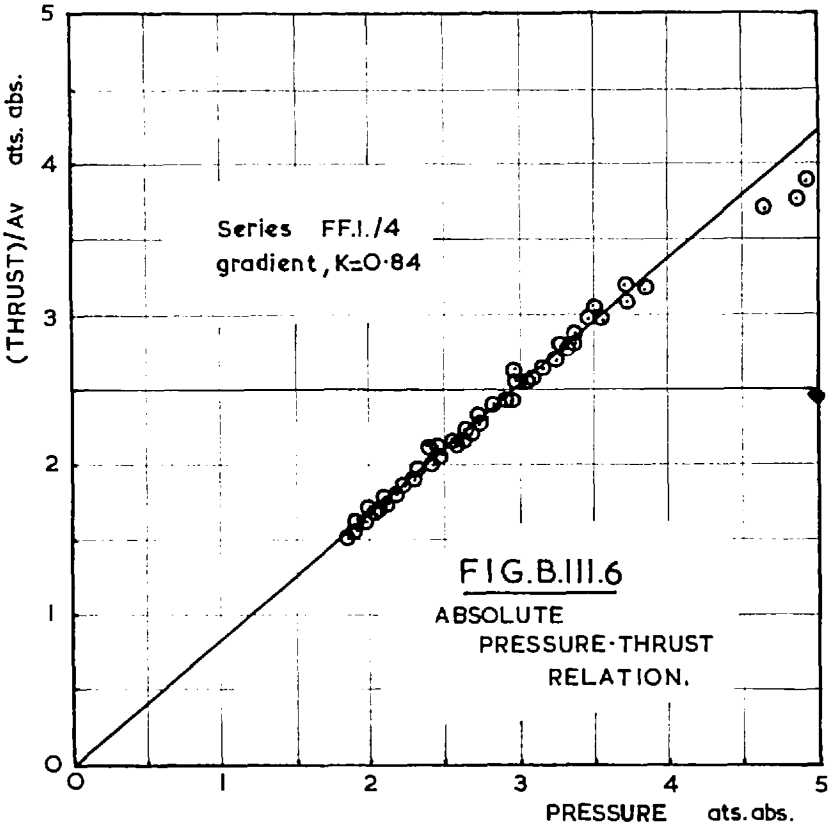

FIG.B.III.6
ABSOLUTE PRESSURE-THRUST RELATION.

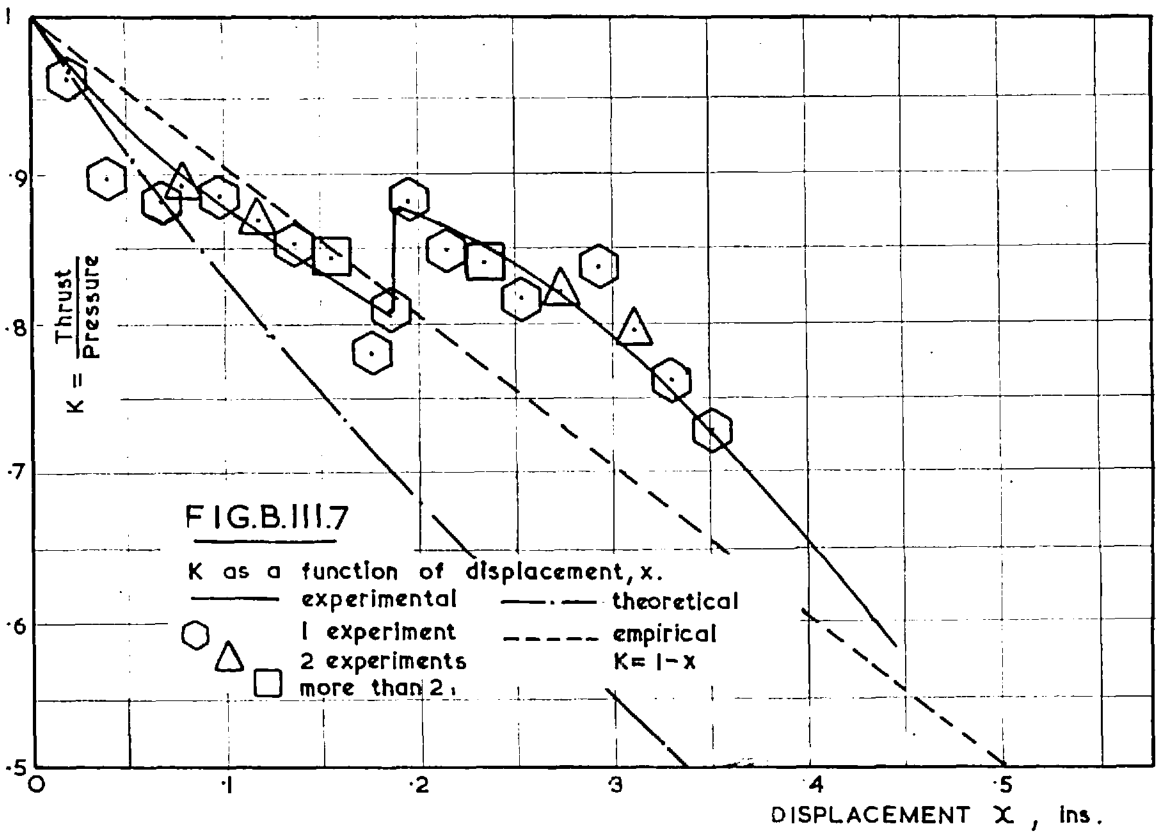

FIG.B.III.7
K as a function of displacement, x.

slope, K, of this line has been measured for each position of the obstruction and is plotted in Fig. B.III.7 against the distance, x, between the plate and the vent. Since the thrust has been calculated in pressure units, as the thrust divided by the vent area, the reservoir pressure equals the thrust when the valve is closed and K is a measure of the momentum change the fluid undergoes in passing through the valve.

In this way, the thrust on the obstruction can be related to the pressure in the reservoir by a single curve. However, a more useful relation is that between the thrust on the obstruction and its distance from the vent for a given pressure in the reservoir. In Fig. B.IV.5 in Chapter B.IV a series of curves has been constructed on the basis of the approximate relation shown in Fig. B.III.7. Each curve corresponds to a particular reservoir pressure as measured by the appropriate pressure ratio: from unity at the bursting pressure to a value representing the transition from supersonic to subsonic flow.

Flash shadowgraphs for a number of displacements of the obstruction and at different intervals after the disc has burst are shown in Plates VII and VIII. Measurements from these photographs cannot be used quantitatively since there are density gradients perpendicular to the photographic plate and the image is distorted

Pressure ratios, p

a.	0·941
b	0·871
c	0·801
d	0·629
e	0·582
f	0·431

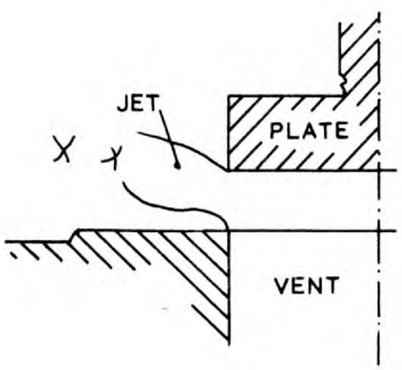

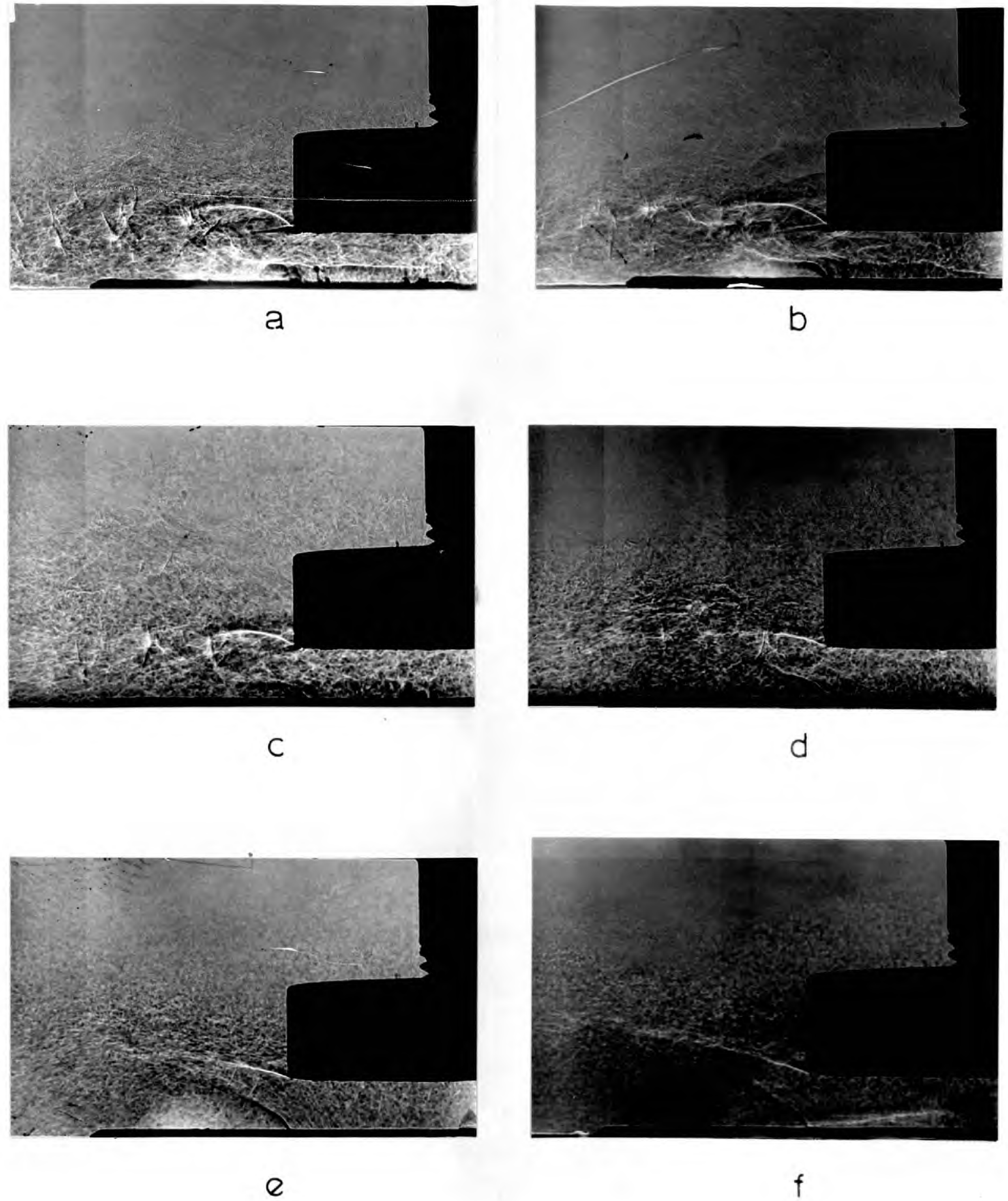

PLATE VII. Shadowgraphs - Flat plate SERIES FF1/ Constant displacement of 0·154 ins.

(ii) Cone, hemisphere and cusped cone.

The experiments are listed in Table B. III.2. It can be seen that variation in bursting pressure has not been considered and in determining the pressure-thrust relations shown in Fig. B.III.8 it has been assumed that the correlation used for the flat plate is applicable. Flash photographs have been taken for each obstruction and samples are shown in Plate IX.

In certain positions the conical and hemispherical obstructions were found to vibrate in the vent and in these experiments the discharge was accompanied by a high pitched whistle. These vibrations appear on the recordings as shown in Fig. B.III.4 (b) and they were found to occur under particular conditions of pressure for each of the positions. It is suggested that the thrust transducer was such that, at its resonant frequency, the wave length of the sound waves under these conditions equal or are an exact fraction of the gap between the vent walls and the obstruction. Hence, the frequency of these oscillations and the size of the gap should be a measure of the state of the gas passing through the valve.

(iii) The accuracy of the results.

Fig. B.III.5 indicates the reproducibility of the results and where more than a single experiment has been carried

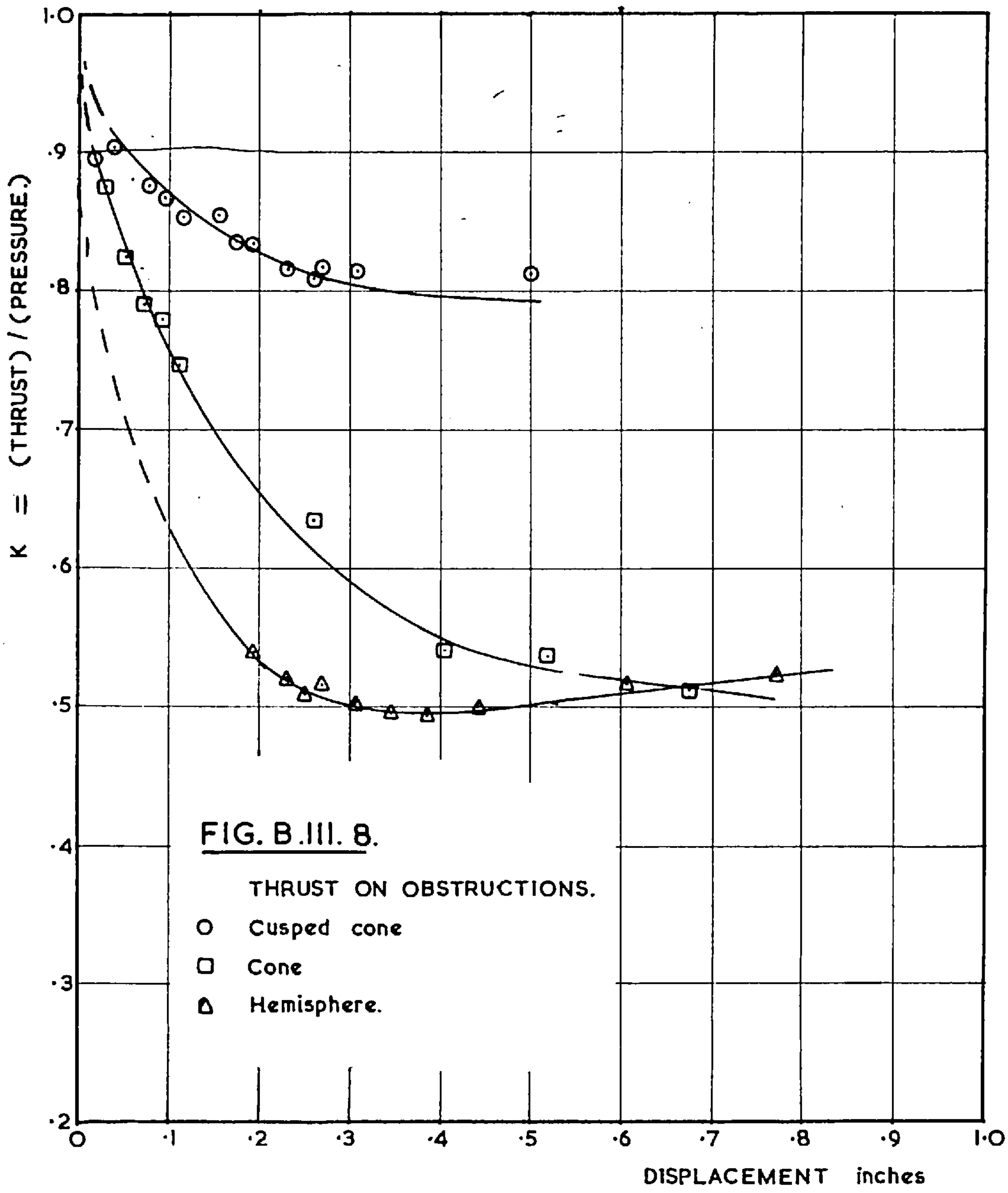

FIG. B.III. 8.

THRUST ON OBSTRUCTIONS.

out for a single displacement the accuracy of K depends upon the measurement of pressure and thrust. The pressure recordings carried out in Chapter A.III were accurate to 0·1% but here direct calibration was not used and the records were measured to the nearest $\frac{1}{2}$ p.s.i.g. The thrust recordings were read to the nearest tenth of a pound so that the slope of the pressure-thrust curve could be measured to $\pm$ 1%. In Fig. B.III.7 the accuracy of each point is given by the size of the symbol.

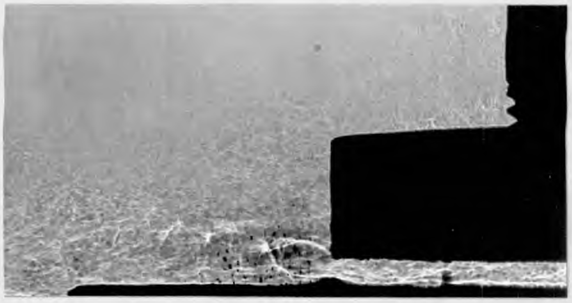

Displacement 0·077"
Pressure ratio 0·663

a Flow through a slit

FF II/10.2/16

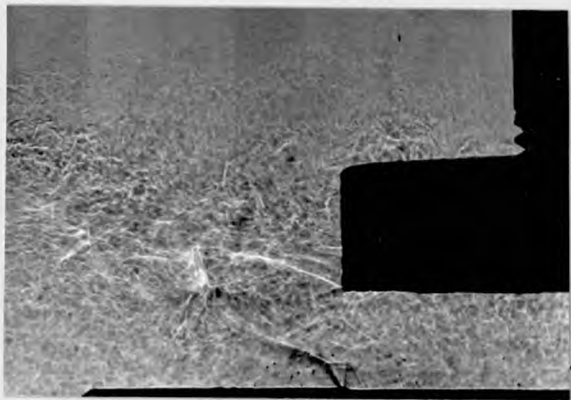

Displacement 0·231"
Pressure ratio 0·910

b Formation of Riemann wave

Riemann wave just visible

FF II/$3\frac{1}{3}$·6/14

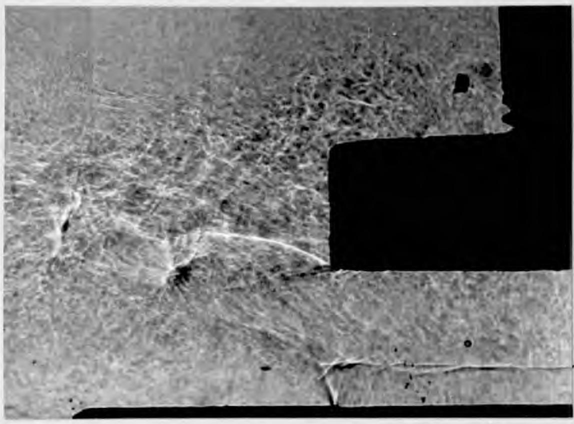

Displacement 0·308"
Pressure ratio 0·858

c Strong Riemann wave

Riemann wave

FF II/$2\frac{1}{2}$.8/13

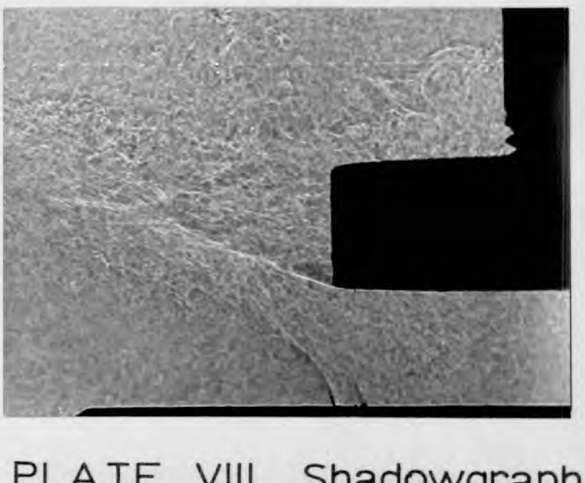

Displacement 0·308"
Pressure ratio 0·536

d Low pressure flow

No Riemann wave

FF II/$12\frac{1}{2}$.8/13

PLATE VIII. Shadowgraphs - Flat plate.
SERIES FF II/

B.III. : Discussion.

(i) Flat plate.

It can be seen from the shadowgraphs in Plate VIII that there are two phases in the phenomenon When the plate is close to the vent, as in (a), a jet is formed at the cylindrical slit made by the edge of the plate and the edge of the vent. When the spacing is greater that 0·2 vent diameters, as shown in (b), the jet is formed in the vent itself and is deflected by the plate so that the area of discharge is no longer that of the slit. At these displacements the formation of a normal shock wave becomes apparent and when the spacing is 0·308 vent diameters, as in (c), a strong shock wave extending across the jet can be seen. This wave is termed a Riemann wave and represents a discontinuity in the flow parameter and a reduction in gas velocity from supersonic to subsonic conditions. The thrust on the plate will depend upon the type of flow taking place and the transition is marked by a change in the thrust-displacement curve shown in Fig. B.III.7.

The first phase can be analysed theoretically by assuming that the plate acts as one wall of a converging diverging 'nozzle' and the flow through the valve is such that all stream lines are orthogonal to the conical surfaces BA_o, BA_n, BA_1 ......BA_r as shown in Fig. B.III.9.

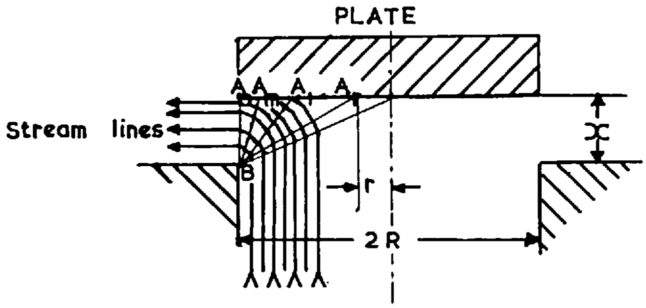

FIG.B.III.9.

Fig. B.III.9.

If the pressure, temperature, density and gas velocity in the reservoir, at one of these surfaces and at the minimum flow area BA_m are P_o, T_o, ρ_o, u_o; P, T, ρ, u; and P_+, T_+, ρ_+, u_+ respectively the equations of motion for each cross sectional area can be written:

$$u_o = 0 \;;$$

$$u = u_o^2 + \frac{2\gamma}{\gamma - 1} \cdot \frac{P_o}{\rho_o} \left\{ 1 - \left(\frac{P}{P_o}\right)^{\frac{\gamma - 1}{\gamma}} \right\} \;;$$

and $$u_+ = u_o^2 + \frac{2\gamma}{\gamma - 1} \cdot \frac{P_o}{\rho_o} \left\{ 1 - \left(\frac{P_+}{P_o}\right)^{\frac{\gamma - 1}{\gamma}} \right\} .$$

(equations B.III.1)

Therefore, the pressure P at a given section will depend upon the velocity, u, of the gas

i.e., $$\frac{P}{P_o} = \left\{ 1 - \frac{\rho_o}{P_o} \cdot \frac{\gamma - 1}{2\gamma} \cdot u^2 \right\}^{\frac{\gamma}{\gamma - 1}} \qquad \text{B.III.2.}$$

The velocity will depend upon the gas density and the cross-sectional area, A, according to:

$$\text{Mass flow} = A, \rho, u$$

where the mass flow will be determined by the minimum flow area, A_+. The mass flow has been given in Chapter A.III as

$$\text{Mass flow} = A_+ \sqrt{\gamma \left(\frac{2}{\gamma+1}\right)^{\frac{\gamma+1}{\gamma-1}} \cdot P_o \rho_o}$$

so that

$$u^2 = \left[\frac{\text{Mass flow}}{A \cdot \rho}\right]^2 .$$

$$\left.\begin{aligned} \therefore \quad u^2 &= \frac{\gamma . P_o . \rho_o . B^2}{\rho^2 \alpha^2} \\ \text{where} \quad B &= \left(\frac{2}{\gamma+1}\right)^{\frac{\gamma+1}{2(\gamma-1)}} \quad \text{and} \\ \alpha &= \frac{A}{A_+} \end{aligned}\right\} \qquad \text{B.III.3.}$$

Substituting B.III.3 in B.III.2 and putting $\frac{\rho}{\rho_o} = \left(\frac{P}{P_o}\right)^{\frac{1}{\gamma}}$ for isentropic flow

$$\left(\frac{P}{P_o}\right)^{\frac{\gamma-1}{\gamma}} = 1 - \frac{\gamma-1}{2} \cdot \frac{B^2}{\alpha^2} \cdot \left(\frac{P_o}{P}\right)^{\frac{2}{\gamma}} . \qquad \text{B.III.4}$$

Therefore, when $\gamma = 1{\cdot}4$, $B^2 = 0{\cdot}3353$ and

$$\alpha^2 = \frac{0{\cdot}0671}{p^{1{\cdot}428} \; (1 - p^{0{\cdot}2856})} \qquad \text{B.III.5}$$

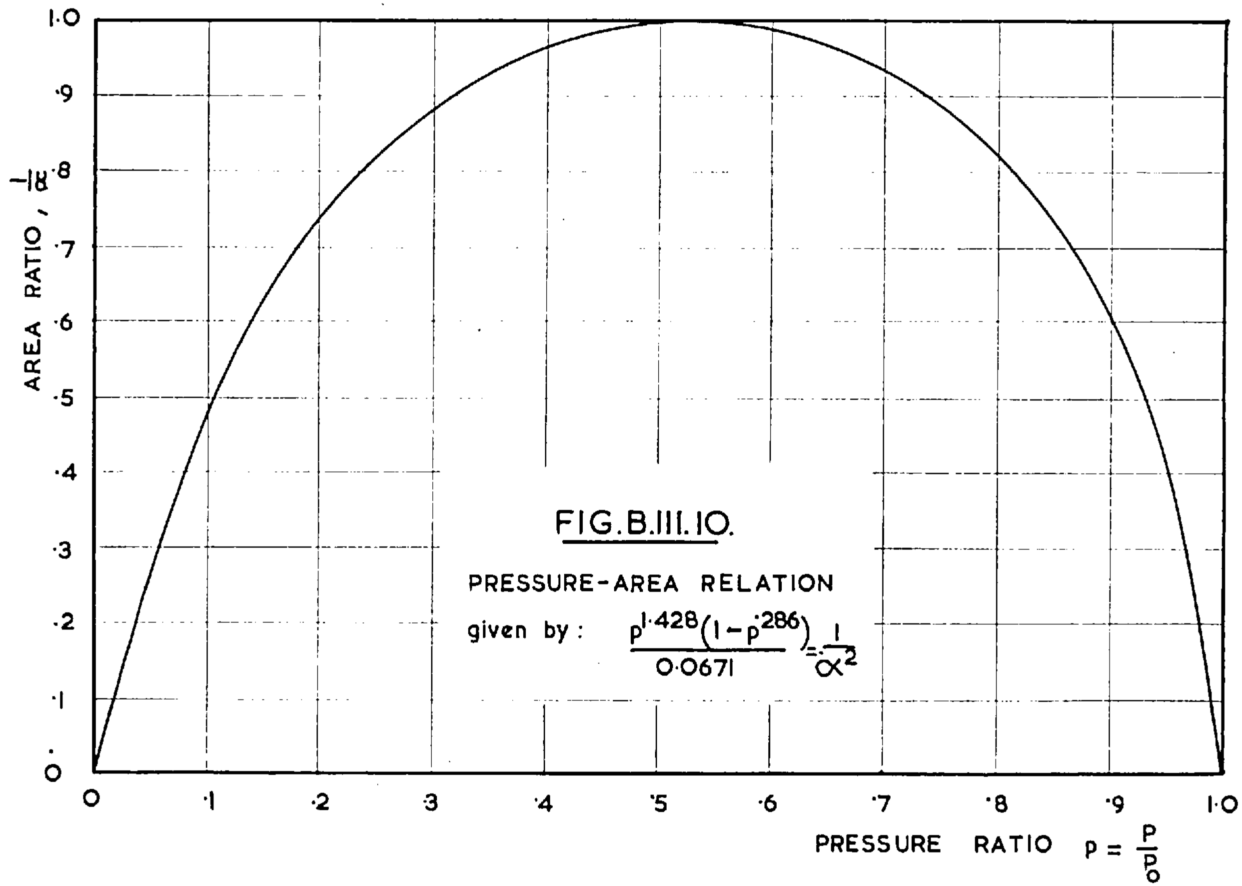

FIG. B.III.10.

PRESSURE-AREA RELATION

given by : $\frac{p^{1\cdot428}(1-p^{\cdot286})}{0\cdot0671} = \frac{1}{\alpha^2}$

where $p = \frac{P}{P_o}$.

Hence, the pressure exerted at any point on the flat plate can be related to the flow area associated with that point as shown in Fig. B.III.10.

To complete the solution, it is necessary to compute the flow areas formed by the frustrums of the cones between the rim of the vent and a circle on the flat plate of radius r. This area is given by

$$A = 2\pi \left(\frac{R + r}{2}\right) \cdot y$$

$$\text{and} \quad y = \sqrt{x^2 + (R - r)^2}$$

$$\therefore A = 2\pi \left(\frac{R + r}{2}\right) \cdot \sqrt{x^2 + (R - r)^2}$$

$$\left.\begin{aligned} &= \left[\frac{1 + \eta}{2} \sqrt{1 + \left(\frac{1 - \eta}{X}\right)^2}\,\right] 2\pi x R \\ &\text{where } \eta = \frac{r}{R}, \\ &X = \frac{x}{R} \quad \text{and} \end{aligned}\right\} \quad \text{B.III.6}$$

$2\pi x R$ = area of cylindrical aperture between plate and vent.

Since the variation of A with η is required in the calculation, the minimum flow area has not been determined analytically but graphically from the plot of A against η. (not shown). The minimum flow area as a function of x is shown in Fig. B.IV.1 in Chapter B.IV.

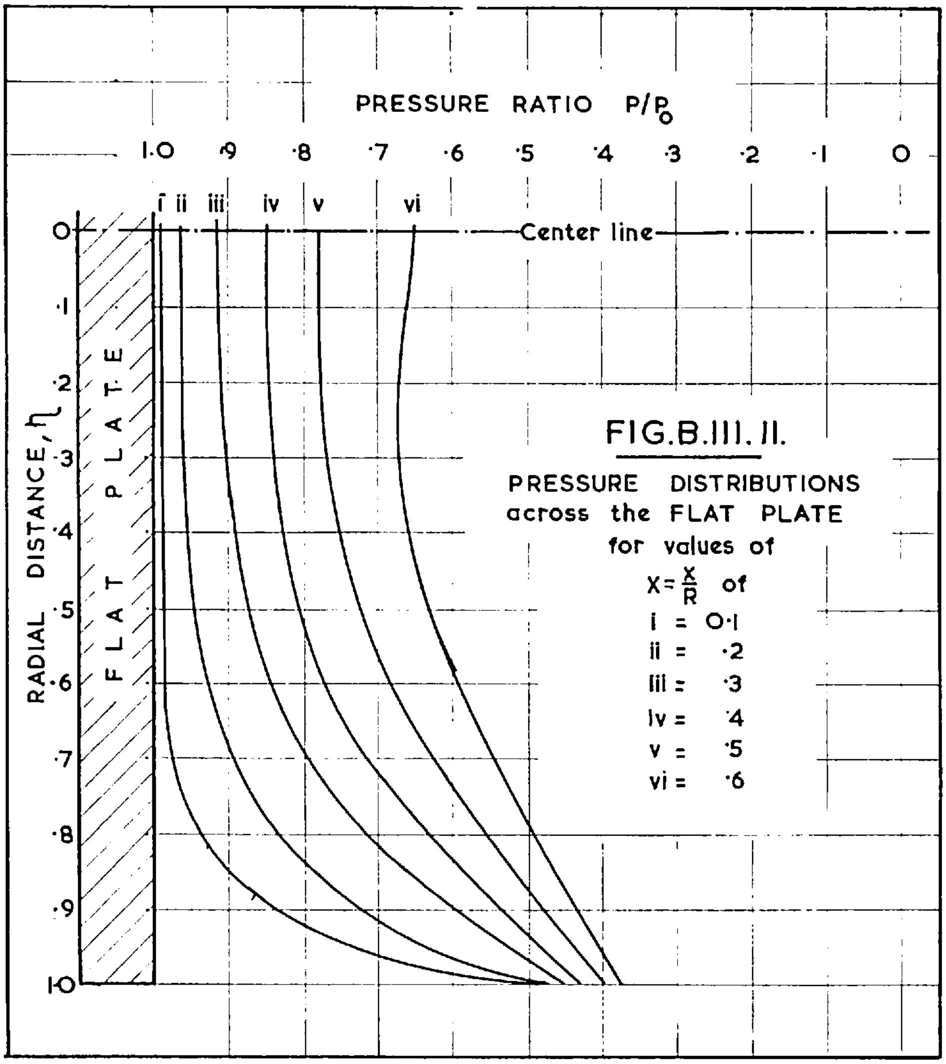

FIG.B.III.II.

PRESSURE DISTRIBUTIONS across the FLAT PLATE for values of $X = \frac{x}{R}$ of

i = 0·1
ii = ·2
iii = ·3
iv = ·4
v = ·5
vi = ·6

The pressure at any section is obtained from equation B.III.5 and it is assumed that this is the pressure on the plate at a point at a radial distance r from the centre. The pressure distributions across the plate for a number of values of X are given in Fig. B.III.11. For each value of x the pressure can be integrated over the area of the plate and the total thrust calculated from

$$F = 2\pi \int_0^R P.r.\, dr$$

$$\text{or} \quad \frac{F/(\pi R^2)}{P_o} = 2\int_0^1 p.\eta.\, d\eta. \qquad \text{B.III.7}$$

The right hand side of equation B.III.7 is a definite integral and a constant for a given displacement so that the thrust is directly proportional to the reservoir pressure P_o. It should be noted that P_o is the absolute pressure and that F is the thrust on one side of the plate only and the atmospheric pressure must be subtracted from it before the true thrust is obtained. If the gauge pressure is P_{og} and the true thrust F_g equation B.III.7 can be rewritten

$$\frac{\frac{F_g}{\pi R^2} + 1}{P_{og} + 1} = K$$

where $K = 2 \int_0^1 p.\eta.d\eta$

= the slope of the curve obtained from Fig. B.III.6.

Therefore, by rearranging,

$$\frac{F_g}{A_v} = K.P_{og} - (1 - K) \qquad \text{B.III.8}$$

where $A_v = \pi R^2$ = maximum vent area,

F_g is in atmospheres ins^2.,

P_{og} is in atmospheres and

R is in inches.

B.III.8 is the equation to a straight line having a slope K and an intercept on the P_{og} axis of $(1 - K)$.

The relation between K and x calculated in this manner is compared with the experimental results in Fig. B.III.7. Within the range $0 < X < 0{\cdot}5$, reasonable agreement is obtained although the theory predicts lower values of K. This is due to the assumption that the pressure is constant across each section. The pressure is probably greater near the plate since the momentum of the gas will cause a concentration of stream lines at the plate surface.

When the displacement is greater than 0·2 vent diameters the flow mechanism changes and the jet is formed in the vent giving rise to the Riemann wave. Under these conditions the

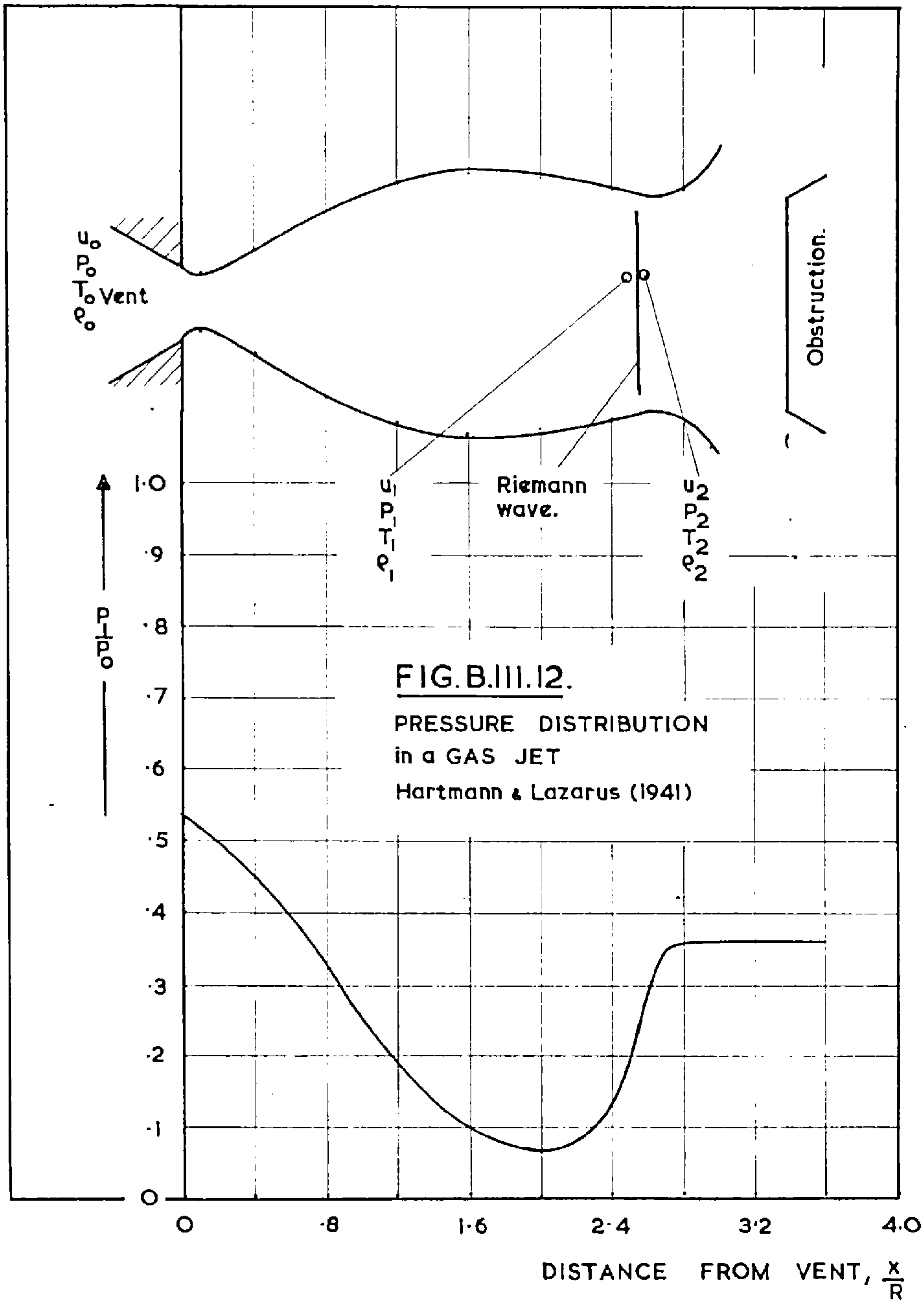

FIG. B.III.12.

PRESSURE DISTRIBUTION in a GAS JET

Hartmann & Lazarus (1941)

pressure on the plate is a function of both the pressure just ahead of the Riemann wave and the pressure in the reservoir. If the pressure just ahead of the wave is P_1 the pressure on the plate is

$$\frac{P}{P_o} = \frac{\left(\frac{\gamma+1}{\gamma-1}\right)^{\frac{\gamma+1}{\gamma-1}}\left[\left(\frac{P_o}{P_1}\right)^{\frac{\gamma-1}{\gamma}} - 1\right]}{\frac{P_o}{P_1}\left[\frac{4\gamma}{(\gamma-1)^2} - \frac{1}{\left(\frac{P_o}{P_1}\right)^{\frac{\gamma-1}{\gamma}} - 1}\right]^{\frac{1}{\gamma-1}}} \qquad \text{B.III.9}$$

Hartmann and Lazarus (1941) have measured the static pressures in gas jets and a typical pressure-distance relation is shown in Fig. B.III.12. The increase in pressure at the Riemann wave is associated with the decrease in velocity across the shock wave. When the shock wave is present this pressure change is discontinuous but even when conditions are such that there is no shock an increase in pressure is found to occur at a similar point in the jet.

Hence, as the obstruction moves away from the vent the pressure should increase fairly rapidly at a certain value of x, as shown in Fig. B.III.7. This value of x cannot be related to the results obtained by Hartmann and Lazarus since the flat plate itself effects the flow conditions in the jet.

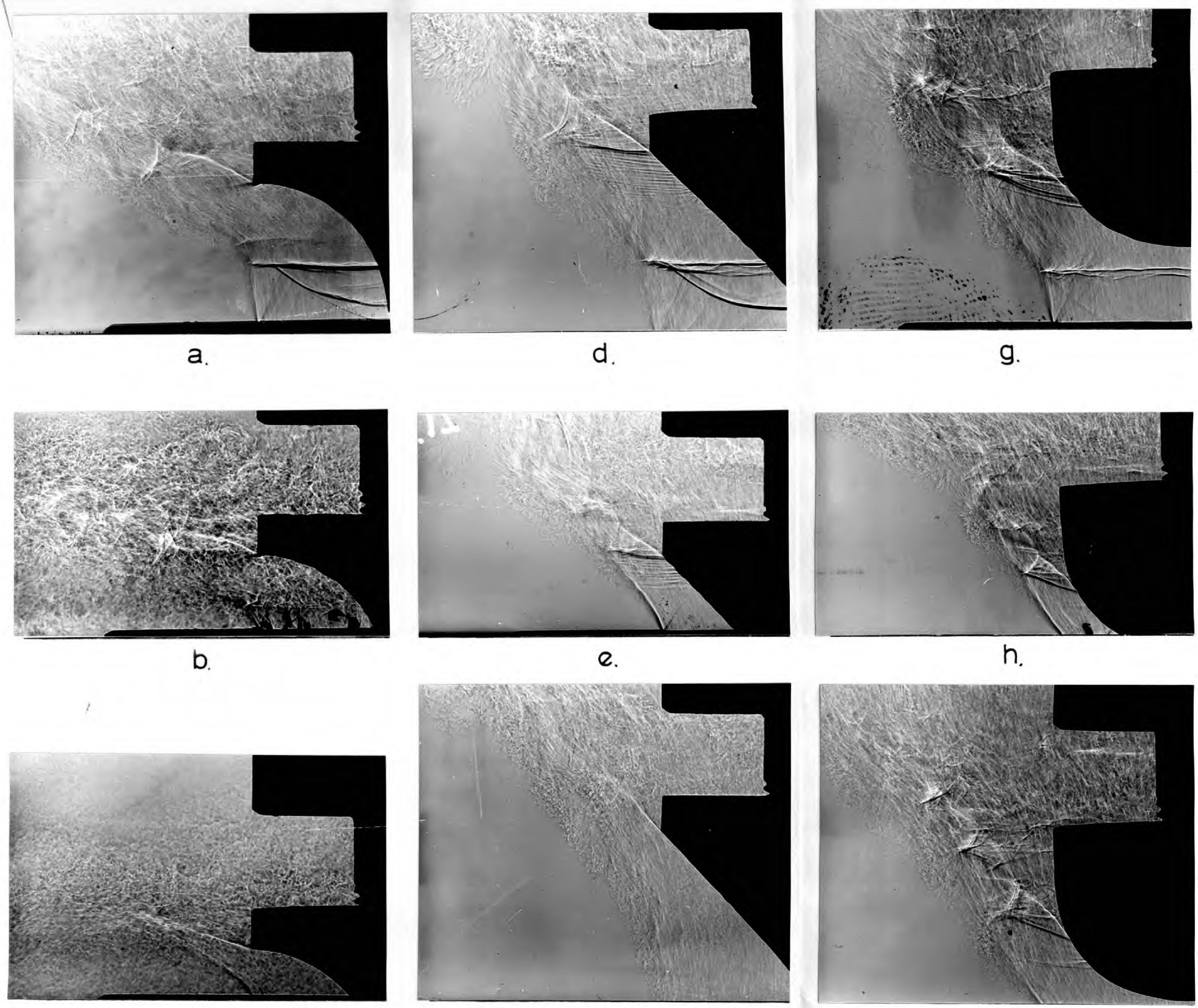

a. d. g.

b. e. h.

c. f. i.

Cusped cone — Cone — Hemisphere

PLATE IX. Shadowgraphs - Other obstructions.

a, d, g. Formation of normal shock wave ;

b, e, h. High pressure discharge ; and

c, f, i Low pressure discharge.

(ii) Other obstructions.

The results for the other obstructions are shown in Fig. B.III.8 and are similar in form to those for the flat plate. However, the values of x at which the transition occurs are much greater since the displacement required before the obstruction is clear of the vent is at least one half vent diameter. The formation of the Riemann wave is shown in Plates IX (a), (d) and (g) but they cannot be related to any value of K since controlled experiments were not carried out at these large displacements.

The normal shock waves shown in (a), (d) and (g) are similar to those found in wind tunnel experiments and in the case of the sharp ended obstructions these waves are attached whereas they are formed ahead of the blunt obstructions (compare Plate VIII (c)). The weak shock waves formed on the cone are due to small irregularities of the surface and the angle they make to the direction of flow is a measure of the velocity of the gas. The shock wave at the edges of the two conical obstructions and part way along the hemisphere are caused by a sudden change in direction of the boundary. If the obstructions were in a wind tunnel the angle these waves make with the axis of the obstruction could be calculated. However the gas is expanding in the vent into an ifinite atmosphere and the problem requires the analysis of the flow from the vent.

CHAPTER B.IV. DISCHARGE RATES PAST THE OBSTRUCTIONS AND THE CALCULATION OF VALVE PERFORMANCE

B.IV.1 Calculation of discharge coefficients.

Theoretically, the discharge rate through a valve is known if the minimum cross-sectional area can be determined. The equations involving the state of the gas entering the valve, the discharge area and the mass flow through the valve are given in Chapter A.III. However, the true discharge rate is a function of the shape of the gas passage and a discharge coefficient must be included to account for the three-dimensional effects and the presence of a boundary layer. The mass flow rate is

$$G = Cd.A.\ \rho_o \sqrt{\gamma \frac{P_o}{\rho_o} \left(\frac{2}{\gamma + 1} \right)^{\frac{\gamma + 1}{\gamma - 1}}} \qquad \text{B.IV.1}$$

where A = minimum flow area,

G = mass flow rate,

ρ_o = density of the gas in the reservoir,

P_o = the pressure of the gas in the reservoir and

Cd = the discharge coefficient.

The minimum flow area is computed from the geometry of the valve. The minimum areas for the flat plate have been calculated in the previous chapter and those for the cone, hemisphere and cusped cone are obtained in a similar manner and shown in

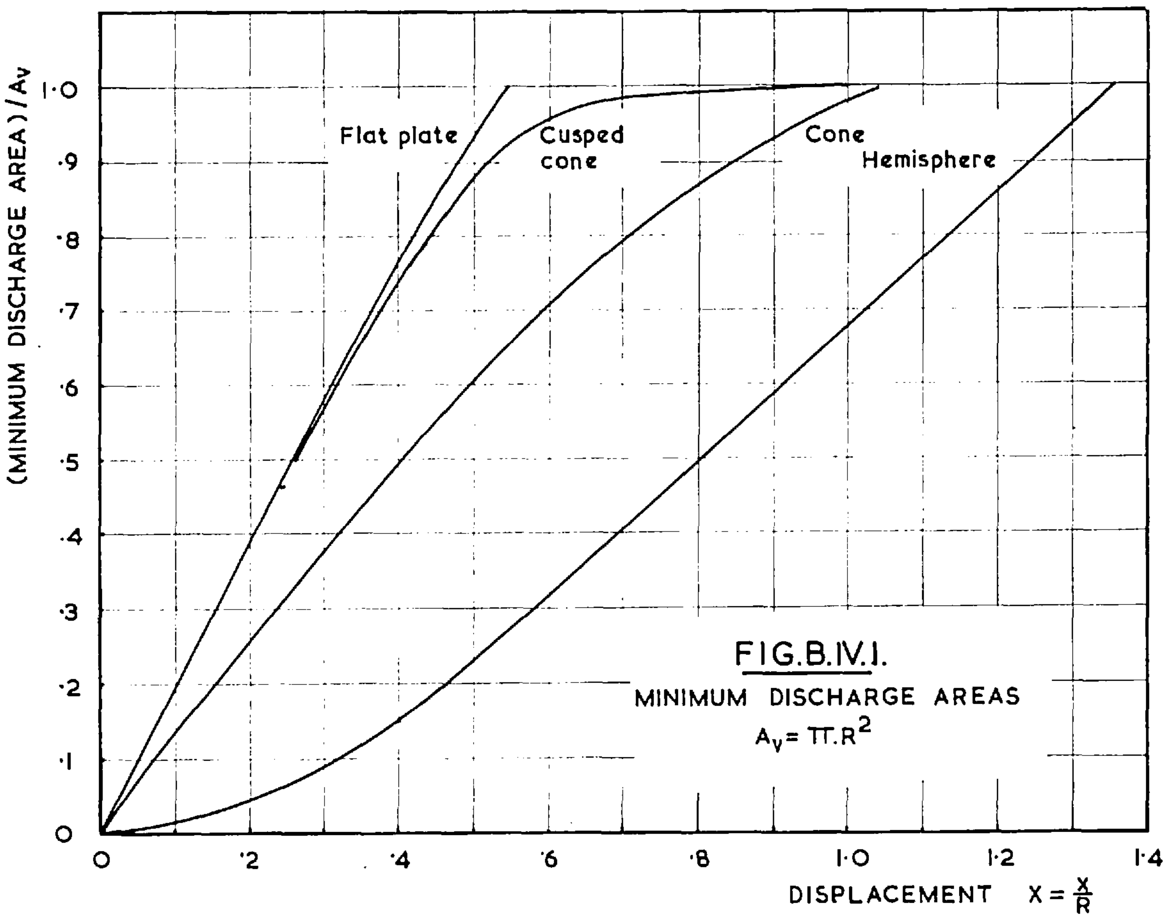

FIG.B.IV.1.

MINIMUM DISCHARGE AREAS

$A_v = \pi . R^2$

Fig. B.IV.1.

For instance in the case of the cone shown in Fig. B.IV.2 the area of the section AB is

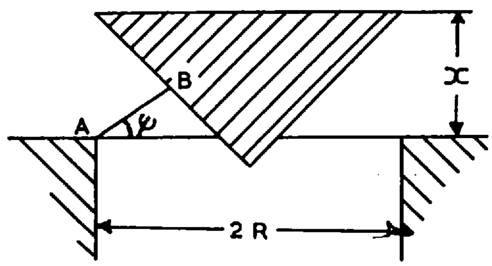

FIG.B.IV.2.

Fig. B.IV.2

$$\frac{\text{Area frustrum AB}}{\text{area of vent}} = \frac{X}{\cos \Psi}\left[\frac{2}{1 + \tan \Psi} - \frac{X}{(1 + \tan \Psi)^2}\right]$$

where $X = \frac{x}{R}$

which is a minimum when

$$\tan \Psi = \frac{X \pm \sqrt{16 - 7X^2 - 8X}}{2X + 4}$$

These two equations give the minimum cross-sectional area for any value of X.

The mass flow rate from a pressure reservoir is given by equation A.III.2 on Page 127 as

$$\frac{dp}{dt} = k\,(1-\theta)^{\frac{5}{4}} - \frac{\gamma\, G}{V\,\rho_o}\,.\,P$$

$$\frac{d\theta}{dt} = \left[k(1-\theta)^{\frac{5}{4}} - \frac{\gamma - 1}{V\,\rho_o}\,.\,G.\,P \right] \frac{\theta}{P}\,.$$

Hence, by measuring the change in pressure and by establishing the value of k, all the terms in equation B.IV.1 except Cd can be determined.

This process has been applied to the pressure recordings obtained experimentally in Chapter B.III.

The corrected discharge area, Cd.A, is calculated as described in Chapter A.III. on page 147 from the differential form of the discharge equation.

$$\text{i.e.,}\quad CdA = \frac{V}{a_o B}\left\{ \frac{1}{\theta^{\frac{1}{2}}} \quad \frac{d}{dp}\left(\ln\frac{\theta}{p}\right) \right\} \frac{dp}{dt}$$

where V = the volume of the pressure reservoir,

a_o = the speed of sound in the gas in the reservoir at time $t = 0$,

θ = $\dfrac{\text{the temperature of the gas at } t = t}{\text{the temperature of the gas at } t = 0}$

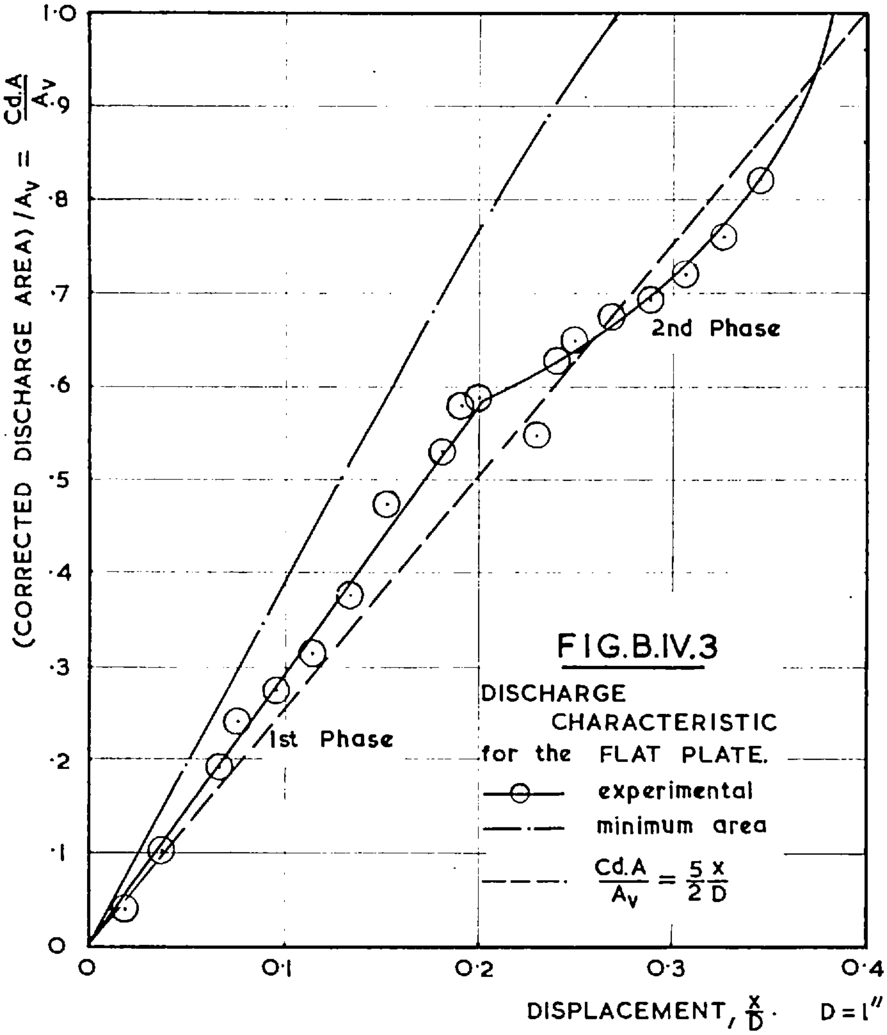

(CORRECTED DISCHARGE AREA) /A_v = $\frac{Cd.A}{A_v}$
1·0
·9
·8
·7
·6
·5
·4
·3
·2
·1
0
0
0·1
0·2
0·3
0·4
DISPLACEMENT, $\frac{x}{D}$. D = 1″
1st Phase
2nd Phase
FIG.B.IV.3
DISCHARGE CHARACTERISTIC for the FLAT PLATE.
experimental
minimum area
$\frac{Cd.A}{A_v} = \frac{5}{2}\frac{x}{D}$

$$p = \frac{\text{pressure of gas at } t = t}{\text{pressure of gas at } t = 0},$$

$$B = \left(\frac{2}{\gamma + 1}\right)^{\frac{\gamma + 1}{2(\gamma - 1)}}$$

In this way, the corrected discharge area has been computed (as a fraction of the unobstructed vent area) for a series of displacements of each obstruction and related to the distance between the obstruction and the vent by the curves shown in Figs. B.IV. 3 and 4. The difference between one of these curves and the corresponding minimum area curve is a measure of a discharge coefficient which varies with the displacement. These coefficients have not been calculated since it is the actual discharge rates which are required in the assessment of valve performance.

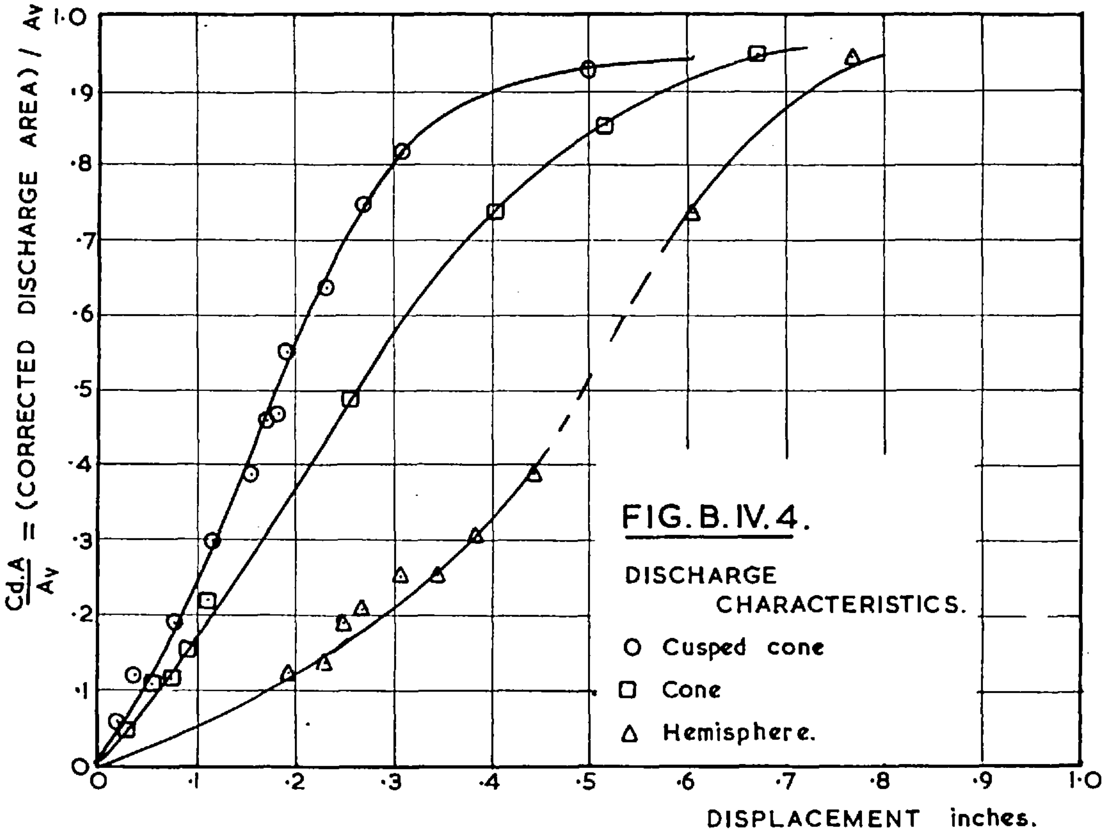
$\frac{Cd.A}{Av}$ = (CORRECTED DISCHARGE AREA) / Av
DISPLACEMENT inches.
DISCHARGE CHARACTERISTICS.
O Cusped cone
□ Cone
Δ Hemisphere.
O
·1
·2
·3
·4
·5
·6
·7
·8
·9
1·0

FIG. B. IV. 4.

B.IV.2 Discussion

(i) Discharge rates past the flat plate.

These results are used later in this Chapter to determine the performance of the valve. However, some comment on the mechanism of discharge is required here.

The difference between the minimum area curve and the corrected area curve, a measure of the efficiency of the valve, is almost entirely due to the change in direction forced on the gas by the shape of the valve. This effect is similar to that for the sharp edged orifice and the deviation from maximum flow will depend upon the abruptness of the change in direction

The discharge of gas past the flat plate occurs in two phases. In the first phase, when the distance between the plate and the vent is small, the momentum of the gas impinging on the plate is negligible. The gas discharges through the cylindrical space as if through an orifice of equivalent area. This process continues until the displacement of the plate is about 0·2 D when the area between the plate and the vent tends towards the maximum area. The Riemann wave forms across the jet and the discharge rate remains nearly constant as the plate is moved away from the vent. Finally, the discharge rate equals that

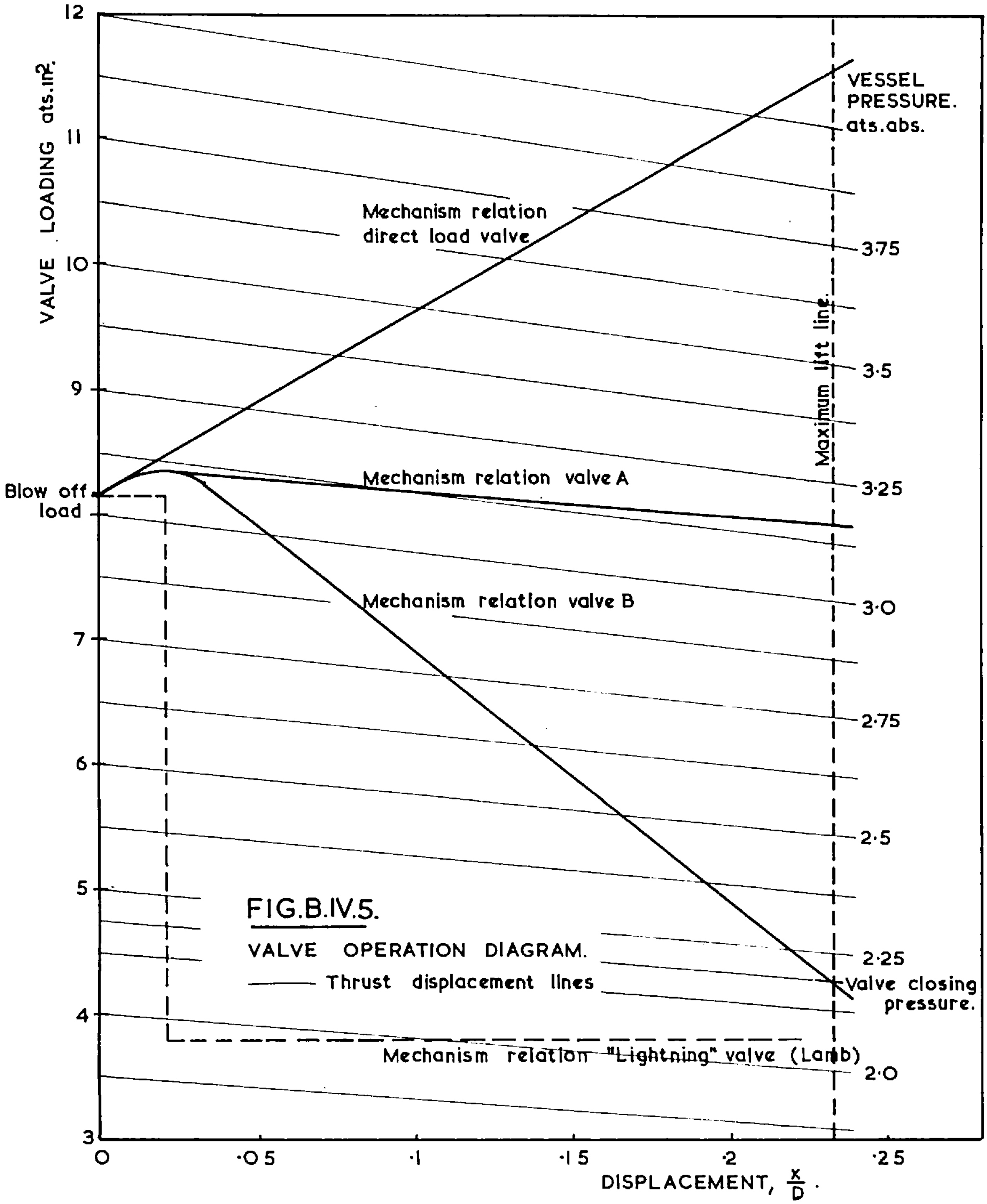

FIG.B.IV.5.

VALVE OPERATION DIAGRAM.

of an unobstructed vent when the displacement is about 0·4 diameters. This change in flow mechanism has already been noted in Chapter B.III. and the discharge characteristic confirms that a transition occurs when the plate is a distance of 0·2 diameters from the vent. It is not clear whether the change is sudden or gradual and a more detailed investigation at the transition point is required.

(ii) Comparison between the direct and link loaded flat plate valves.

(a) The force displacement relation for direct and link loaded systems has been considered in Chapter B.II and the 'mechanism relations' for two such systems are shown in Fig. B.IV.5. Both have the same blow off load, F_{go}, and are represented by

$$\left.\begin{aligned} F_g &= m\left(\frac{x}{D}\right) + F_{go} \\ \text{and} \quad F_g &= \text{function}\left(\frac{x}{D}\right) \end{aligned}\right\} \qquad \text{B.IV.2}$$

respectively.

(b) The thrust exerted by the discharging gas is a linear function of the pressure in the reservoir and has been obtained experimentally in Chapter B.III as

$$\frac{F_g}{A_v} = K.\ P_{og} - (1 - K) \qquad \text{B.IV.3}$$

where P_{og} is the gauge pressure in atmospheres and K is a constant for a given displacement x. If the straight line

$$K = 1 - \frac{x}{D} ,$$

shown in Fig. B.III.7, is taken to represent the experimentally determined curve, equation B.IV.3 can be rewritten

$$\frac{F_g}{A_v} = - P_o \left(\frac{x}{D}\right) + (P_o - 1) \qquad \text{B.IV.4}$$

where P_o is the absolute pressure in atmospheres.
This is the equation of a series of lines on the force-displacement diagram of gradient $- P_o A_v$ and intercept $(P_o - 1) A_v$.

If these lines are plotted in Fig. B.IV.5 each line represents all the possible positions the valve head can take up for a given vessel pressure. For a particular system of restraining forces this position is further limited by the 'mechanism relation' and the equilibrium position of the valve head will be given by the intersection of the two curves.

(c) The pressure in the reservoir is a function of its capacity, the discharge rate through the valve and the blow off pressure, P_{oo}. Using equation A.III.1 for adiabatic expansion in the vessel, the rate of pressure fall is

$$- \frac{dP_o}{d_t} = \gamma . B . \frac{CdA}{V} . P_{oo} . a_{oo} . \left(\frac{P_o}{P_{oo}}\right)^{\frac{3\gamma - 1}{2\gamma}} \qquad \text{B.IV.5}$$

where P_{oo} is the pressure at $t = 0$,

a_{oo} is the velocity of sound in the gas in the reservoir at $t = 0$,

$$B = \left(\frac{2}{\gamma + 1}\right)^{\frac{\gamma + 1}{2(\gamma - 1)}},$$

V = the volume of the vessel and

CdA = the corrected discharge area and a function of the displacement, x.

This function has been obtained experimentally, earlier in this Chapter and can be approximated by

$$\frac{Cd.A.}{A_v} = 2 \cdot 5 \left(\frac{x}{D}\right) \qquad \text{B.IV.6}$$

where A_v = unobstructed area.

Substituting this in equation B.IV.5,

$$\frac{dP_o}{d_t} = M(P_o)^{\frac{3\gamma - 1}{2\gamma}} \cdot \left(\frac{x}{D}\right) \qquad \text{B.IV.7}$$

where $M = 2 \cdot 5. \gamma . B. \frac{A_v}{V} . a_{oo} . \left(\frac{1}{P_{oo}}\right)^{\frac{\gamma - 1}{2\gamma}}$.

(d) The valve performance is obtained by the simultaneous solution of the equations B.IV. 2, 4 and 7. For the direct loaded valve, which has an explicit 'mechanism relation', a differential equation is obtained which can be solved graphically

$$-\frac{dP_o}{d_t} = M. \left[\frac{P_o - (1 + \frac{F_{go}}{A_v})}{P_o + \frac{m}{A_v}}\right] . P_o^{\frac{3\gamma - 1}{2\gamma}} \qquad \text{B.IV.8}$$

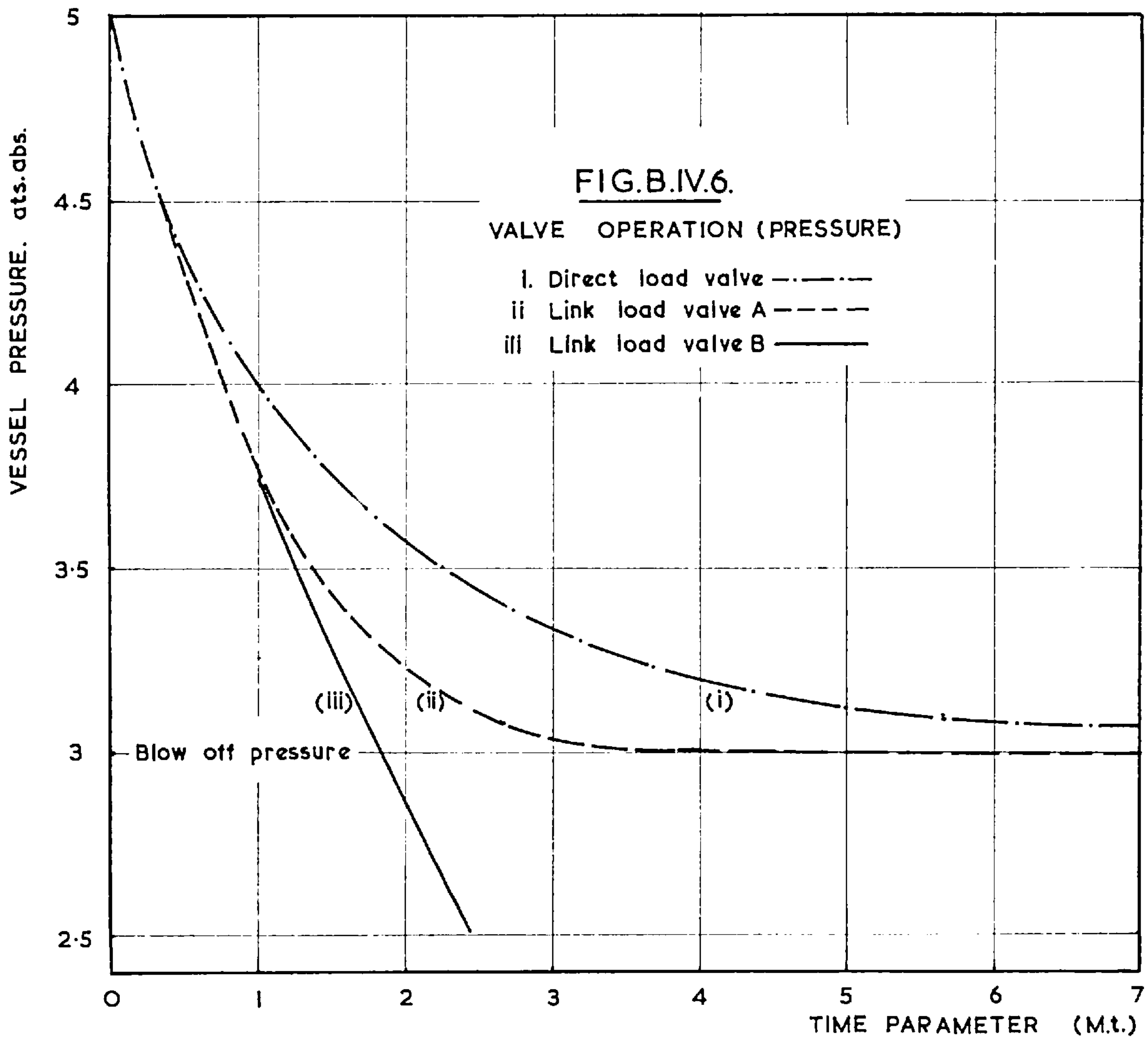
FIG.B.IV.6.
VALVE OPERATION (PRESSURE)
I. Direct load valve
ii Link load valve A
iii Link load valve B
VESSEL PRESSURE. ats.abs.
5
4.5
4
3·5
3
2·5
Blow off pressure
(iii)
(ii)
(i)
0
1
2
3
4
5
6
7
TIME PARAMETER (M.t.)

where: m and F_{go} are fixed by the strength of the spring loading; and M depends upon the vessel and valve sizes and the initial conditions at the blow off pressure.

If $m = 13{\cdot}60$ ats.in^2,

$F_{go} = 8{\cdot}16$ ats.in^2 and

$A_v = 4{\cdot}0$ in^2

equation B.IV.8 becomes

$$-\frac{dP_o}{d_t} = M \left(\frac{P_o - 3{\cdot}04}{P_o + 3{\cdot}40} \right) P_o^{1{\cdot}143}$$

whence

$$Mt = -\int_{P_{oo}}^{P_o} \frac{(P_o + 3{\cdot}40)\ dP_o}{(P_o - 3{\cdot}04)\ P_o^{1{\cdot}143}} \quad .$$

The solution of this equation gives the variation of reservoir pressure with time as shown in Fig. B.IV.6 and by combining equations B.IV.2 and B.IV.3

$$\frac{x}{D} = \frac{P_o - 3{\cdot}04}{P_o + 3{\cdot}4}$$

determines the valve head displacement, shown as a function of time in Fig. B.IV.7. It should be noted that as the pressure tends towards the blow off pressure the valve closes and theoretically it would require an infinite time before the valve closed completely.

For the link load valve a graphical 'mechanism relation' has to be used and the differential equation solved by the finite

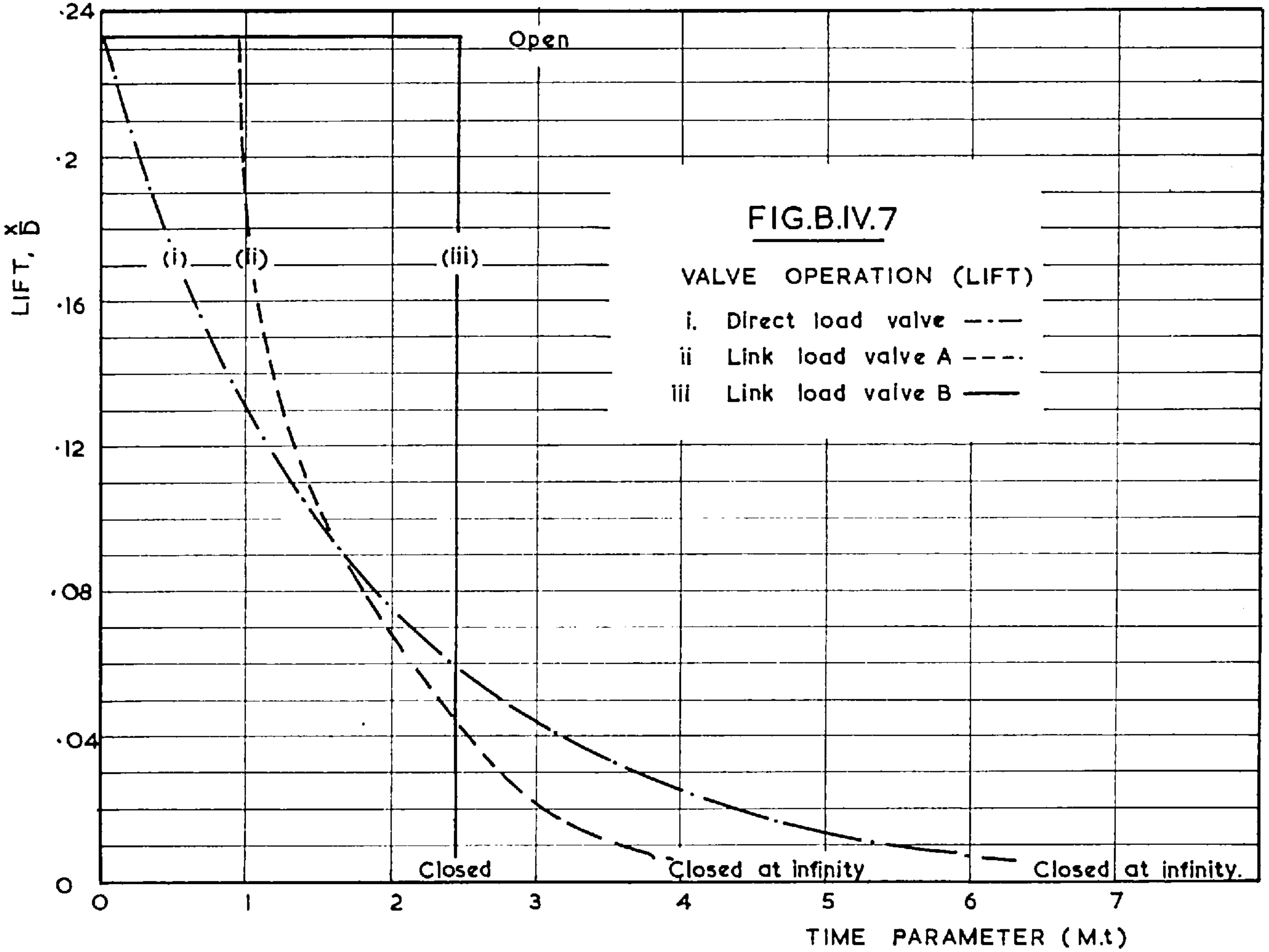

·24
·2
·16
·12
·08
·04
0
LIFT, $\frac{x}{D}$
0
1
2
3
4
5
6
7
TIME PARAMETER (M.t)
Open
(i)
(ii)
(iii)
Closed
Closed at infinity
Closed at infinity.
VALVE OPERATION (LIFT)
i. Direct load valve
ii Link load valve A
iii Link load valve B

FIG.B.IV.7

difference method. Equation B.IV.7 can be written

$$M. \delta t = \frac{\delta P_o}{(P_o)^{\frac{3\gamma - 1}{2\gamma}} . (\frac{x}{D})}$$

and, if sufficiently small intervals of pressure are used in a step by step solution of this equation with equations B.IV 2 and 4, a solution can be obtained graphically. However, in most cases this solution is not required and an examination of the mechanism relation and equation B.IV.4 drawn on the same diagram of F_g against $(\frac{x}{D})$ will determine the function of the valve. Consider the two valve mechanisms shown in Fig. B.IV.5 each with the same blow off load and the same maximum load but differing in the rate of fall in load beyond the maximum.

In the first, the slope of the 'tail' of the mechanism relation is less than the slope of the thrust relation given by equation B.IV.4. As the pressure in the vessel falls the valve slowly closes according to the magnitude of the gradient. Hence, the valve is discharging at less than full lift for a considerable time.

If the slope of the 'tail' is greater than that of the thrust relation the valve will remain at maximum lift until the pressure in the vessel falls to such a level that the thrust line intersects the mechanism curve at the maximum lift position and the valve then closes instantaneously. Thus, the valve will remain fully open until the pressure is less than the blow off pressure.

In both these cases the solution has been obtained graphically and the pressure-time and valve-lift-time relations are plotted in Figs. B.IV. 6 and 7 respectively. F_{go} and A_V have the same values (of 8·16 ats.in^2 and 4·0 in^2) as the direct loaded valve and it is assumed that the maximum lift is 0·233 D. This is not the full lift position for the valve but makes possible a comparison with the direct loaded valve which, for m = 13·60 and a pressure of 5 ats.g. in the vessel, can only rise this far.

These results clearly show that the second type of valve is the most efficient. It remains fully open throughout the discharge and closes instantaneously once the pressure is well below the blow off value. Hence, the design requirements for a link loaded mechanism are that the slope of the mechanism relation must be negative towards full lift and the magnitude of this slope must be greater than that of the thrust-distance line for the particular shape of valve head.

(e) Dynamic loading.

When the valve operates under dynamic conditions the inertia of the valve has to be taken into consideration. The equation of motion is that described in the introduction:

$$\phi\,(P,T).f(X_i) \;-\; R(X_i) \;=\; \sum_j \left(\frac{\partial^2 X_i}{\partial t^2}\right)_j .\; w_j$$

where

$\phi\,(P,T).\; f(X_i)$ is the force exerted by the fluid on the valve head,

$R(X_i)$ is the restraining force exerted by the loading system and

$\left(\dfrac{\partial^2 X_i}{\partial t^2}\right)_j$ is the acceleration of the j.th element of mass w_j ,

all these values being determined in the i.th direction, at a value configuration determined by X_i and at the time t.

The equations derived in Chapter B.IV can be used to solve these equations of motion and, since the motion of the valve is along the axis of the valve, a single equation is obtained in which:

$\phi(P,T)$ is represented by the first half of equation B.IV.4 which relates the thrust to the conditions behind the valve for a given displacement of the valve head and

$f(X_i)$ is represented by the second half which relates the thrust to the displacement so that

$$\phi(P,T)\; f\;(X_i) \;=\; -\,P_o\, A_V\, \left(\frac{x}{D}\right) \;+\; (P_o - 1)\, A_V$$

is the thrust exerted by the expanding air.

The term $R(X_i)$ is represented by the mechanism relation and for most loading systems can be written

$$R(X_i) = m\left(\frac{x}{D}\right) + F_{go}$$

where m is the slope of the line and is positive for the direct loaded valve, negative for the link loaded valve and zero for the compressed air valve (with the additional stipulation, in the third case, that F_{go} has some value determining the closing load and less than the blow off load.)

The term $\sum_j \left(\frac{\partial^2 X_i}{\partial t^2}\right)_j w_j$ can be simplified by assuming

that most of the moving mass resides in the valve head and spindle and the inertia terms corresponding to the links, springs and other moving parts can be included as an increased mass at the valve head.

$$\therefore \sum_j \left(\frac{\partial^2 X_i}{\partial t^2}\right)_j . w_j = (w + \Delta w) \frac{\partial^2 X}{\partial t^2}$$

where w = mass of valve head and spindle

and Δw = the correction for other moving parts.

Hence, the equation of motion is:

$$P_o A_v \left(\frac{x}{D}\right) + (P_o - 1) A_v - m\left(\frac{x}{D}\right) - F_{go}$$

$$= (w + \Delta w) \frac{\partial^2 X}{\partial t^2}$$

Rearranging and substituting the following dimensionless terms for displacement and time, a second order linear differential equation is obtained

$$\frac{\partial^2 X}{\partial \tau^2} + \left(\frac{P_o(\tau)}{P_{oo}} + \frac{m}{P_{oo} A_v} \right) . X = \frac{P_o}{P_{oo}} - 1$$

where $X = \frac{x}{D}$,

$$\tau = \sqrt{\frac{P_{oo} A_v}{(w + \Delta w) D}}$$

A solution of the equation requires the knowledge of the pressure function $P_o(\tau)$ and this will have to be specified arbitrarily. By assuming a step pressure function the maximum response time can be ascertained and compared with that for a bursting disc. It is also necessary to assume that the pressure is maintained at a constant level during the venting of the gas.

i.e. $P_o(\tau) < P_{oo}$ at $\tau = 0$

$P_o(\tau) = n.P_{oo}$ at $\tau > 0$

$$\therefore \frac{d^2 X}{d \tau^2} + \left(n + \frac{m}{P_{oo} A_v}\right) X = n - 1$$

which has the solution

$$X = \frac{A}{B^2} \left[1 - \cos B \tau \right]$$

where $A = n - 1$ and

$$B = n + \frac{m}{P_{oo} . A_v}$$

for the boundary conditions

$X = 0$ at $\tau = 0$

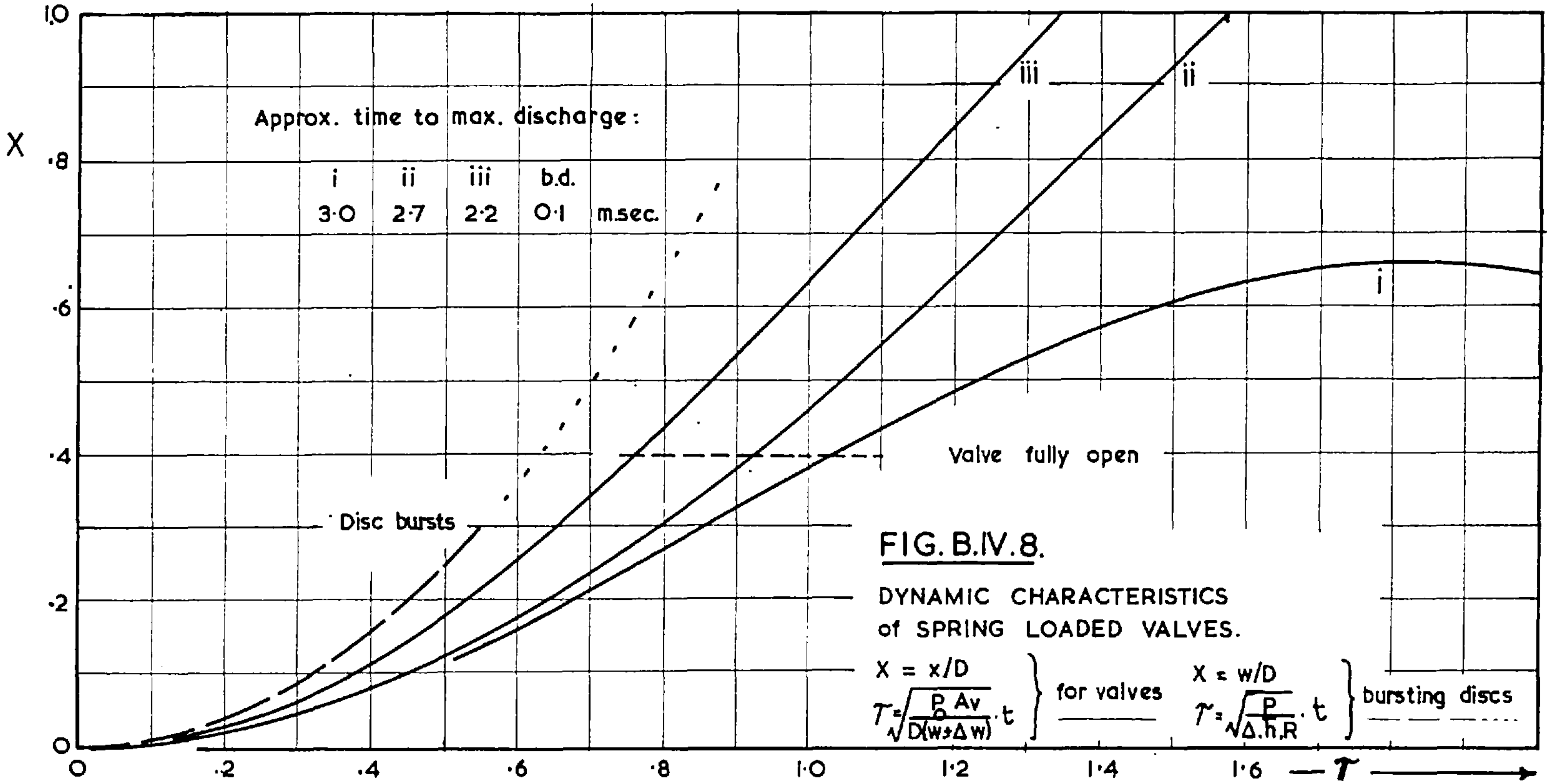

FIG. B.IV.8.

DYNAMIC CHARACTERISTICS of SPRING LOADED VALVES.

$X = x/D$, $\tau = \sqrt{\dfrac{P_o A_v}{D(w+\Delta w)}} \cdot t$ } for valves ———

$X = w/D$, $\tau = \sqrt{\dfrac{P}{\Delta . h . R}} \cdot t$ } bursting discs - - - - - -

$\frac{dX}{d\tau} = 0$ at $\tau = 0$

That is, initially the valve is stationary and closed.

A numerical solution has been obtained for the valves described below and the result is shown in Fig. B.IV.8.

(i) A direct-spring-loaded valve with a dimensionless mechanism slope and loaded to twice the blow off pressure.

$$\frac{m}{p_o A_v} = 1 \cdot 0 \quad \text{and} \quad n = 2 \quad \text{so that} \quad A = 1, \quad B = 3.$$

(ii) A link-loaded valve

$$\frac{m}{p_o A_v} = -1 \cdot 0, \quad n = 2 \quad \text{so that} \quad A = 1, \quad B = 1.$$

(iii) A compressed-air-loaded valve

$$\frac{m}{p_o A_v} = 0, \quad n = 2, \quad F_{go} = \tfrac{1}{2} \quad \text{so that} \quad A = \frac{3}{2}, \quad B = 2.$$

A comparison is made with the equivalent bursting disc and absolute values have been calculated for valves having a blow off pressure (bursting pressure for the disc) of 85 p.s.i.g; a diameter of 4" and a reasonable thickness of valve head of ½"

These calculations take no account of the reduced thrust caused by the rapid movement of the valve head and an analysis similar to that carried out by Goldsworthy (1953) would be required. However, the small differences obtained taking this into account do not warrant the lengthy procedure and can usually be neglected.

CHAPTER B.V. CONCLUSIONS

The conventional spring loaded valve suffers from two main disadvantages:

(a) Loading requirements necessary for good valve seating are detremental to rapid relief. That is, the springs have to be extremely strong and large pressures in excess of the operating pressures must be applied before the valve opens appreciable. This means that the valve only operates efficiently well above the blow off pressure.

(b) The valves suffer from what is known as chatter. The valve opens and discharges just sufficient of the vessel contents to allow the valve to close and this is followed by an increase in pressure necessitating the reopening of the valve.

The first of these features can be discussed with reference to the valve operation diagram in Fig. B.IV.5. In order to produce good seating properties the slope of the mechanism relation has to be large and in order to obtain a large displacement intersection (large discharge area) a thrust-displacement-line associated with a high vessel pressure must be chosen. For example, an excess vessel pressure of 30% is required to open the direct loaded valve, whose mechanism relation is shown in Fig. B.IV.5, to an extent of $\frac{x}{D} = 0{\cdot}2$.

It can be seen from this that an obvious improvement is available. A valve can be made which has a mechanism relation with a negative slope when the valve is open but has the required applied-force-displacement for good seating when the valve is closed. Then the pressure for maximum lift need be only slightly in excess, or even less than, the blow off pressure. Thus valve A (Fig. B.IV.5) requires only 4% excess pressure for full lift. Further, if the valve has a mechanism relation having a slope greater than that of the thrust-displacement lines (as shown for valve B), it will remain open at a pressure considerably lower than the blow off pressure and yet maintain good seating.

This type of valve also overcomes the problem of chatter. The pressure in the vessel falls considerably below the blow off level before the valve closes so that the pressure will take some time to rise before the valve is required to open again.

An improvement on this last valve is obtained when the mechanism relation is discontinuous. When the valve is closed the applied force must equal the blow off load but as soon as the head has lifted some small distance the applied force falls immediately to a level just sufficient to close the valve when discharge ceases (as shown in Fig. B.IV.5). Such a valve is described by Lamb (1952) and is actuated by compressed air. When the valve is closed the compressed air acts on a large area but the action of the valve opening diverts the air so that the pressure is applied to a smaller area. (The valve also incorporates flame quenching devices but those are not relevent in the present context).

The valve operation diagram has been obtained from the experimental investigation into the thrust exerted on, and the discharge rate past, obstructions in a vent. The relations have been simplified by using linear plots whereas the thrust-displacement-curves would not in practice be straight lines. This does not invalidate the qualitative results discussed above but will effect the calculated performance and the true curves should be used. This leads to the interesting point introduced by the sudden change in thrust at a displacement of about $\frac{x}{D} = 0{\cdot}2$. This increase in pressure, as the valve opens in this range, appears to represent the condition when the valve head "jumps" the Riemann wave but, since neither its magnitude nor its exact function are known, no predictions can be made.

Quantitative assessment of valve performance is limited to the flat plate and can be divided into three parts.

(a) The most efficient valve is obtained if the mechanism relation has a slope greater than that of the thrust-displacement lines.

$$\text{i.e.,} \quad - \frac{d\,F_g}{d(\frac{x}{D})} > - P_o A_v$$

where F_g is the thrust on the plate,
x is the displacement,
D is the diameter of the vent,
P_o is the operation pressure and
A_v is the area of the vent.

Under these conditions the valve will fully open once the blow off pressure, P_o, has been exceeded and then will close when the pressure falls below the valve closing pressure.

(b) The operation of the valve under equilibrium conditions (c.f. page 43) can be determined from the following equations:

$$F_g = \text{function } \left(\frac{x}{D}\right), \qquad \text{B.IV.2.}$$

the mechanism relation:

$$\frac{F_g}{A_v} = K.P_{og}. - (1 - K) \qquad \text{B.IV.4}$$

where $K = \text{function } \left(\frac{x}{D}\right)$

and is determined experimentally and given in Fig. B.III.7 and 8; and

$$-\frac{d\,P_o}{dt} = \gamma\, B\, \frac{Cd\, A}{V} \cdot P_{oo} \cdot a_{oo} \cdot \left(\frac{P_o}{P_{oo}}\right)^{\frac{3\gamma - 1}{2\gamma}} \qquad \text{B.IV.5}$$

where $Cd\, A = \text{function } \left(\frac{x}{D}\right)$

and obtained experimentally (given in Figs. B.IV.3 and 4)

F_g = Force on the obstruction as produced by the loading,

x = the displacement,

P_{og} = gauge pressure in the vessel,

P_o = absolute pressure in the vessel,

P_{oo} = absolute pressure in the vessel when the valve first opens

a_{oo} = the speed of sound in the vessel when the valve opens,

$B = \left(\frac{2}{\gamma + 1}\right)^{\frac{\gamma + 1}{2(\gamma - 1)}}$,

γ = the ratio of specific heats,

D = the diameter of the valve,

A_v = the area of the vent and

V = the volume of the vessel.

The simultaneous solution of these three equations by analytical or graphical methods determines the valve performance. In the case considered under (a) in which the valve opens instantaneously to its full lift position, equations B.IV.2 and B.IV.4 are redundent and equation B.IV.5 with Cd A a constant at its maximum value determines the pressure in the vessel.

(c) The operation of the valve under dynamic conditions.

Fig. B.IV.8 shows the performance of the three types of valve and it can be seen that the response time improves, but only slightly. Comparison with bursting disc valves, however, indicates the poor dynamic qualities of such valves and the orders of magnitude given in B.IV.2 express a 20 fold increase in response time.

SECTION C THE SIZE, POSITION AND RATE OF OPENING OF VALVES AS RELATED TO THE RELIEF OF EXPLOSIONS

CHAPTER C.I INTRODUCTION

The performance of valves has been discussed in the previous sections and the rates of discharge of gases through two types of valve obtained. Some comments have been made on the mechanism of discharge and the rate of pressure fall in a vessel, and equations have been derived to calculate the pressure and temperature changes under these conditions. Hence, for pressure release from vessels in which only small increases in pressure are expected the venting area can be specified by:

(i) the equation for the discharge area, Cd.A., of the particular valve;

(ii) the adiabatic expansion equation corresponding to equation A.III.9a; and

(iii) the expected rate of pressure increase in the vessel which has to be relieved.

These relations can be written:

valve size = function of Cd.A;

$$Cd\ A = \frac{\gamma V}{a_o\ B}\ \frac{1}{P}\ \frac{dP}{dt} \qquad \text{C.I.1.}$$

and $\frac{dP}{dt}$ = rate of pressure rise.

That is, equation C.I.1. gives the discharge area as a function of the operating pressure and the volume of the vessel. (The term operating pressure has been introduced in this section to include both the bursting pressure for bursting disc valves and the blow off pressure of spring loaded valves.)

In this section, the discharge areas required to protect vessels subjected to explosive pressure rises will be determined theoretically. It will be shown that, using a comparatively simple analysis, the discharge area required to maintain the pressure in the vessel below a certain value is a function of that pressure and the position of the valve. Using these results a method has been developed to determine the minimum discharge area required for constant pressure venting for any explosive system. The theoretical predictions have been tested by the application of experimental data derived from the literature and in most cases there is a close agreement between theory and practice.

However, pressure fluctuations during combustion and during pressure relief have been noted by a number of workers. Since these cannot be accounted for by the simple theory an extension, based on techniques developed for non-combustive discharge from vessels, is suggested. To indicate the complexities of the problem an analogue has been constructed to depict the variation in pressure under non-combustive discharge conditions.

Although the analogue has not materially assisted in the solution of the problem, it may be of interest in other fields and it has therefore been described in detail.

Before introducing the problem and deriving the equations, the assumptions made throughout the analyses will be listed.

(i) No appreciable heat transfer within the gas or to the walls of the vessel. The conduction of heat through the gas is small and, since turbulent mixing is not considered, the temperature rise is mainly due to the heat evolved in combustion and the compression of the gas.

(ii) The movement of the gas is caused by the expansion of the burnt gases and the venting during pressure relief only. All random turbulence before and during combustion is neglected.

(iii) Except for the combustion, all processes are assumed to be adiabatic. viz; the compression of the burnt and unburnt gases; the expansion of the contents of the vessel when venting occurs; and the discharge through the vent.

(iv) The combustion occurs at constant pressure for each element and the flame, or combustion zone, is considered to be of infinitesimal thickness. This means that the combustion zone is a temperature discontinuity dividing the burnt and unburnt gases but on either side of which both particle velocity and pressure are the same.

(v) Finally, it is assumed that the gas is inviscid and that the pressure, temperature and density of the gas are related by the equation of state

$$P\,dV = dw\,\frac{1}{m}\mathcal{R}\,T \qquad \text{C.I.2.}$$

where

P = the absolute pressure,

T = the absolute temperature,

dw = the mass of the element,

dV = the volume of the element,

m = the molecular weight of the gas and

$\mathcal{R}$ = the universal gas constant.

CHAPTER C.II THE SIMPLE THEORY

C.II.1 Introduction

Consider a gas element of mass dw and volume dV in a vessel of volume V. Initially the element is at an absolute pressure P_i and an absolute temperature T_i and has a density and molecular weight ρ_i and m_i. The gas in the vessel ignites at a centre a distance x from the element and a combustion zone, or flame, spreads through the gas at a velocity S depending on the pressure and temperature and the combustible gases under consideration. The heat evolved in this process induces a change in pressure, which causes the temperature of the element to rise to T_u according to the adiabatic relation

$$P_u^{\frac{1}{\gamma}} \cdot \epsilon_u = P_i^{\frac{1}{\gamma}} \cdot \epsilon_i = F_u \qquad \text{C.II.1a}$$

and the equation of state $P.dV = dw.\frac{1}{m}.RT$.

Here, subscript u relates to conditions in the unburnt gas at a time t after ignition and ϵ is the volume occupied by one molecule of the gas and given by

$$\epsilon = \frac{m}{\rho}. \qquad \text{C.II.1b.}$$

P_i and ϵ_i are the same for all elements and F_u will be a constant for all the elements of unburnt gas.

When the flame reaches it, the element burns at constant pressure and its temperature instantaneously rises to T_b. Since it has undergone a chemical change, the molecular weight also changes to that of the products, m_e. The temperature rise, $(T_b - T_u)$, will depend upon the properties of the gas and the heat released on combustion so that the temperature of the gas immediately after burning will depend upon the temperature just before burning. Since, each element is burnt at a different temperature level, the "initial" conditions in the burned state, as represented by T_b, will vary from element to element.

The burnt element is compressed adiabatically from the temperature T_b to the temperature T_{bp} as given implicitly by

$$P_{bp}^{\frac{1}{\gamma}} \cdot \epsilon_{bp} = P_b^{\frac{1}{\gamma}} \cdot \epsilon_b = F_b \qquad \text{C.II.3}$$

where the subscript b refers to conditions just after burning and the subscript bp to conditions in the burnt element at a pressure P. Hence, the temperatures of individual elements of burnt gas will vary and the term F_b will only be a constant for each element and will depend on the conditions in the element immediately after burning. This process continues until the flame reaches the walls of the vessel and all the reactants have been burnt.

The mass of any element of gas can be determined from either of equations C.II.1 or 2 and the equation of state, C.I.2. By summing these elements over the volume of the vessel the total mass of gas can be calculated. This summation represents the continuity of the medium and expresses the conservation of mass.

$$\text{i.e.} \quad \int^{V} dw = \text{constant} \qquad \text{C.II.3}$$

The energy contained in each element of gas as it undergoes an adiabatic pressure change is

$$dE = \frac{Cv.T}{m} \cdot dw \qquad \text{C.II.4.}$$

where Cv is the heat capacity at constant volume and is equal to $\frac{R}{\gamma - 1}$

where γ = ratio of specific heats.

The total energy in the system is the sum of all the elements of energy given by equation C.II.4.

$$\text{i.e.} \quad \text{Total energy} = \int^{V} dE \qquad \text{C.II.5}$$

The sum of the heat evolved in the reaction and the initial energy of the system is:

$$\int_{0}^{w_b} \Delta H_i \, dw + \frac{Cv.\ T_i}{m_i} \quad w_i \qquad \text{C.II.6}$$

where ΔH_i is the heat of reaction per unit mass of burnt gas,

w_b is the mass of burnt gas and

w_i is the initial mass of gas.

Since the equation of conservation of energy states that, at any instant of time, the energy in both the burnt and unburnt gases is equal to the initial energy in the combustibles plus the energy made available by the reaction of the quantity of gas burnt in this time;

$$\int^{V} dE = \int_{0}^{w_b} \Delta H_i \, dw. + \frac{C_v . T_i}{m_i} \cdot w_i \qquad \text{C.II.7}$$

These equations represent a thermodynamic examination of the combustion of gases in closed vessels and, although they express the state of the gas as a function of the position of the combustion zone, contain no reference to the time rates of change of properties. To introduce a time scale, the chemical kinetics of the explosive system must be considered and the rate of combustion expressed as a function of temperature and pressure. By assuming that the temperature and pressure are related by an adiabatic law the burning rate can be written as a function of pressure alone. It has been found convenient to express the burning rate per unit flame area as being proportional to the pressure raised to some power.

$$\text{i.e.} \quad \frac{1}{A_f} \cdot \frac{dwb}{dt} = K.\ P^{\beta}$$

where A_f = area of the flame at time t and

K and β are constants for the system under consideration. This relation has been tested for a number of systems and found to give a reasonable approximation. The extent of agreement is shown for the particular example of a 3% pentane air mexture in Fig. C.II.3.

Equations C.II. 3, 7 and 8 cannot be solved without the knowledge of the pressure variation from element to element. Since pressure disturbances are transmitted at a finite velocity, the pressure will vary across the vessel if the ratio of flame velocity to the speed of sound is appreciable. In the simple theory this variation in pressure is neglected and it is assumed that, at any instant of time, the pressure is constant throughout the vessel. Hence, the equations derived above are sufficient for the complete solution of this problem.

A more exact solution requires an equation of motion based on the principle of conservation of momentum in which the pressure is related to the velocity of the gaseous elements. This leads to a problem of the Lagrangian type and a solution is obtained by an analysis of the formation and movement of pressure waves within the vessel; examined in Chapter C.IV.

If pressure relief is applied to the vessel at a certain time, t_o, the mass and energy of gas vented from the vessel must be included in the two balances. In a time dt, the mass vented, dw_v, is given by equation A.III.4 as

$$dw_v = Cd.A \sqrt{P \rho \gamma \left(\frac{2}{\gamma + 1}\right)^{\frac{\gamma + 1}{\gamma - 1}}} \cdot dt \qquad \text{C.II.9}$$

where Cd.A is the discharge area of the relief valve.

Therefore

$$w_v = (\gamma B)^{\frac{1}{2}} \int_{t_o}^{t} Cd.A \ (P \rho)^{\frac{1}{2}} \cdot dt \qquad \text{C.II.10}$$

$$\text{where} \quad B = \left(\frac{2}{\gamma + 1}\right)^{\frac{\gamma + 1}{\gamma - 1}} .$$

Since the gas discharged may be reactants or combustion products, the pressure and density terms can bear the subscript u or b and the corresponding mass terms will be w_{vu} and w_{vb} respectively.

The term

$$Ev = (\gamma B)^{\frac{1}{2}} \frac{Cv}{m} \int_{t_o}^{t} Cd.A \ (P \rho)^{\frac{1}{2}} \cdot T. \ dt. \qquad \text{C.II.11}$$

the energy in the vented gases, is introduced in equation C.II.7 and, again, may represent burnt or unburnt gases.

Before solving these equations, the boundary conditions must be stipulated. Two problems are examined so that the solution can be applied to any shape of vessel. The first configuration covers approximately cubic vessels and the second deals with elongated vessels having a large aspect ratio $\left(\frac{\text{major length}}{\text{minor length}}\right)$.

(i) In spherical combustion the flame expands as a spherical shell from a point of ignition at the centre of the vessel until it reaches the walls when it is completely extinguished. When the vent opens the flame will be distorted but it is assumed that this effect is equivalent to the increased expansion of the burning spherical shell which would be caused by an equal venting area evenly distributed over the entire surface of the vessel.

(ii) In one-dimensional plane combustion a flat flame travels along the length of the vessel and is considered to commence as a plane flame extending across the smaller section. Ignition can occur at any plane and the discharge area is evenly distributed over either or both ends but not along the length of the vessel. This particular form of the problem can be adapted to incorporate the effects of non-planar flames and the central venting of long ducts. These extensions of the theory are not dealt with in deriving the equations but are included in the analysis of two problems in the next chapter.

To summarise, the combustion wave moves through the unburnt gas and raises the temperature of the burnt gas during the process of combustion. Heat is not transmitted in significant quantities through the gas but the increase in temperature and change of volume of the burnt gas cause a rise in pressure accompanied by adiabatic heating of the gas in the vessel. Thus every element of gas has its temperature raised in three operations: initially in its unburnt condition by adiabatic compression due to burning of elements of gas nearer the ignition centre; then in combustion; and finally in its burnt condition by adiabatic compression due to the burning of elements of gas further away from the ignition centre. As the combustion wave progresses through the gas, the pressure (as measured by a gauge) rises evenly throughout the vessel but the temperature of each element of gas increases at a rate depending upon the past history of the element and its state immediately after combustion. A thermodynamic examination of the combustion is carried out and mass and energy balances obtained. An assumption of a power law for the variation of flame velocity with pressure is introduced and, by solving these three equations, the state of the system at any instant of time is determined.

Before ignition the combustible gas is at its initial state signified by the subscript i. After ignition the burned gas occupies a core surrounded by the unburned gas which has been compressed to the temperature T_u. Each element burns from T_u to a temperature T_b, due to combustion, and is then compressed adiabatically to temperature T_{bp}. All compressions are adiabatic but each element of burnt gas is compressed from a different initial temperature T_b and hence the ' adiabatic function ' varies from element to element in the burnt medium.

This adiabatic function is defined as

$$F = P^{\frac{1}{\gamma}} \epsilon$$

P = pressure in the vessel - constant throughout the vessel,

ϵ = volume occupied by one mole of gas,

m = molecular weight (average molecular weight of a mixture),

w = mass of gas and the subscripts e and f represent conditions when the combustion is complete and in the combustion zone respectively.

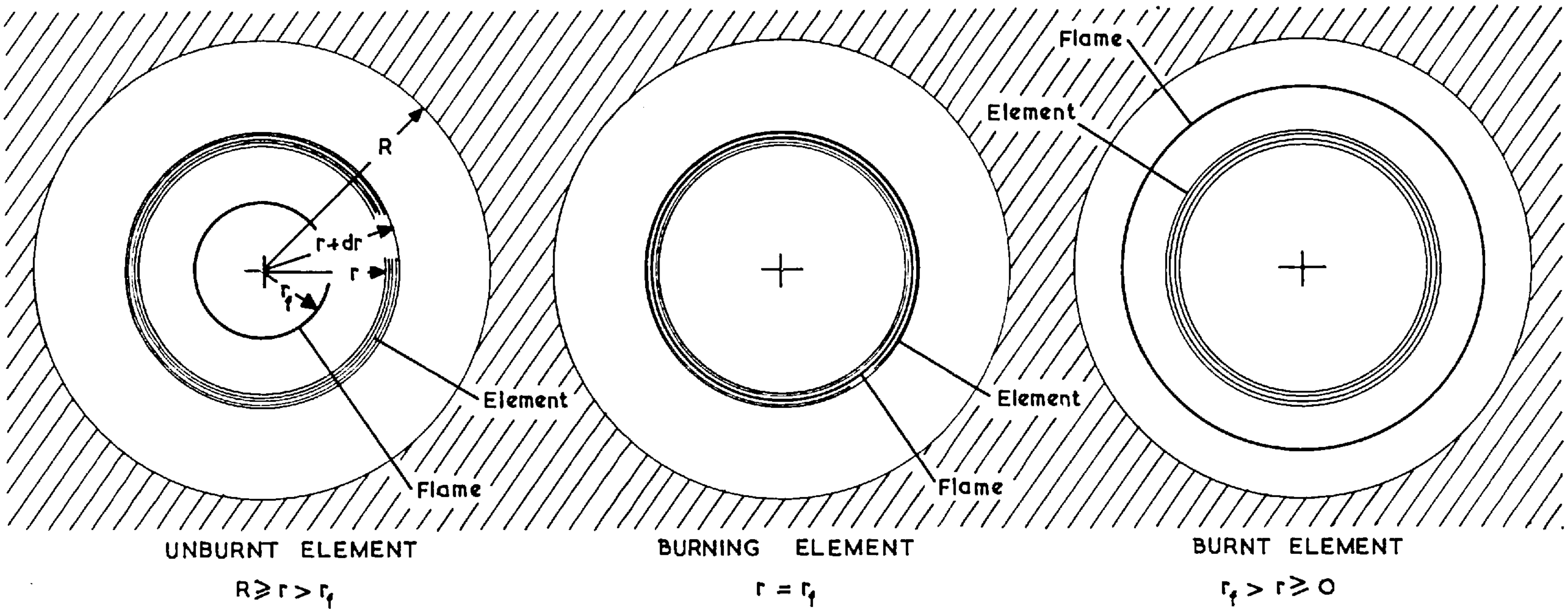

FIG.C.II.1. SPHERICAL COMBUSTION

C.II.2 Spherical combustion.

Before writing the mass and energy balances, it should be noticed that in this case only unburnt gas can be vented during combustion.

The following equations are obtained from the geometry of the element and equations C.I.2, C.II.1a, 1b, 2, 3, 4, 6, 10 and 11.

(i) Mass balance

Mass of unburnt gas

$$= \int_{r_f}^{R} 4\pi \rho_u \, r^2 \, dr$$

$$= \frac{4}{3}\pi (R^3 - r_f^{\,3}) \, m_i \, \frac{P^{\frac{1}{\gamma_u}}}{F_u}$$

where R = radius of vessel and

r_f = radius of the flame.

Mass of unburnt gas vented from time t_o

$$= \frac{(\gamma_u m_i \, B)^{\frac{1}{2}}}{F_u^{\frac{1}{2}}} \int_{t_o}^{t} Cd.A. \, P^{\frac{\gamma_u + 1}{2\gamma_u}} \, dt.$$

Mass of burnt gas

$$= 4\pi \int_{o}^{r_f} \rho_b \, . \, r^2 \, dr$$

$$= 4\pi . \, m_e \, P^{\frac{1}{\gamma_b}} \int_0^{r_f} \frac{r^2}{F_b} \, . \, dr \, .$$

The total of these is a constant and therefore equal to the initial mass, w_i. Summing these terms, equating to w_i and dividing through by

$$w_i = \frac{4}{3} \pi R^3 \frac{m_i P_i}{\mathcal{R} T_i}$$

the first equation is

$$(1 - \eta_f^{\,3}) \, p^{\frac{1}{\gamma_u}} + \frac{C}{V} \int_{t_o}^{t} Cd.A. \; p^{\frac{1+\gamma}{2\gamma}} \, dt$$

$$+ \, 3 \, \frac{m_e}{m_i} \, . \, p^{\frac{1}{\gamma_b}} \int_0^{\eta_f} \frac{\eta^2}{F_p} \, . \, d\eta = 1 \qquad \text{C.II.12}$$

where $\eta = \dfrac{r}{R}$,

$p = \dfrac{P}{P_i}$,

$C = \left[\mathcal{R} \gamma \, T_i \, \dfrac{1}{m_i} \, B \right]^{\frac{1}{2}}$,

V = volume of the vessel,

$F_p = \dfrac{F_b}{F_u}$

Equation C.II.12 is more useful in the form of the two equations

$$1 - n = (1 - \eta_f^3)\, p^{\frac{1}{\gamma_u}} + \frac{C}{V} \int_{t_o}^{t} Cd.A.\; p^{\frac{1+\gamma_u}{2\gamma_u}} .dt$$

C.II.13

and $$n = 3\ \frac{m_e}{m_i}\, p^{\frac{1}{\gamma_b}} \int_o^{\eta_f} \frac{\eta^2}{F_p} \cdot d\eta$$

(where $n = \frac{w_b}{w_i}$ = fraction of gas burnt) representing the masses of unburnt and burnt gases respectively.

(ii) The energy equation is obtained in a similar manner and, by dividing through the equation by the term representing the compression energy in the combustibles,

$$\frac{W_i}{m_i} \cdot T_i \cdot (Cv)_u ,$$

$$\frac{3m_e}{m_i} \cdot b.\ p^{\frac{1}{\gamma_b}} \int_o^{\eta_f} \frac{\eta^2}{F_p} d\eta + 1$$

$$= (1 - \eta_f^3)\left(\frac{\gamma_b - \gamma_u}{\gamma_b - 1}\right) p + \left(\frac{\gamma_u - 1}{\gamma_b - 1}\right) p$$

$$+ \frac{C}{V} \int_{t_o}^{t} Cd.A.\; p^{\frac{3\gamma_u - 1}{2\gamma_u}} .dt.$$ C.II.14

Where $b = \frac{m_i}{m_e} \cdot \frac{\Delta H_i}{T_i\ (Cv)_u}$.

(iii) The rate of combustion has been given in equation C.II.8 as

$$\frac{d\, w_b}{dt} = A_f \, . \, K \, . \, P^{\beta} .$$

Hence, the rate of combustion is zero at ignition when the flame area, A_f, is zero. It is assumed that the power low is valid above a critical flame area A_f^{*} and the rate of combustion can be written

$$\frac{d\, w_b}{dt} = w_i \, \frac{dn}{dt} \qquad (\text{since } w_b = n . w_i)$$

$$= M_i \, \frac{A_f}{A_f^{*}} \, . \, p^{\beta}$$

where $M_i = K \, A_f^{*} \, . \, p_i^{\beta}$

$$= \left(\frac{d\, w_b}{dt} \right)_{initial} .$$

Because $\frac{A_f}{Av} = \left(\frac{r_f}{R} \right)^2 = \eta_f^{\,2}$

where Av = surface area of the vessel,

$$\frac{dn}{dt} = \frac{M_i}{w_i} \, . \, \frac{Av}{A_f^{*}} \, . \, \eta_f^{\,2} \, p^{\beta} \qquad \text{C.II.15.}$$

(iv) Combining equations C.II.13, 14, 15

$$b.n. = \frac{\gamma_b - \gamma_u}{\gamma_b - 1}\left\{1 - n - \frac{A_f^{*}\, C.w_i}{V.\, M_i}\int_{n_o}^{n} \alpha\, p^{\frac{\gamma_{u+1}}{2\gamma_u} - \beta} \cdot \frac{1.d\eta}{\eta_f^2}\right\} p^{1 - \frac{1}{\gamma_u}}$$

$$+ \frac{\gamma_{u} - 1}{\gamma_b - 1} \cdot p - 1$$

$$+ \frac{A_f^{*}\, C\, w_i}{V\, M_i}\int_{n_o}^{n} \alpha\, p^{\frac{3\gamma_u - 1}{2\gamma_u - 1} - \beta}\, \frac{1}{\eta_f^2}\, d\eta \qquad \text{C.II.16}$$

where n_o = fraction gas burnt when the relief valve opens and

$$\alpha = \frac{Cd\ A}{A_v}$$

= fraction of available area for discharge.

This equation is solved for a particular case in which $\gamma_u = \gamma_b$ but an approximate solution is available for any values of γ_u and γ_b if one assumption is made. This assumption is given in Appendix C.1 and the solution leads to the relation

$$\left\{ p^{\frac{1}{\gamma_u}} + (1 - n)\left(\frac{\gamma_b - \gamma_u}{\gamma_u}\right)\right\}\frac{dp}{dn} =$$

$$b.\left(\frac{\gamma_b - 1}{\gamma_u - 1}\right) \cdot p^{\frac{1}{\gamma_u}} + \frac{\gamma_b - \gamma_u}{\gamma_u - 1} - \left(\frac{A_f^{*} . C.w_i}{V\, M_i}\right) p^{\frac{3\gamma_u + 1}{2\gamma_u} - \beta} \cdot \frac{1}{\eta_f^2}\,\alpha$$

$$\text{where } \eta_f^3 = \frac{1 + nb - \frac{\gamma_b - \gamma_u}{\gamma_b - 1} \cdot p - (1 - n)\, p^{1 - \frac{1}{\gamma_u}}}{\frac{\gamma_u - 1}{\gamma_b - 1} \cdot p} .$$

When $\gamma_u = \gamma_b$ the solution is exact and

$$\left.\begin{aligned} \frac{dp}{dn} &= b - \frac{\alpha}{H} \cdot p^{\frac{3\gamma-1}{2\gamma} - \beta} \cdot \frac{1}{\eta_f^2} \\ \text{and} \quad \eta_f^3 &= \frac{1 + bn - (1-n)\ p^{1-\frac{1}{\gamma}}}{p} \end{aligned}\right\} \qquad \text{C.II.17a}$$

where $H = \dfrac{M_i\ V}{A_f^{*} . C. w_i}$.

Equation C.II.17 can be solved by finite difference methods and the variation with time obtained from equation C.II.15 as

$$\frac{dp}{d\tau} = \frac{dp}{dn} \cdot \frac{dn}{d\tau}$$

$$= H \frac{dp}{dn} \cdot \eta_f^2 \cdot p^{\beta} \qquad \text{C.II.17b}$$

where $\tau = \dfrac{C.\ Av.}{V}\ t$, the dimensionless time term.

(v) Up to the valve operation pressure, P_o, the valve is closed and $\alpha = 0$. The first of equations C.II.17 becomes

$$\frac{dp}{dn} = b \qquad \text{C.II.18a}$$

which can be integrated to give

$$p = 1 + bn \qquad \text{C.II.18b}$$

Substituting in the second of the equations it becomes

$$\eta_f^3 = 1 - (1 + \frac{1}{b})\ p^{-1} + \frac{1}{b} \cdot p^{1-\frac{1}{\gamma}} \qquad \text{C.II.19}$$

and equation C.II.17 b remains unaltered as

$$\frac{dp}{d\tau} = H.b.\eta_f^{\,2}\; p^{\beta}.$$

(Vi) After the valve has opened the condition that the pressure no longer rises is the only criterion for safe venting

$$\therefore \quad \frac{dp}{dn} = 0$$

and $\alpha = H.\ b\ .\ p_o^{\;\beta - \frac{3\gamma - 1}{2\gamma}} \cdot \eta_f^{\,2}$

Since combustion will continue after the valve has opened η_f will increase and the valve area will have to increase at an appropriate rate. To ensure that the pressure does not rise, the maximum value of α at $\eta_f = 1$ is used and

$$\alpha_c = H.\ b.\ p_o^{\;\beta - \frac{3\gamma - 1}{2\gamma}} \qquad \text{C.II.20}$$

This equation can be applied to approximately cubic vessels with central ignition and evenly distributed vents.

When the valve opens to give a discharge area A_c = α c.Av.

$$\left.\begin{aligned} \frac{dp}{dn} &= b\left\{1 - \left(\frac{p}{p_o}\right)^{\frac{3\gamma-1}{2\gamma} - \beta} \cdot \frac{1}{\eta_f^{\,2}}\right\} \leqslant 0 \\ \eta_f^{\,3} &= \frac{1 + bn - (1 - n)\, p^{1 - \frac{1}{\gamma}}}{p} \\ \frac{dp}{d\tau} &= \frac{dp}{dn} \cdot \eta_f^{\,2} \cdot p^{\beta} \end{aligned}\right\} \qquad \text{C.II.21}$$

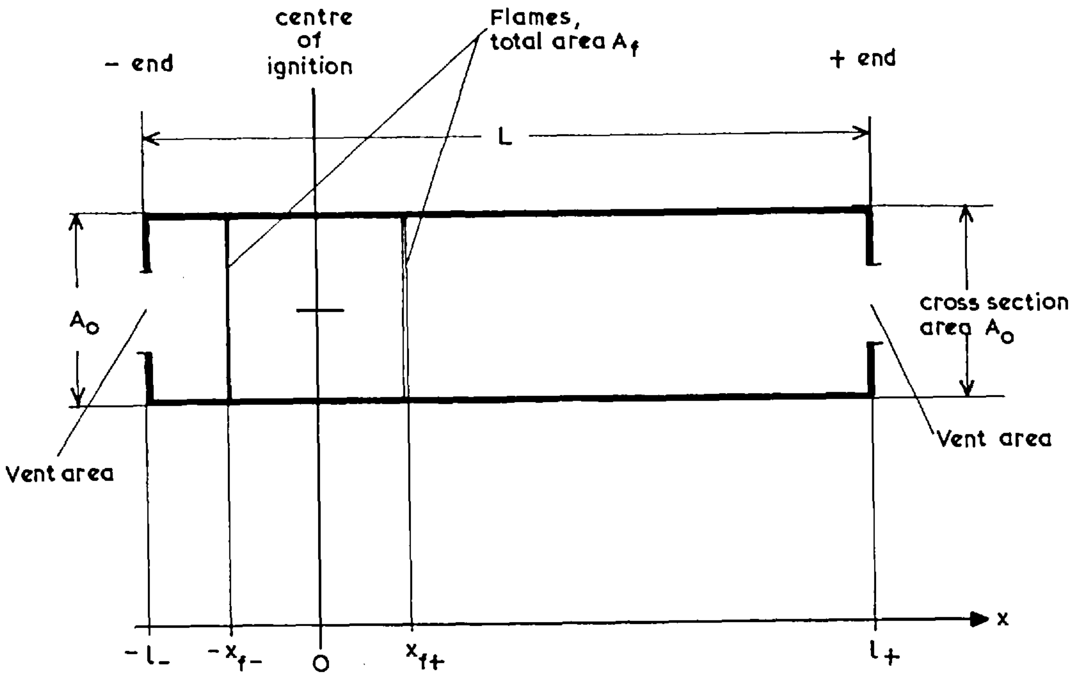

FIG.C.II.2 a. ONE-DIMENSIONAL COMBUSTION

C.II.3 One-dimensional combustion.

In the one-dimensional theory an exactly similar treatment of the problem is pursued. The inclusion of a centre of combustion and variation of the venting direction is attained by the use of a series of coefficients.

One assumption beyond those expressed in the spherical case is included: the flame, initiated at the centre of ignition, is instantaneously established as a plane across the vessel section. This assumption can be justified on the basis that, in treating a one-dimensional vessel with a large aspect ratio, the plane flame is established before the question of venting arises.

The problem of a one-dimensional system introduces the questions of: direction of flow; position of vents; and the centre of ignition. The centre of ignition is made the origin of the system and the two ends of the vessel are identified by the subscripts + and - as shown in Fig. C.II.2. The analysis is detailed in Appendix C.I and the results will be summarised below and compared with those for the spherical vessel.

(i) Up to the valve operating pressure:

$$\left.\begin{aligned} \frac{dp}{dn} &= b \quad \text{and} \\ p &= 1 + bn \ ; \end{aligned}\right\} \qquad \text{C.II.22}$$

$$\frac{dn}{d\tau} = H.\frac{A_f}{A_v} \cdot p^{\beta} = \frac{1}{b} \cdot \frac{dp}{d\tau} \ ; \quad \text{and} \qquad \text{C.II.23}$$

$$X_{f+} - X_{f-} = 1 - \left(1 + \frac{1}{b}\right) p^{-\frac{1}{\gamma}} + \frac{1}{b} \cdot p^{\left(1 - \frac{1}{\gamma}\right)} \qquad \text{C.II.24}$$

where $X = \frac{x}{L}$, the subscripts are defined in Fig. C.II.2

and A_v = available venting area.

(ii) When the valve opens

$$\frac{dp}{dn} = b - \frac{\alpha}{H} \cdot S \frac{A_v}{A_f} \cdot (p)^{\frac{3\gamma - 1}{2\gamma} - \beta} \ ; \qquad \text{C.II.25}$$

$$\frac{dn}{d\tau} = H.\frac{A_f}{A_v} \cdot p^{\beta} \ ; \quad \text{and} \qquad \text{C.II.26}$$

$$(X_{f+} - X_{f-}) = \frac{\left(1 - \frac{S^u_+ + S^u_-}{S}\right)p + \left(\frac{S^u_+ + S^u_-}{S}\right)(1 + nb) - (1 - n)\, p^{\left(1 - \frac{1}{\gamma}\right)}}{p} \qquad \text{C.II.27}$$

where: S^u_+ and S^u_- are coefficients taking the value 0 when the vent is closed and 1 when the vent is open;

<table>
<tr><th></th><th>CENTRAL IGNITION</th><th>OPEN END IGNITION</th><th>CLOSED END IGNITION</th></tr>
<tr>
<td>ONE VENT
$A_v = A_o$</td>
<td>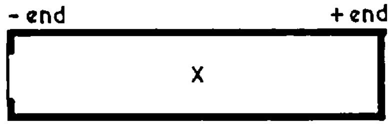

2 Flames $A_f = 2A_o$
Unburnt gas vented till flame reaches vent when burnt gas is vented.
$A_f / A_v = 2$
$S = 1$ <u>or</u>
$S > 1$</td>
<td>

1 Flame $A_f = A_o$
Burnt gas vented
$S_b^- = 1$ $S_u^- = S_u^+ = S_b^+ = 0$
$A_f / A_v = 1$
$S > 1$</td>
<td>

1 Flame $A_f = A_o$
Unburnt gas vented
$S_u^- = 1$ $S_u^+ = S_b^- = S_b^+ = 0$
$A_f / A_v = 1$
$S = 1$</td>
</tr>
<tr>
<td>TWO VENTS
$A_v = 2A_o$</td>
<td>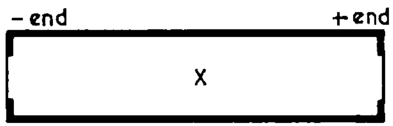

2 Flames $A_f = 2A_v$
Unburnt gas vented
$S_u^- = S_u^+ = 1$ $S_b^- = S_b^+ = 0$
$A_f / A_v = 1$
$S = 1$</td>
<td>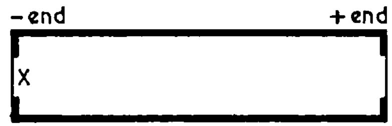

1 Flame $A_f = A_v$
Both burnt and unburnt gas vented
$S_b^- = S_u^+ = 1$ $S_b^+ = S_u^- = 0$
$A_f / A_v = 1/2$
$S > 1$</td>
<td><u>FIG.C.II.2b.</u>

ONE-DIMENSIONAL COMBUSTION

Definitions of coefficients $S_u^+, S_u^-, S_b^+, S_b^-$.</td>
</tr>
</table>

$$S = \frac{S^u_+ + S^u_- + \frac{m_e}{m_i} \frac{S^b_+ + S^b_-}{(F_{po})^{\frac{1}{2}}}}{S^u_+ + S^u_- + S^b_+ + S^b_-}$$

and $F_{po} = \frac{m_e}{m_i} \cdot \frac{F_b}{F_u}$ (at $x = 1$, $t = t$).

The venting area for constant pressure conditions is obtained by putting $\frac{dp}{dn} = 0$ in the first equation.

$$\alpha_c = H.\ b.\ \frac{A_f}{S.A_v} \cdot \left(p_o\right)^{\beta - \frac{3\gamma - 1}{2\gamma}} \qquad \text{C.II.28.}$$

Both S and $\frac{A_f}{A_v}$ depend upon the centre of ignition so that the venting area cannot be determined but, for any one gaseous system, the maximum value of the ratio $\frac{A_f}{SA_v}$ can be calculated and the safe venting area is

$$\alpha_c = \text{constant} \left(p_o\right)^{\beta - \frac{3\gamma - 1}{2\gamma}} \qquad \text{C.II.29}$$

$\frac{A_f}{A_v}$ equals either $\frac{1}{2}$, 1 or 2 and $S \geqslant 1$

Hence α has a maximum when $S = 1$ and $\frac{A_f}{A_v} = 2$

Therefore the constant in equation C.II.29 is (2H.b.) and the maximum area is required when the ignition takes place near the centre of the vessel and it is vented at one end only.

C.II.4 Comparison of the two systems.

The equations derived in the previous chapters are summarised in Table C.II.1. The two equations for the venting area show that the spherical vessel requires a smaller proportion of its surface area for discharge. However, this is due to the implicit assumption of central ignition in spherical combustion and a true comparison should be made with the corresponding case of central ignition in the one-dimensional vessel. Then by substituting the appropriate values of S = 1 and $\frac{A_v}{A_f} = 1$ the equations are equivalent, being

$$\alpha = H.\ b.\ p_o^{\,\theta - \frac{3\gamma - 1}{2\gamma}} .$$

Each of the parameters required in the calculation of discharge area and rate of change of pressure have a physical meaning. Also, the two equations for the safe venting area can be rearranged to give a single relation in terms of the energy of compression and the energy of combustion in the unburnt gas. Both these aspects are considered below.

(i) $b = \frac{m_i}{m_e} \cdot \frac{\Delta H_i}{T_i (Cv)_u}$

b can also be calculated from equations C.II.18 or 22

$$p = 1 + bn$$

and the final pressure is given by this equation when $n = 1$

$$\text{i.e.} \quad p_e = 1 + b$$

$$\therefore \quad b = p_e - 1. = \frac{P_e}{P_i} - 1$$

Since we are dealing with adiabatic operations, the energy per unit volume of gas is proportional to the pressure. In the closed vessel the volume of gas is the same at the beginning and the end so that

$$b = \frac{P_e - P_i}{P_i}$$

$$= \frac{\text{Energy available from combustion}}{\text{Energy initially in combustibles.}}$$

which is a property of the gaseous system. This expression can also be derived from the first definition of b.

$$\text{(ii)} \qquad H = \frac{M_i . V}{A_f^{*} . C . w_i}$$

and $\frac{w_i}{V} = \rho_i$, initial density of the gas,

$M_i = \left(\frac{dw_b}{dt}\right)_i$, initial combustion rate.

$$C = \left[\gamma R \, T_i \quad \frac{1}{m_i} \quad B\right]^{\frac{1}{2}}$$

$$= a_i \; B^{\frac{1}{2}}$$

where a_i = initial velocity of sound

$$\text{and} \quad B = \left(\frac{2}{\gamma + 1}\right)^{\frac{\gamma+1}{\gamma-1}} .$$

$$\therefore \quad H = \frac{1}{A_f^{*} . \rho_i} . \left(\frac{d\,w_b}{dt}\right)_i . \frac{1}{a_i\, B^{\frac{1}{2}}}$$

and $\dfrac{1}{A_f^{*}\ \rho_i}\left(\dfrac{dw_b}{dt}\right)_i$ = initial burning velocity.

$$\therefore \quad H = \frac{1}{B^{\frac{1}{2}}} . \frac{\text{initial burning velocity}}{\text{initial velocity of sound}}$$

which is a property of the gaseous mixture.

(iii) $\tau = \dfrac{C.A_v}{V} . t.$

where $C = B^{\frac{1}{2}}.a_i$

$\dfrac{V}{A_v}$ = dimensional characteristic of the vessel

= $\dfrac{R}{3}$ for the sphere

= L for the one-dimensional vessel.

Therefore, $\dfrac{V}{C.A_v}$ is a measure of the time it takes a sound wave to travel the greatest distance in the vessel at the initial temperature and, hence, is a measure of the size of the vessel as it effects the propagation of pressure changes.

(iv) By substituting these physical interpretations in the equations for the venting area it can be shown that the criterion for constant pressure venting for both types of vessel is:

Volume rate of discharge required

$$= \text{(volume rate of burning)} \times \frac{\text{Combustion energy in unburnt gas}}{\text{Compression energy in unburnt gas}}$$

FOR BOTH VESSELS

The absolute pressure	P
Ratio of pressure at time t to initial pressure	$p = P/P_i$
Mass of gas	w
Fraction of total gas burnt at time t	$n = w_b/w_i$
Time interval after ignition	t
Dimensionless time	$\tau = \frac{CA_v}{V}$
Volume of the vessel	V
Vent area as a fraction of available area	α
"Safe" venting area fraction	α_c
Explosive potential in combustibles	$b = p_e - 1$
Initial flame velocity	G
A measure of initial burning velocity	$H = G/C$
A measure of the initial speed of sound	C
Exponent governing rate of increase of combustion	β

SPHERICAL VESSEL

Radius of vessel	R
Radius of gaseous element in vessel	r
Dimensionless radial distance	η

ONE-DIMENSIONAL VESSEL

Length of vessel	L
Distance of gaseous element from centre of ignitio	x
Dimensionless distance	X
Cross-sectional area of vessel	A_o
Area available for venting	A_v
Coefficients to account for conditions of venting	S

SUBSCRIPTS

Initial conditions	i
Final conditions	e
Pertaining to the flame	f
Pertaining to unburnt gas	u
Pertaining to burnt gas	b

	SPHERICAL	ONE-DIMENSIONAL
CLOSED VESSEL $1 \leq p \leq p_o$ $0 \leq n \leq n_o$ $0 \leq \tau \leq \tau_o$	$\frac{dp}{dn} = b \quad \therefore \; p - 1 = b.n$ $\frac{dp}{d\tau} = \frac{1}{b}\frac{dn}{d\tau} = H\eta_f^2 p^{\beta}$ $\eta_f^3 = 1 - (1+\frac{1}{b})p^{-\frac{1}{\gamma}} + \frac{1}{b}p^{1-\frac{1}{\gamma}}$	$\frac{dp}{dn} = b \quad \therefore \; p - 1 = b.n$ $\frac{dp}{d\tau} = \frac{1}{b}\frac{dn}{d\tau} = H\frac{A_f}{A_v}p^{\beta}$ $X_f - X_f = 1 - (1+\frac{1}{b})p^{-\frac{1}{\gamma}} + \frac{1}{b}p^{1-\frac{1}{\gamma}}$
VENTED VESSEL $p_o \leq p$ $n_o \leq n$ $\tau_o \leq \tau$	$\frac{dp}{dn} = b - \frac{1}{H}\alpha(p)^{\frac{3\gamma-1}{2\gamma}-\beta}.\left(\frac{1}{\eta_f}\right)^2$ $\frac{dn}{d\tau} = H.\eta_f^2.p^{\beta}$ $\eta_f^3 = \frac{1 + b.n - (1-n)p^{1-\frac{1}{\gamma}}}{p}$	$\frac{dp}{dn} = b - \frac{1}{H}\alpha(p)^{\frac{3\gamma-1}{2\gamma}-\beta}.\frac{S.A_v}{A_f}$ $\frac{dn}{d\tau} = H\frac{A_f}{A_v}.p^{\beta}$ $\Delta X_f = \left[\left(1 - \frac{S_u^+ + S_u^-}{S}\right).p + \frac{S_u^+ + S_u^-}{S}(1 + n.b.) - (1-n).p^{1-\frac{1}{\gamma}}\right]\frac{1}{p}$
"SAFE" VENTING	$\alpha_c = H.b(p_o)^{\frac{3\gamma-1}{2\gamma}-\beta}$ $\frac{dp}{dn} \leq 0$	$\alpha_c = H.b.\frac{A_f}{S A_v}(p_o)^{\frac{3\gamma-1}{2\gamma}-\beta}$ $\frac{dp}{dn} = 0$

TABLE.C.II.1. COMBUSTION EQUATIONS.

C.II.5 Comparison with experimental results.

Equations C.II.17 to C.II.27 predict the behaviour of gaseous explosions in closed and vented vessels. By solving these equations the theory can be examined in the light of experimental evidence obtained from the literature. In most cases, the solution requires a step by step calculation using a finite difference method. Hence, each case must be considered separately and the tedious computations make any comprehensive comparison with experimental results difficult. Only three experimental studies will be considered and, although these are primarily concerned with the venting of explosions, the results for closed vessels will have to be considered first. Pressure relief above the critical pressure can be examined from the theoretical standpoint but in most cases insufficient information is available for a direct comparison and certain assumptions have to be made.

Before considering these results a brief comment on a previous analysis of the combustion of gases in closed vessels is necessary. Lewis and von Elbe (1935) were the first to suggest any quantitative theory to account for the pressure rise in a closed spherical vessel. Their theory has been used as the basis for the present work. However, certain improvements have been introduced and by basing the analysis on the fundemental concepts of conservation ofmass and energy a solution has been obtained which does not require the additional assumptions of small changes in heat capacities. An exact solution is available for non-vented explosions in the form:

$$bn = \left(\frac{\gamma_b - \gamma_u}{\gamma_b - 1}\right)(1 - n)\, p^{\left(1 - \frac{1}{\gamma_u}\right)} + \left(\frac{\gamma_u - 1}{\gamma_b - 1}\right) \cdot p - 1 .$$

A comparison with the approximate solution

$$bn = p - 1$$

obtained by Lewis and von Elbe shows that the errors introduced are less then 1%. However, the calculated value of the final pressure as determined from these two expressions with $n = 1$ and $b = \frac{m_i}{m_e} \cdot \frac{\Delta H_i}{T_i\ (Cv)_u}$

may differ by as much as 10%. For example, in an experiment on the combustion of ozone as carried out by Lewis and von Elbe (1934) the final pressure ratio, p_e, was 5·72. Calculating the pressure ratio from the properties of the gases two values of the final pressure ratio are obtained: 5·69 using the exact relation; and 6·20 using the approximate one.

Lewis and von Elbe used these equations to calculate the fundamental burning velocity from experimental results. Since the present theory is to be used to calculate pressure rises in closed and vented vessels, an additional equation relating the burning velocity to the pressure has been introduced. This step is difficult to justify theoretically, particularly in view of the increase in flame speed due to turbulent mixing of the gases. This means that the rate of burning for any mixture in a given vessel should be obtained experimentally. Bearing this in mind, the following comparisons between the analysis and experimental results show remarkable agreement.

(i) Pentane-air explosions in a nearly spherical vessel - Wilson (1954)

These experiments were carried out to determine the effectiveness of vents for the relief of explosions. Unfortunately, all these results are either for venting pressures less than critical or for spring loaded valves about which insufficient information is available. Therefore, only the closed vessel results have been used and a pressure-time curve constructed for the explosion assuming the vessel to be approximately spherical.

The initial burning velocity has been taken as 1•2 ft/sec as suggested by Wilson and the exponent β, which determines the effect of pressure on the burning rate, as 1•3. This latter assumption can be justified theoretically by comparing the

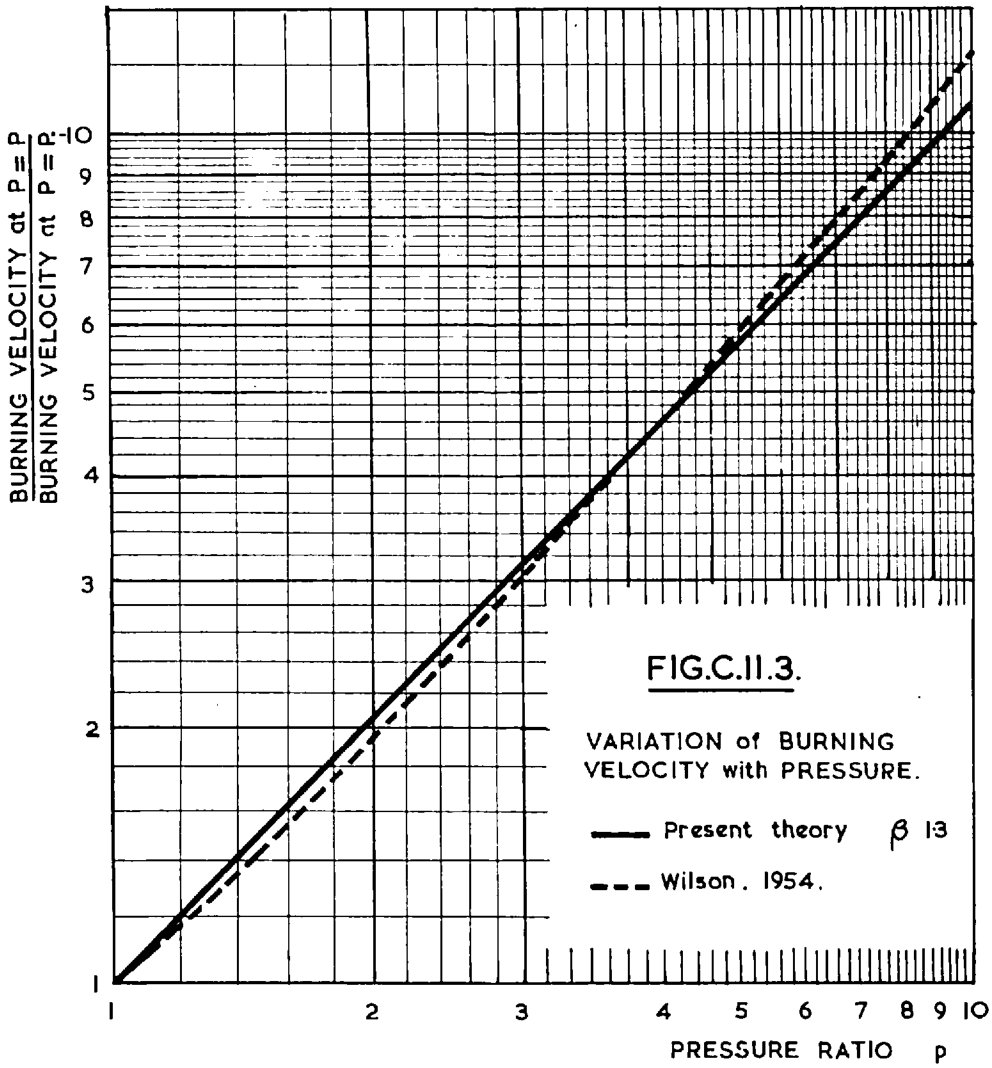

FIG.C.II.3.

VARIATION of BURNING VELOCITY with PRESSURE.

change of burning rate with pressure predicted by Dugger (1951) and Manson (1953) and that predicted by the present theory when $\beta = 1{\cdot}3$. Although agreement is good, as shown in Fig. C.II.3, the value of this exponent was determined from the maximum rate of pressure rise given by Wilson. Using equation C.II.17b.,

$$\text{i.e.} \quad \frac{dp}{d\tau} = H.\ b.\ \eta_f^{\,2} \cdot p^{\beta} \quad ,$$

the maximum rate of pressure rise occurs when the flame first touches the vessel walls so that the only unknown, β, can be calculated from this expression. In this case: $(\eta_f)_{max} = 0{\cdot}862$;

$$\left(\frac{dp}{dt}\right)_{max} = 78 \text{ sec}^{-1} \quad \text{at} \quad p = 5{\cdot}5; \quad b = 7{\cdot}55;$$

$$\text{and } H\tau = S_u \cdot \frac{A_v}{V} \cdot t = 1{\cdot}478\ t; \quad \text{whence} \quad \beta = 1{\cdot}315$$

Equations C.II.17, 18a and 19 have been solved simultaneously and the results plotted in Fig. C.II.4 in terms of the pressure ratio p and the dimensionless time group $H\tau .b$. Wilson's results are plotted on the same figure together with the pressure-time curves for stirred explosions using an increased initial flame velocity. Agreement between theoretical prediction and experimental measurements is good up to $p = 6$. Above this pressure the flame diameter reaches a value of 4 ft.

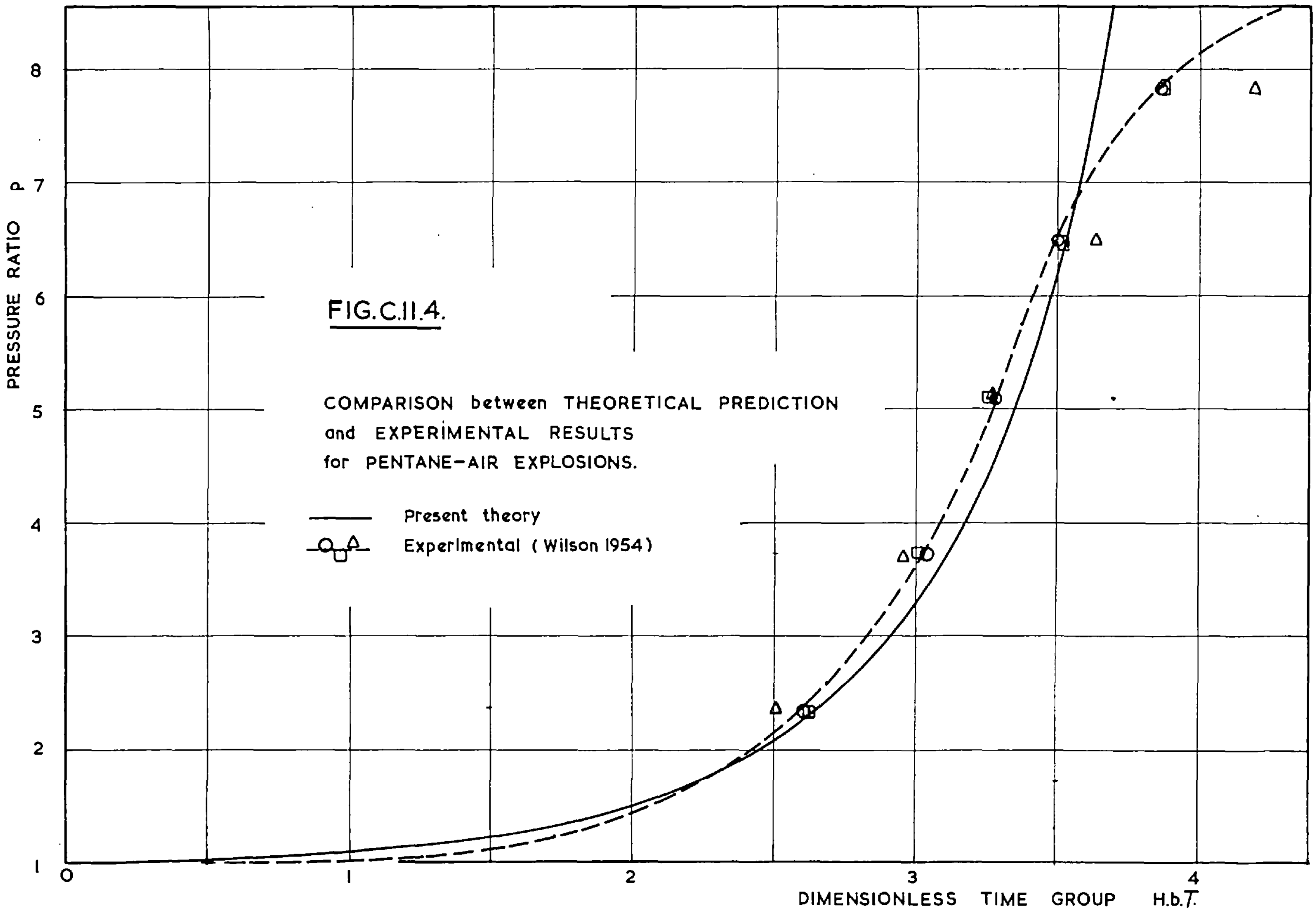
FIG. C.11.4.
COMPARISON between THEORETICAL PREDICTION and EXPERIMENTAL RESULTS for PENTANE-AIR EXPLOSIONS.
Present theory
Experimental (Wilson 1954)
PRESSURE RATIO P
DIMENSIONLESS TIME GROUP H.b.T.
1
2
3
4
5
6
7
8
0
1
2
3
4

and the flame touches the wall of the vessel so that the analysis is no longer applicable.

The similarity between the pressure-time curves for stirred explosions was noted by Wilson. Fig. C.II.4 shows that these results can be correlated by using different values for the initial burning velocity in the dimensionless time group H.b τ and it indicates a possible method for calculating the effect of stirring and turbulence on explosion and venting problems. This aspect presents the greatest defect in the present theory since the action of venting effects the burning rate. This difficulty becomes apparent in sections (ii) and (iii) which deal with vented explosions and a possible solution will be discussed in Chapter C.II.6.

(ii) Propane-air explosions in a nearly spherical vessel vented at one end - Cousins & Cotton (1951).

Mixtures of propane and air were exploded under different initial pressures. The explosions were vented using various bursting discs so that a number of bursting pressures and venting areas could be examined. Additional information was obtained for closed vessels and the maximum pressure and maximum rate of pressure rise recorded for two initial pressures. This latter work agrees with the analysis given above in as much as the final pressure ratio is a constant. That is, the relation between maximum pressure and initial pressure is linear. Unfortunately the shape of the vessel in which these experiments were carried out is not specified and further ommissions limit the usefulness of this work, making exact comparison with theory unreliable. Nevertheless, a comparison has been made by assuming central ignition and supposing that the vessel used was the one designed for high pressure explosions having a length of 1·54 ft and a diameter of 1 ft.

After the vent has opened the pressure will increase if

$$\alpha < H.b.\ p_o^{\beta - \frac{3\gamma - 1}{2\gamma}}\ \eta_f^2 \ .$$

A maximum will be reached if

(a) the rate of venting is such that at some stage the rate of pressure increase exactly balances the rate of discharge through the vent and

$$\frac{dp}{dn} = b - \frac{\alpha}{H} \cdot p_{max}^{\left(\frac{3\gamma - 1}{2\gamma} - \beta\right)} \cdot \frac{1}{\eta_f^2} = 0 \qquad \text{C.II.30}$$

or (b) The gas continues to burn until some part of the flame reaches the vent and the resulting reduction in flame area causes the pressure to fall.

In the first case, the maximum pressure is independent of the operating pressure, p_o, at which the vent opens. Maximum

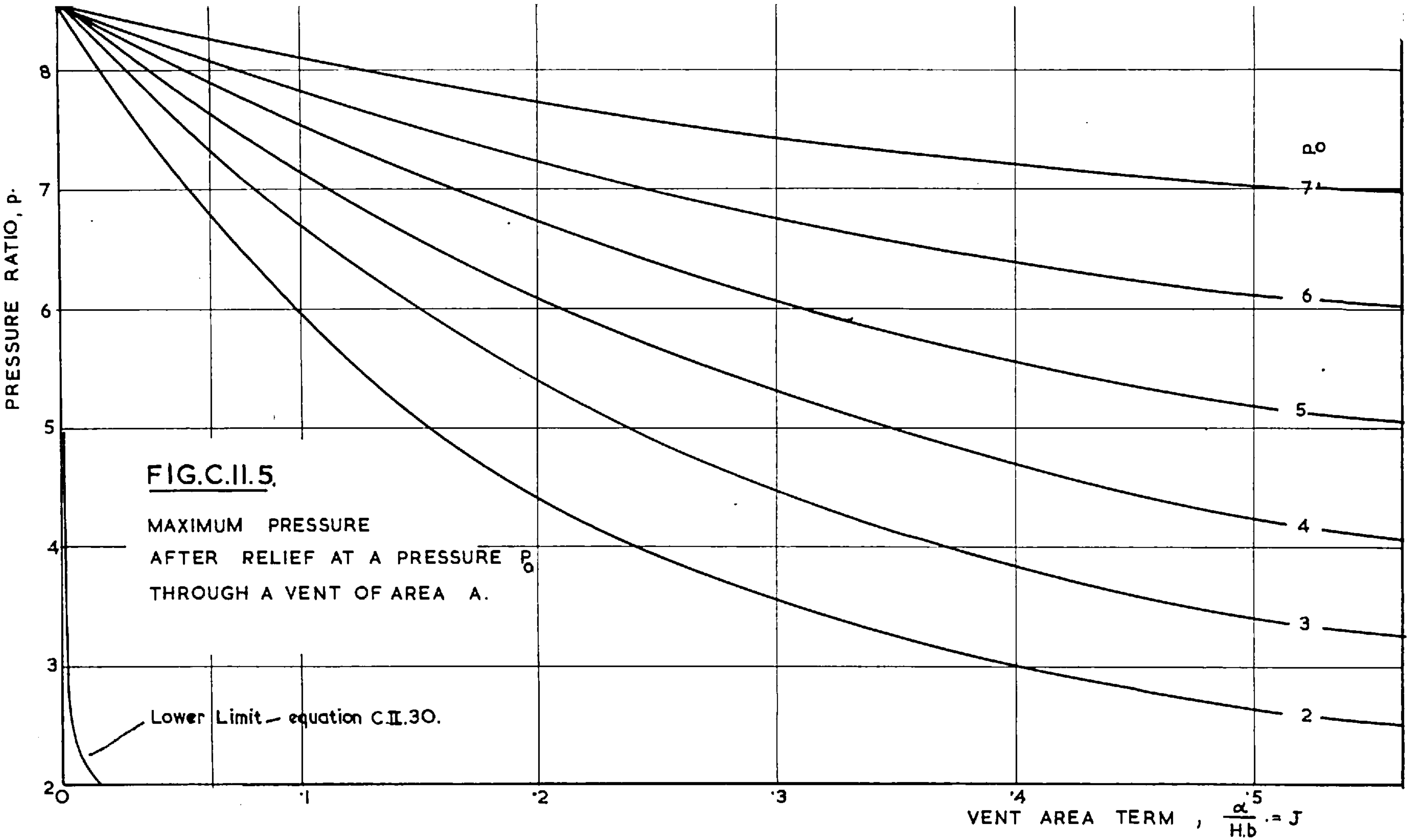

FIG.C.II.5.

MAXIMUM PRESSURE
AFTER RELIEF AT A PRESSURE P_o
THROUGH A VENT OF AREA A.

pressures calculated from equation C.II.30 are usually less than $p = 2$ so that these are the lower limits of maximum pressure as shown in Fig. C.II.5. In the second case, the maximum pressure will depend upon the bursting pressure because it will be affected by the distance between the flame and the vent at the instant the vent opens. The calculation of the maximum pressure requires the step-by-step solution of equation C.II.17 for different values of p_0 and α, the maximum pressure being that corresponding to $\eta_f = 1{\cdot}0$. The results of these calculations are shown in Figs. C.II.5 and 6.

In Fig. C.II.5 the maximum pressure ratio is related to the vent area for a series of values of the operating pressure ratio. The diagram has been calculated using $\beta = 1{\cdot}3$ and is applicable to propane-air mixtures only but can be used for any initial pressure and any vessel which is approximately spherical. Using these results, the variation of maximum pressure with bursting pressure for three vent areas and two initial pressures have been calculated and compared in Fig. C.II.6 with the results obtained by Cousins & Cotton. In this case the values of $\frac{\alpha}{Hb}$ have been chosen to give those curves which best fit the results and in Table C.II.2 these values are compared with the experimental values of vent area.

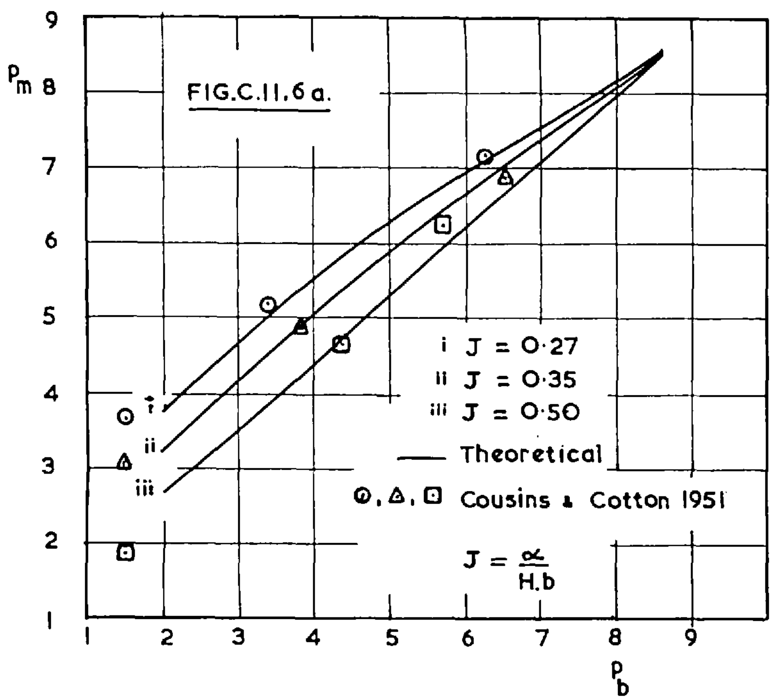

FIG.C.11.6 a.

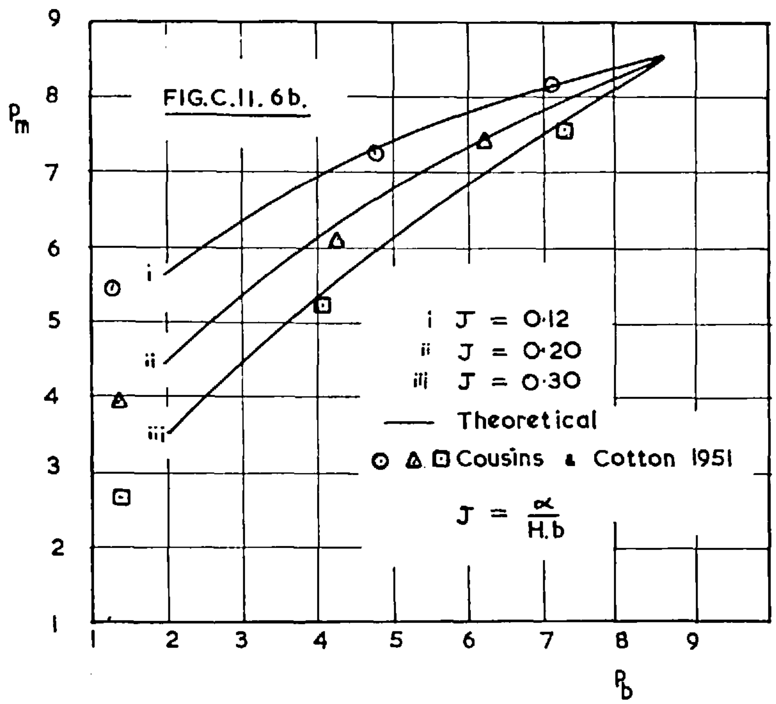

FIG.C.11.6b.

INITIAL PRESSURE. psig.	15			45		
VENT DIAMETER ft	·0510	·0751	·1167	·0510	·0751	·1167
VENT AREA RATIO 10^3	2·61	5·64	13·61	2·61	5·64	13·61
REYNOLDS NUMBER $Re^* \; 10^{-6}$	5·70	8·40	13·02	11·39	16·78	26·06
INITIAL BURNING VELOCITY S_u^* ft/sec	1·300	1·678	2·835	2·78	3·61	5·81

TABLE C. II. 2.

Table C.II.2

The discrepancy between experimental and theoretical results for turbulent conditions has already been noticed and a suggested correlation employing a Reynolds number is considered. In this case the Reynolds number depends upon the diameter of the vent and the density of the gas and, if the initial flame velocity, S_u^*, required to give the correct value of $\frac{\alpha}{Hb}$ is plotted against the appropriate Reynolds number, Re^*, based on the vent diameter and the initial density, a direct relation is obtained. This is shown in Fig. C.II.6c and the equation

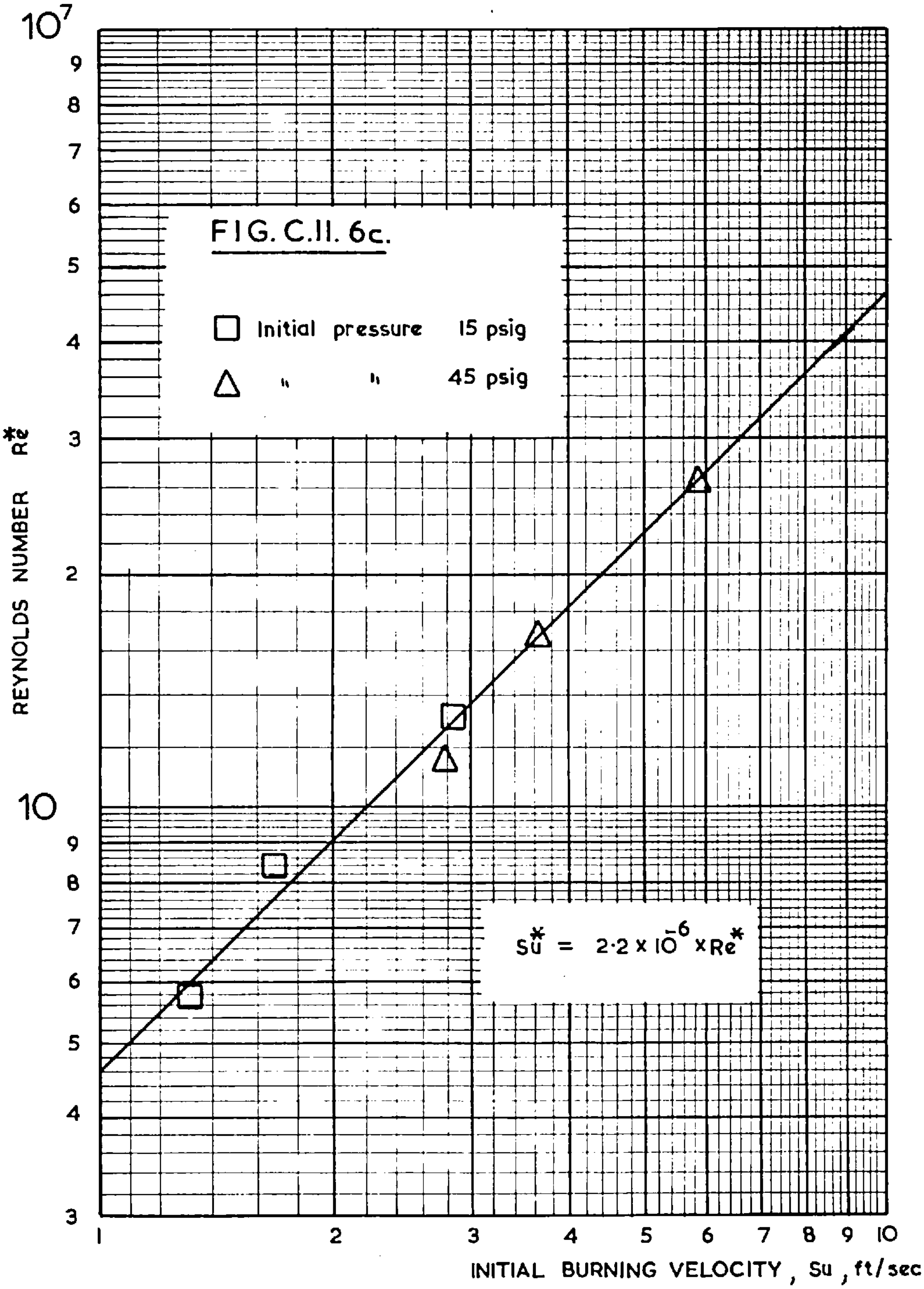
FIG. C.II. 6c.
Initial pressure 15 psig
" " 45 psig
$S_u^* = 2{\cdot}2 \times 10^{-6} \times Re^*$
REYNOLDS NUMBER Re^*
INITIAL BURNING VELOCITY, Su, ft/sec
10^7
9
8
7
6
5
4
3
2
10
9
8
7
6
5
4
3
1
2
3
4
5
6
7
8
9
10

$Su^{H} = k. (Re^{M})$ has been obtained. Since the initial flame velocities used to calculate the pressure-time curves in section (i) were proportional to the fan diameter it is possible that the correction factor to be applied to turbulent conditions is directly proportional to the Reynolds number.

(iii) Pentane-air explosions in a duct - Rasbash and Rogowski (1956).

In these experiments a tube 6" in diameter and 6' long was used and pentane-air mixtures were ignited at one end. Pressure-time records were obtained for explosions vented at either end using bursting discs or open vents. Again all but a few experiments involved venting at pressures below the critical ratio and the closed vessel experiments will be analysed first.

The explosion takes place in three phases. In the first, the gas burns as a spherical shell until the flame reaches the wall. During this process the sphere is displaced alone the tube due to the flow of gas away from the ignition end. The analysis of this phase is identical to that for spherical combustion using equations C.II.17, 18a and 19 and taking the radius of the vessel to be the "equivalent radius". That is, the radius of a sphere which has the same surface area

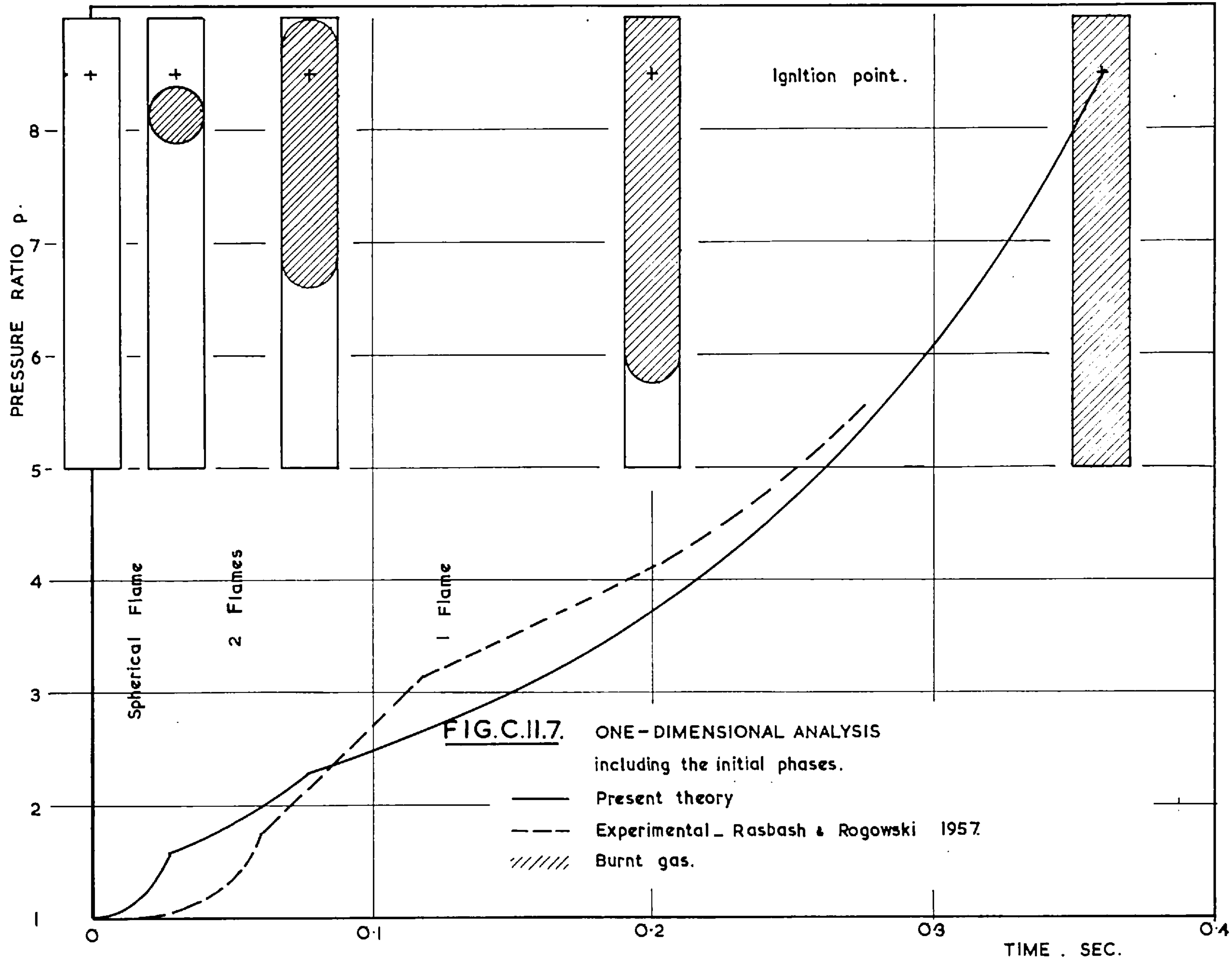

FIG.C.11.7. ONE-DIMENSIONAL ANALYSIS including the initial phases.

to volume ratio as the vessel under consideration. The displacement can be calculated from the equation for the movements of elements by assuming that the centre of the sphere is such an element. In the second phase, two flames exist, travelling in opposite directions. Gerstein et al (1951) have shown that the two flames will be approximately hemispherical in shape and have a surface area of about twice the cross-sectional area of the tube. This means that equations C.II.22, 23 and 24 must be solved with $\frac{Af}{Av} = 4$. This stage is completed when one flame reaches the wall and the time and pressure at which this occurs can be determined from equation C.II.24. In the final stage, a single flame travels down the tube and an analysis similar to that used in the second stage but with $\frac{Af}{Av} = 2$ is used.

These calculations are detailed in Appendix C.II.2 and the results are shown in Fig. C.II.7. Both the pressure-time curve and the flame positions at various stages in the process are shown. The three stages are clearly shown in the experimental curve and, although it does not coincide with that predicted by the theory, it is evident that there is reasonable agreement.

Information on the venting of this duct at supercritical pressures is not directly available but an examination of the pressure-time curves for a series of experiments indicates that constant pressure venting will occur when the vent diameter is between 2" and 3" and the bursting pressure is less than 30 p.s.i.g. Under these conditions there are two flames in the duct and $\frac{Af}{SAv} = 2$. Substituting this figure and appropriate values of H, b, β and γ in equation C.II.28.

$$\alpha_c = 57\cdot2 \times 10^{-3}\ p^{0\cdot167}$$

at an average value of p = 2·5

$$\alpha_c = 66\cdot6 \times 10^{-3}$$

and the vent diameter is 1·85 inches - assuming a discharge coefficient of 0·70. This is small compared with the experimental value and the difference is probably due to the increased turbulance. If H is calculated using an initial burning velocity determined by the Reynolds number, as plotted in Fig. C.II.6c, the vent diameter for constant pressure ventirg is D = 2·9"

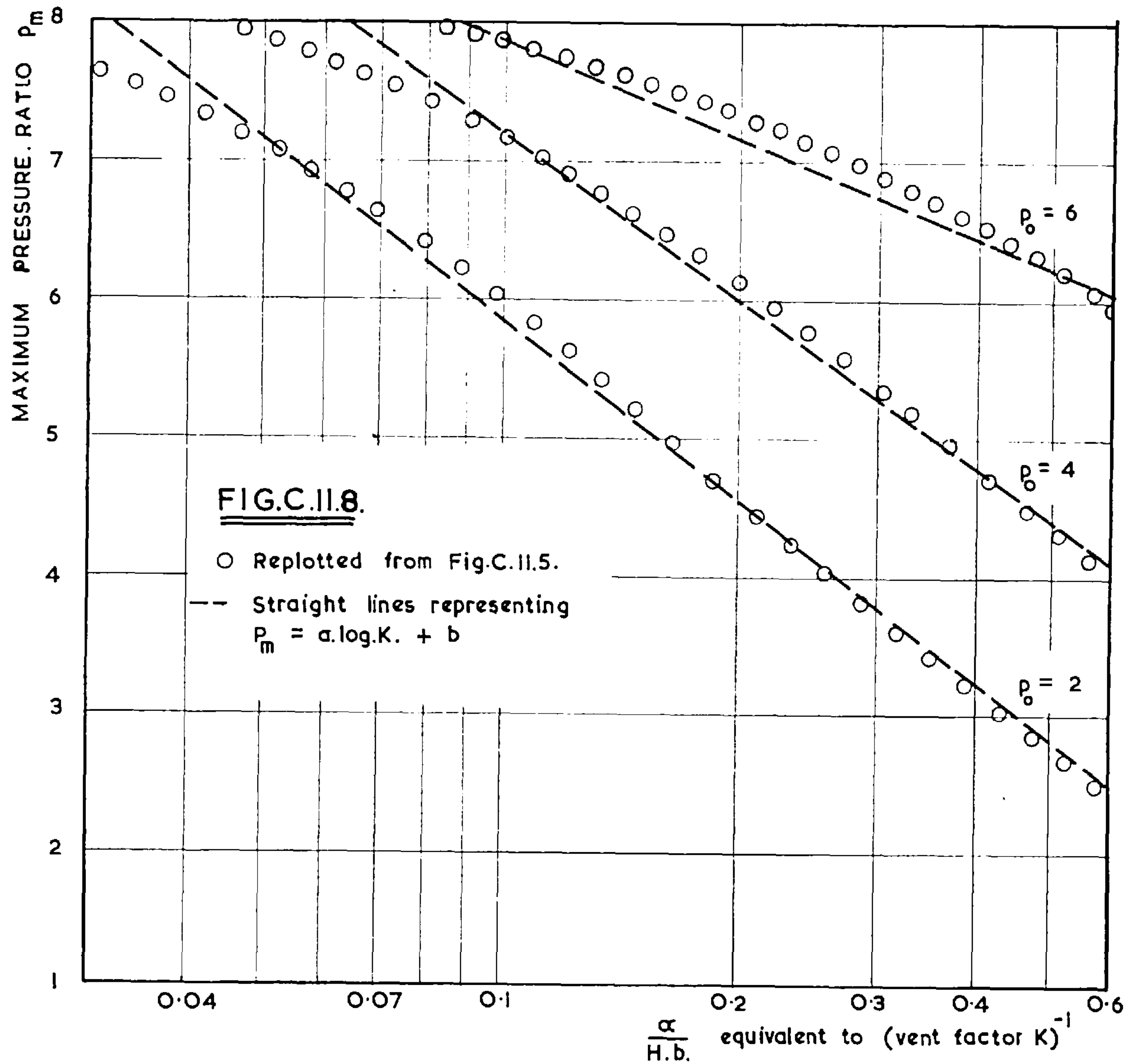

MAXIMUM PRESSURE. RATIO P_m
8
7
6
5
4
3
2
1
FIG.C.II.8.
Replotted from Fig.C.II.5.
Straight lines representing
$P_m = a.\log.K. + b$
$P_o = 6$
$P_o = 4$
$P_o = 2$
0·04
0·07
0·1
0·2
0·3
0·4
0·6
$\frac{\alpha}{H.b.}$ equivalent to (vent factor K)$^{-1}$

C.II.6 Assessment of the importance of the simple theory and its reliability.

In the last chapter the theory was used to calculate the pressure-time curves for unvented explosions and the maximum pressures in vented explosions. The theory predicts the performance of unvented explosions with remarkable accuracy but underestimates the maximum pressures once relief has been applied. A method has been suggested for accounting for the difference but further experimental results are required to check this.

In spite of these deviations this theory provides a sound basis for further experiments and also confirms certain empirical correlations put forward by other workers. For instance, the K factor suggested by Burgoyne & Newitt (1960) and used by Rasbash (1959) would appear to bear a logarithmic relation to the maximum pressures and to illustrate this the results given in Fig. C.II.5 have been replotted in Fig. C.II.8.

However, an extended experimental programme is required to test the validity of the theoretical expressions. The simultaneous measurement of pressure and flame position must be made so that the several phases of combustion can be delineated and the effect of the venting on the burning rate examined.

At the same time, the equations should be solved for various combustion systems and the results tabulated so that any explosive mixture can be treated theoretically once its rate of combustion is known.

CHAPTER C.III THE HYDRAULIC ANALOGUE AND ITS USE IN DEMONSTRATING THE INTERACTION AND REFLECTION OF WAVES IN A VESSEL.

C.III.1 Introduction

In the previous chapter equations were derived to predict the pressure variation within a vessel when a gaseous explosion is vented. Agreement with experimental results was obtained by the introduction of a correction factor which increased the initial flame velocity in direct proportion to a Reynolds number dependent on venting conditions. It was suggested that this correction factor had to be introduced to account for the turbulence set up by the sudden expulsion of gas as the vent opened. That is, the effect of venting on the explosion was accounted for empirically.

The effect of venting on explosions could be determined using a fundamental approach but this would require the introduction of the equation of motion for the gas in the vessel. This is obtained by applying the principle of conservation of momentum to the movement of gas and accounts for the variation in pressure in the vessel at a given instant of time. When the explosion is unvented the assumption of quasi-steady-state conditions (no variation in pressure in the vessel) is adequate so long as

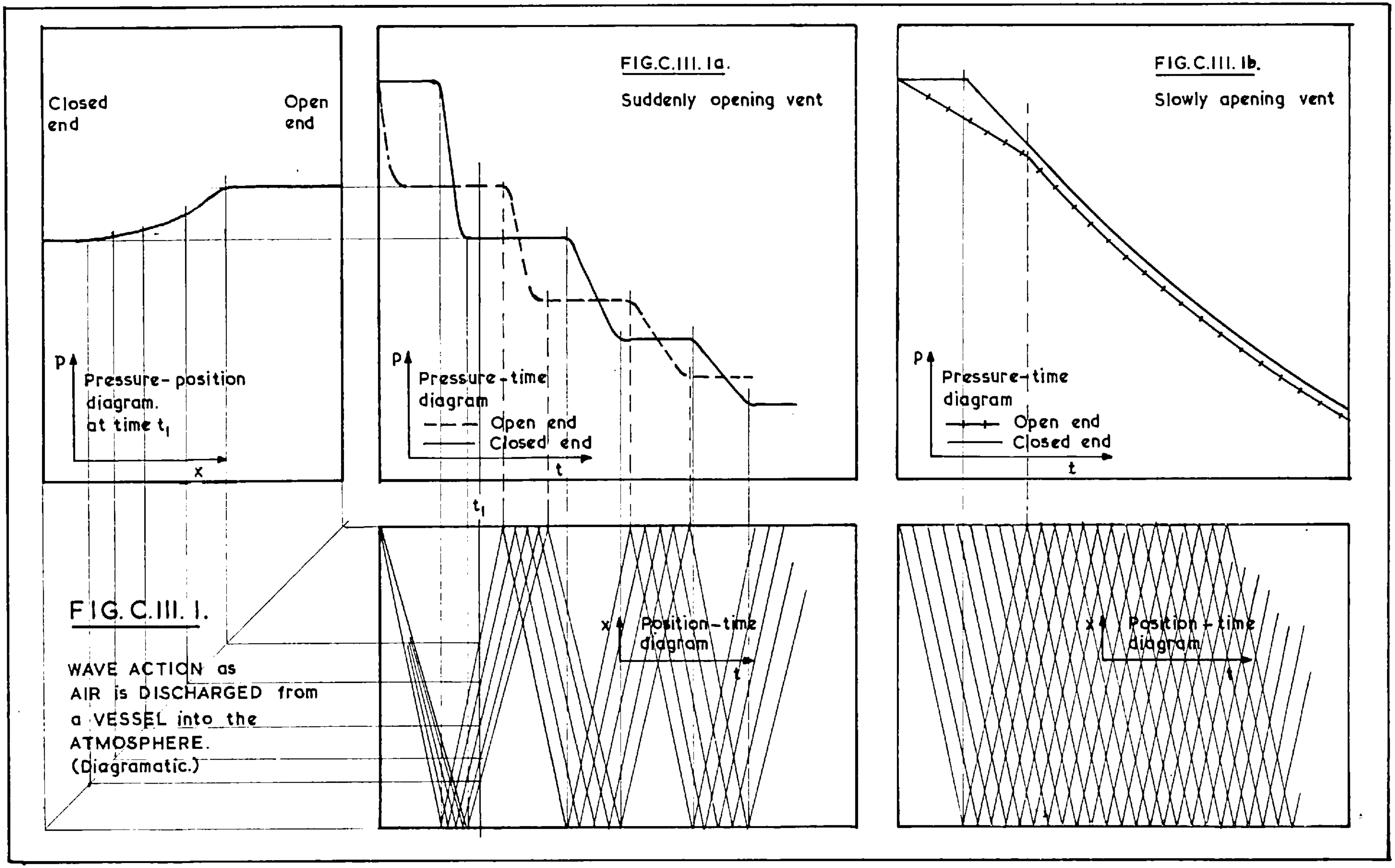

FIG. C.III. 1.

WAVE ACTION as AIR is DISCHARGED from a VESSEL into the ATMOSPHERE. (Diagramatic.)

the gas velocity is not appreciable compared with the speed of sound. However, when the vent opens the discharge of gas occurs at the speed of sound and pressure variations do occur. These take the form of rarefaction waves which are formed at the vent and are reflected from the walls of the vessel.

The equations of motion describe the pressure variation in these waves and their movement through the gas and a analysis of the problem under non-combustive conditions and in a one-dimensional vessel has been developed by Giffen (1940) and extended by Kestin & Glass (1951) and Benson (1955). Using the method of characteristics Benson has calculated the pressure variation in the vessel and the formation and reflection of the rarefaction wave for both sudden and slowly opening vents. The results of these calculations are shown diagramatically in Fig. C.III.1 in which the pressure variation is shown on a P-t diagram and the wave formation on an x-t diagram.

When the vent opens suddenly a discrete rarefaction wave is formed because, at a certain pressure level in the wave, the particle velocity completely satisfies the mass flow required to maintain sonic velocities in the vent. Hence, a relatively sudden pressure difference occurs across the wave and the pressure at a given point falls in steps. When the

FIG. C. III. 2.

INTERACTION between
a RAREFACTION WAVE and
a CONTACT SURFACE (FLAME)
(Diagramatic)

R Rarefaction wave
F Contact surface
C Compression wave
S Shock wave

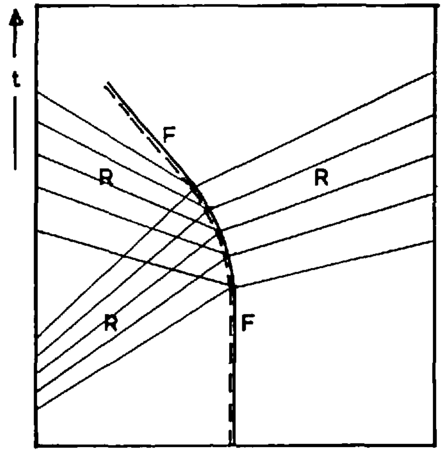

FIG.C.III.2a.

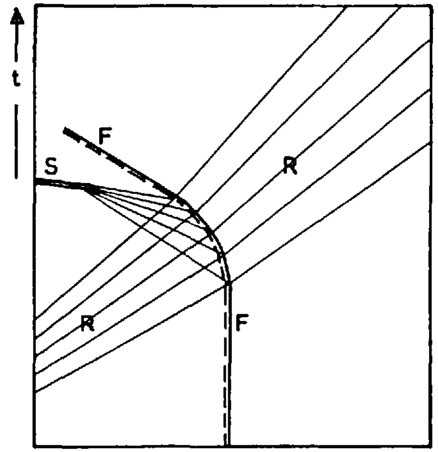

FIG.C.III.2b.

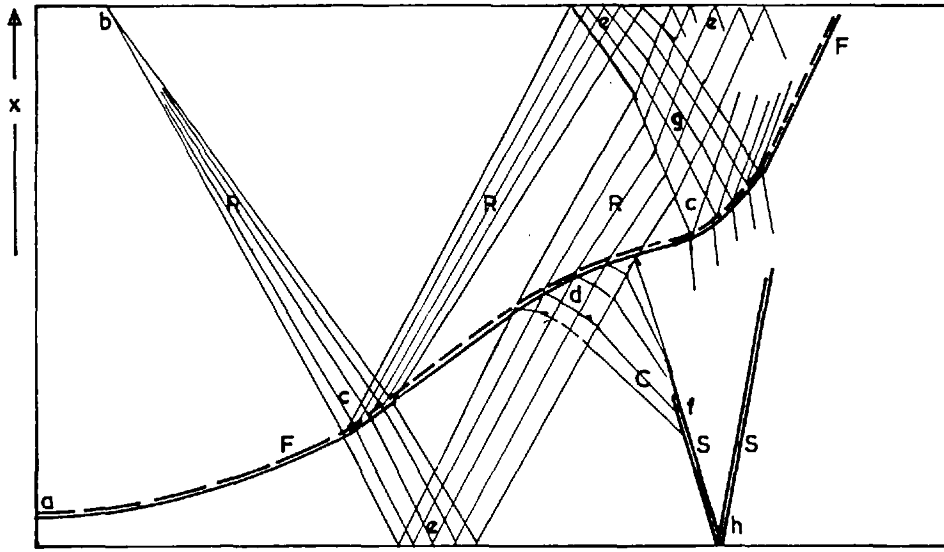

Possible flame-pressure-wave when an explosion is vented.

a ignition
b vent opens _ rarefaction formed.
c flame _ rarefaction interaction.(a)
d " " " (b)
e rarefaction reflected
f shock formed.
g two rarefactions interact
h shock reflected.

see I.I.Glass 1955.

FIG.C.III.2c.

vent opens slowly conditions at the vent never remain the same and the pressure falls continuously once the pressure disturbance associated with the first instant of vent opening has reached the closed end. It should be noted that the lines on the x-t diagram do not represent pressure waves but disturbances travelling at the local speed of sound through the gas. A wave is formed only when a group, or ray, of these disturbances are bounded by undisturbed gas as in Fig. C.III.1a.

T he inclusion of combustion further complicates the issue since the rarefaction waves distort and are distorted by the flame front. Despite this difficulty, the analysis is still possible since the interaction of wave and flame can be predicted if the flame is considered to be a temperature discontinuity separating two different gases. This interaction between a rarefaction wave and a contact surface has already been mentioned in Section A (see Fig. A.I.16) and is shown again in Fig. C.III.2. Depending on the properties of contact surface and rarefaction wave either of two interactions can take place. If the temperature ratio across the contact surface is greater than a certain function of the pressure across the rarefaction wave a shock is formed as in Fig. C.III.2b. But, if the temperature ratio is less, only transmitted and reflected rarefaction waves are formed as shown in Fig. C.III.2a. Thus, it may be supposed that the flame could travel through the vessel as shown in Fig. C.III.2c.

The analysis of such a problem is further complicated by the heat of reaction produced at the flame and the interaction of non-planar flames with complicated wave patterns generated in any real vessel. The former difficulty could be overcome by considering the flame as a source of compression waves, whose interaction with the other waves can be predicted, but the latter complication could not possibly be dealt with by normal computational methods.

In an attempt to demonstrate these difficulties, an hydraulic analogue was constructed and the remaining chapters describe briefly the experiments carried out using it. The analogue does not materially assist the solution of the problem but it has served to show some of the difficulties involved.

C.III.2 Waves on liquid surfaces.

Waves formed on the surfaces of liquids can be divided into two groups: those with wavelengths much greater than the depth of the liquid, known as long waves in shallow water and represented by tidal waves; and those in which the disturbances do not extend far below the surface, so that the wavelength is considerably less than the depth, called surface waves. To this latter group belong most wind waves and surface tension waves and it can be shown that tidal waves represent an approximation of this group and can be derived by assuming vertical accelerations to be negligible. The equations so derived show certain similarities with the equations for two-dimensional compressible irrotational gas flow as shown below.

(i) The continuity equations are:

for surface waves

$$\frac{\partial(hu)}{\partial x} + \frac{\partial(hv)}{\partial y} = -\frac{\partial h}{\partial t}$$

where h is the depth of the fluid and u and v are the velocities in the x and y directions respectively;

and for a compressible gas

$$\frac{\partial(\rho u)}{\partial x} + \frac{\partial(\rho v)}{\partial y} = -\frac{\partial \rho}{\partial t}$$

where ρ is the density of the gas and u, v, x, y have the same meaning as above.

(ii) The equations of motion are:

$$h = \tfrac{1}{2}\bar{u}^2 + \bar{V} - \frac{\partial \phi}{\partial t} = \text{constant}$$

where h is the depth,

$\bar{u}$ is the velocity vector,

$\bar{V}$ is the external force vector (in this case gravitational attraction).

and ϕ is the velocity potential;

and for a compressible gas

$$\int \frac{dP}{\rho} + \tfrac{1}{2} . \bar{u}^2 + \bar{V} - \frac{\partial \phi}{\partial t} = \text{constant}$$

where P is the pressure,

ρ is the density and

the other terms have the same meaning.

(iii) The equations for the velocity potential are:

for the hydraulic analogue

$$\left(1 - \frac{1}{gh}\left(\frac{\partial \phi}{\partial x}\right)^2\right)\frac{\partial^2 \phi}{\partial x^2} + \left(1 - \frac{1}{gh}\left(\frac{\partial \phi}{\partial y}\right)^2\right)\frac{\partial^2 \phi}{\partial y^2} - \frac{2}{gh} . \frac{\partial \phi}{\partial x} . \frac{\partial \phi}{\partial y} . \frac{\partial \phi}{\partial x . \partial y} = 0 \; ;$$

and for the compressible gas

$$\left(1 - \frac{1}{a^2}\left(\frac{\partial\phi}{\partial x}\right)^2\right)\frac{\partial^2\phi}{\partial x^2} + \left(1 - \frac{1}{a^2}\left(\frac{\partial\phi}{\partial y}\right)^2\right)\frac{\partial^2\phi}{\partial y^2}$$

$$- \frac{2}{a^2} \cdot \frac{\partial\phi}{\partial x} \cdot \frac{\partial\phi}{\partial y} \cdot \frac{\partial\phi}{\partial x \cdot \partial y} = 0$$

where a = local velocity of sound waves

$= \sqrt{\gamma \mathfrak{R}T}$.

(iv) Discontinuous flow occurs when:

for the hydraulic analogue, the Froude Number is greater than one.

i.e. $\frac{q}{\sqrt{gh}} > 1$ where q is the fluid velocity.

Under these conditions an hydraulic jump is produced and the flow is said to be shooting;

and for the compressible gas, the Mach Number is greater than one

i.e. $\frac{q}{a} > 1$ where q is the velocity of the gas

Under these conditions the gas is said to be travelling at supersonic velocities and shock waves can be produced.

From the above equations it can be seen that, if the following terms are taken to be analagous, the equations are identical.

Depth ratio	$\frac{h}{h_o}$	Density ratio	$\frac{\rho}{\rho_o}$
		Temperature ratio	$\frac{T}{T_o}$
Square of depth ratio	$\left(\frac{h}{h_o}\right)^2$	Pressure ratio	$\frac{P}{P_o}$
Velocity of water wave	$\sqrt{gh}$	Velocity of sound	$\sqrt{\gamma g R T}$
Froude Number	$F = \frac{q}{\sqrt{gh}}$	Mach Number	$M = \frac{q}{\sqrt{\gamma g R T}}$
Streaming flow	$F < 1$	Subsonic flow	$M < 1$
Shooting flow	$F > 1$	Supersonic flow	$M > 1$

The statement that both $\frac{T}{T_o}$ and $\frac{\rho}{\rho_o}$ are analagous to the depth ratio and that the pressure ratio, $\frac{P}{P_o}$, is analagous to the square of the depth ratio requires the additional stipulation that the analogy lies between surface wave phenomena and compressible gas flow phenomena for a gas which has a ratio of specific heats of two.

Under continuous, shockless, conditions the analogy holds quantitatively but when discontinuous flow occurs agreement is no longer possible. It can be shown that the depth ratio across an hydraulic jump is given by

$$\frac{h_2}{h_0} = \frac{1}{2}\left[(1 + 8F^2)^{\frac{1}{2}} - 1 \right]$$

whereas the density ratio across a shock is

$$\frac{\rho_2}{\rho_0} = \frac{\frac{1}{2}(\gamma + 1)\ M^2}{1 + \frac{1}{2}(\gamma - 1)\ M^2}$$

(the Rankine - Hugoniot relation).

For Froude and Mach numbers above 1·5 there is a considerable difference between the two. It follows that, if an hydraulic jump has formed in the water flow, depth measurement downstream of it cannot bear the same simple relation to gas density as in the continuous case. However, this argument does not effect the patterns the waves form and qualitative agreement is still good.

The analogue was first demonstrated by Raboushinski (1934) and the theory has since been extended by Prieswerk (1938) and Laitone (1954). Several problems have been studied using the analogue and some of them are listed below. Subsonic and supersonic flows past models have been investigated by Laitone (1952) and Manabe and Ohira (1955), flow through nozzles and diffusers has been examined by Binnie and Hooker (1937) and Black and Mediratta (1950) and the problem of gas movement in furnaces by Sammons (1949). An attempt has been made to use the analogue in studies of combustion by both Oppenheim (1953) and Glick et al (1954) and an analagous shock tube has been developed by Gilmore et al (1950), Harleman and Ippen (1954) and Harleman (1956) to study the interaction and diffraction of shock waves. In all, except the last, steady-state conditions have been examined. However, the analogue has its most useful application in non-steady-state phenomena where the time dimension is introduced and the advantages of the reduced wave velocity are apparent.

The discharge of gas from a vessel is a non-steady-state process and the analogue can be used to study the changes both inside and outside the vessel. Such an analogue has been constructed and is described in the next two chapters.

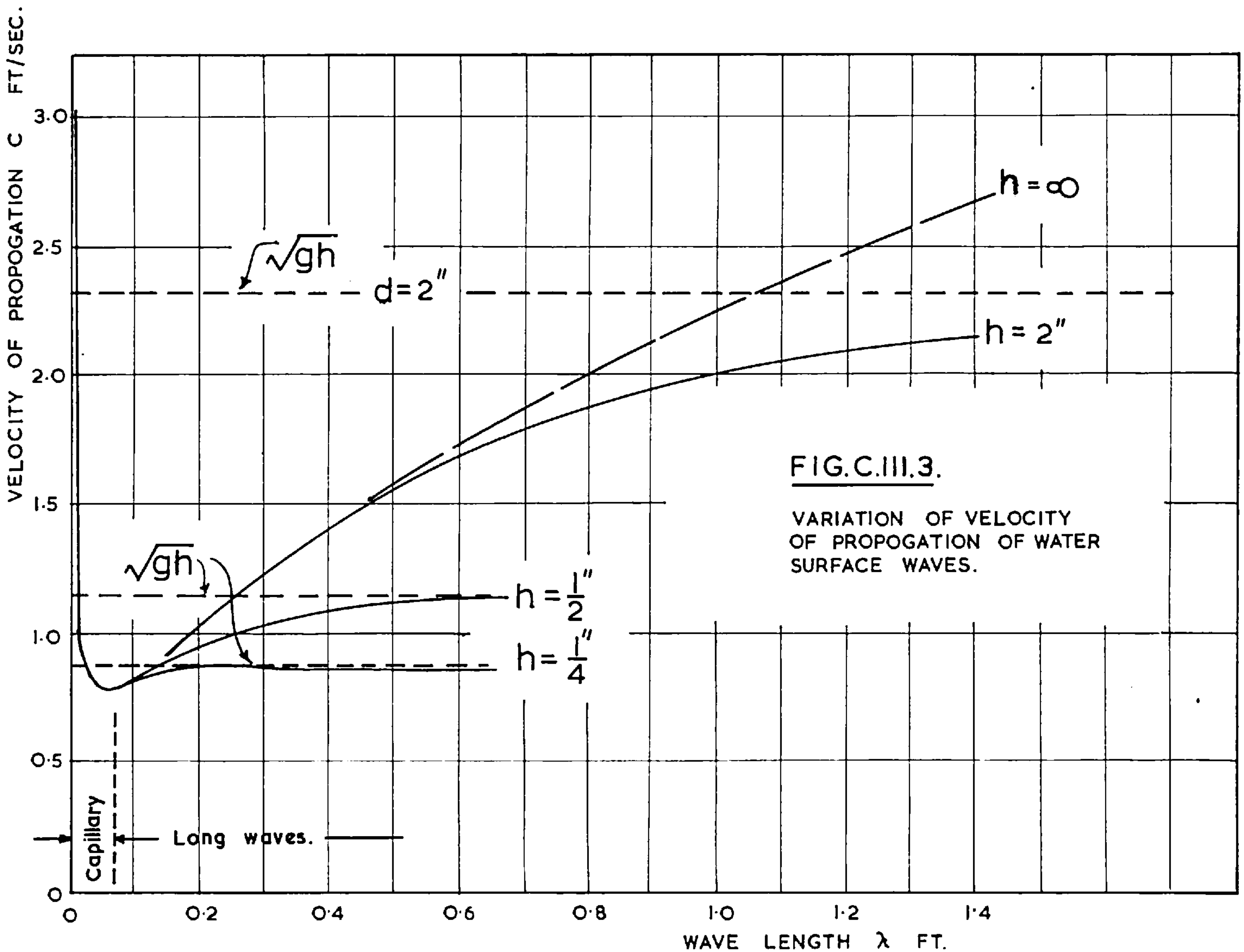

FIG. C.III.3.

VARIATION OF VELOCITY OF PROPOGATION OF WATER SURFACE WAVES.

C.III.3. The construction of the analogue

The three essential features of the analogue are:

(i) The atmosphere into which the vessel discharges. The depth of water representing atmospheric pressure (or more exactly, atmospheric density) must be carefully chosen. It has been pointed out earlier that two types of wave exist depending upon their wavelength and it should also be realised that the second type, the long waves in shallow water, have a velocity of propagation which depends upon the wavelength. The velocity of propagation of any surface wave can be determined from the formula

$$C^2 = \left(\frac{g\lambda}{2\pi} + \frac{2\pi\sigma}{\rho\lambda} \right) \tanh. \frac{2\pi h_o}{\lambda}$$

where C is the velocity of the wave,

λ is its wavelength,

ρ the density of the liquid,

σ its surface tension and

h_o the depth of liquid.

This equation has been derived by Coulson (1955) and is drawn in Fig. C.III.3. The two regions are shown and it can be seen that for depths of $h_o > \frac{1}{2}$" the velocity of the long wave depends upon its wavelength whereas at the depth of $\frac{1}{4}$" the velocity is nearly constant and under these conditions,

$$c^2 = gh$$

For this reason, the "atmospheric" depth of water in the analogue was made $\frac{1}{4}$".

The presence of capillary waves in the analogue does not effect the results as long as the water depth is of the correct magnitude but they are a nuisance when it comes to analysing photographic records.

With such a thin layer of water it was necessary to ensure that the surface used in the analogue was both flat and level. A frame was constructed from aluminium channel over which were distributed sixteen screw jacks. These jacks supported a plate glass sheet 6' x 3' and they were adjusted until the glass was as flat as could be ascertained by a workshop straight edge. The aluminium frame was supported on a table by three adjustable screws and these were used to level the glass sheet. Once the sheet had been levelled further supports were added to ensure that no change in level occurred.

Initially, the depth of water was maintained by perspex walls and a $\frac{1}{4}$" weir at one end. However, it was found that the waves were reflected from the walls and interfered with flow patterns. To eliminate these wall effects the water level was maintained by rubber strips, $\frac{1}{8}$" thick stuck on the glass near the edge. A meniscus was formed on these strips, by coating them with petroleum jelly, and $\frac{1}{4}$" depth of water was obtained. When the waves reached the edge they broke the meniscus and the excess water was drained away by a gutter placed round the glass sheet. Once the wave had passed, the meniscus reformed and "atmospheric" conditions were maintained.

(ii) The vessel.

The vessel consists of four perspex walls fixed to the glass sheet by plasticine. It is rectangular in shape - 16" long and 9" wide - so that the analogue can be examined using a squat or long vessel. Hence, provision is made to fit the vent in either side of the vessel.

(iii) The vent.

To produce an analagous state of affairs the vessel must be filled with water to a given level and a gap in the walls opened suddenly to discharge the water. This was achieved by making the vent in the form of a shaped "orifice" closed by a lifting gate.

A stainless steel plate slides in grooves in the uprights supporting the shaped vent walls. These walls just touch the sliding plate on knife edges making a water tight seal. The gate is raised by a rod passing through the lintel of the supporting

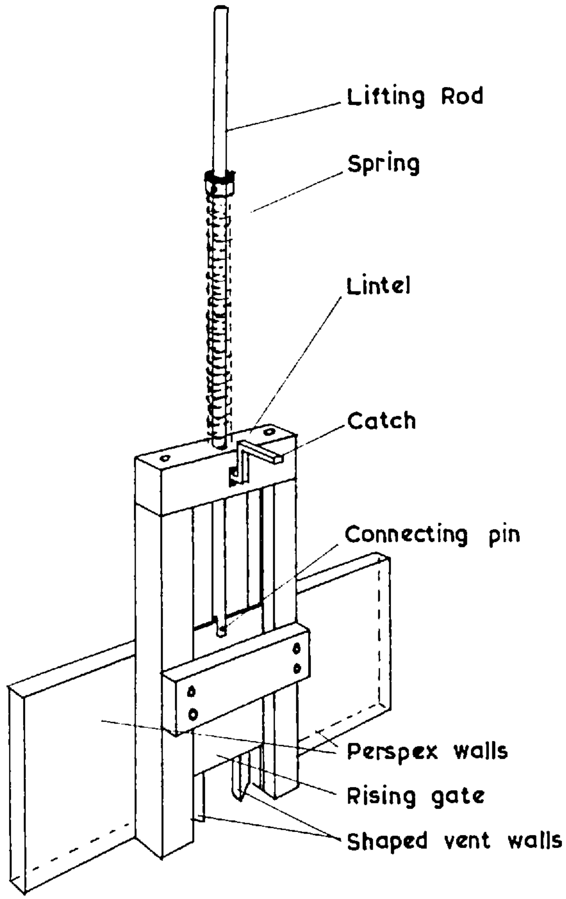

FIG.C.III.4.

VENT for HYDRAULIC ANALOGUE

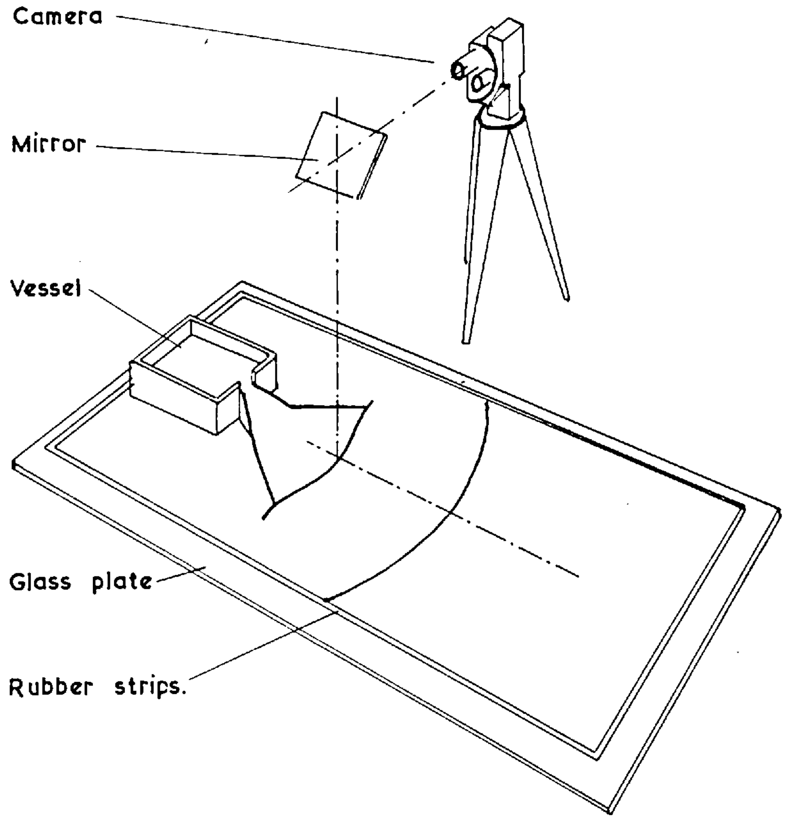

FIG.C.III.5.

WATER TABLE

arch and loaded by a spring to lift the gate. The plate is attached to the lifting rod by a pin through an elongated hole. This allows the plate to rest on the glass sheet representing the base of the analogue and prevents leakage below the gate. The gate is held closed by a catch which engages on the rod. A tap on the end of the lever dislodges the catch and the gate rises. The tap is provided by a solenoid and spring so that the gate can be opened without touching the vessel.

The time taken for the gate to open has been measured and, although there is some variation in this interval, it is less than 50 m.secs. Two sets of vent walls have been constructed so that the discharge width can be one or two inches.

(iv) The recording of wave patterns and the measurement of water depth inside the vessel.

The formation of the jet in the vent was investigated photographically. The photographic technique is best described with the aid of Fig. C.III.5. A cine camera was used to observe, through a mirror, the field ahead of the vessel. The camera and the gate catch were operated simultaneously and the wave patterns on the glass recorded. The table could be lighted from above or below and a centimetre grid was used as a background to facilitate spatial measurements. A thirty seconds timer was placed in the field of view of the camera

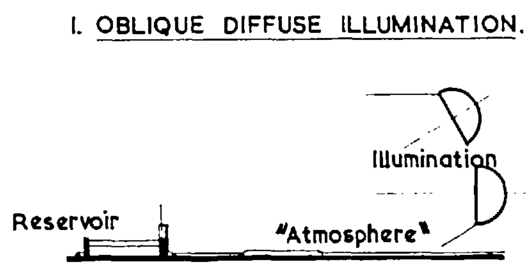

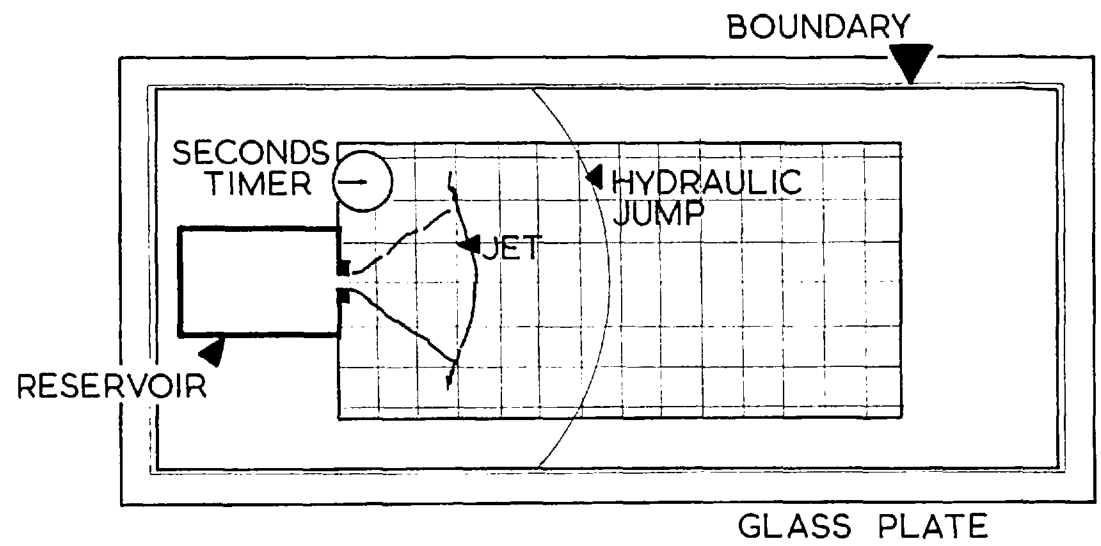

FIG.C.III.6

Water Table (plan)

so that independent timing was available. The overall picture, as seen by the camera, is shown in Fig. C.III.6. Three techniques were used to illustrate different facets of the phenomenon and they will be described in the section dealing with the experimental results.

The depth of liquid in the vessel was measured electronically using the proximity meter described in section A. The water surface constituted the earth plate of the condenser and the live end was supported over the water in the vessel. The change in output from the proximity meter was recorded on an oscilliscope using a drum camera. Unfortunately the calibration of the depth probe is non-linear (see Fig. C.III.7) and the gain of the amplifying circuit had to be increased as the depth fell. The resultant recording is shown in Fig. C.III.7 together with the derived pressure-time curve.

Although the analogue was intended as a tool for examining the effect of waves within the vessel a great deal of the work concerned the formation of the jet outside the vessel. Also, difficulties in measuring and photographing the waves in the vessel precluded any extensive investigation into these effects and the experimental programme was concluded with the examination of the reflection of an hydraulic jump in a series of obstructions. These two aspects are described very briefly in the chapters that follow.

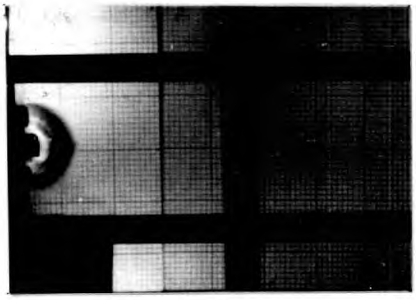

a

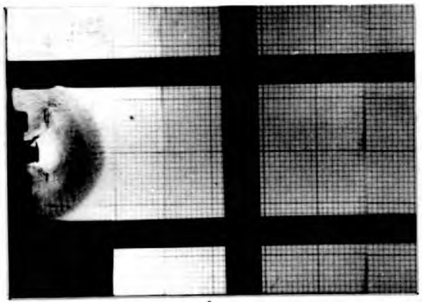

b

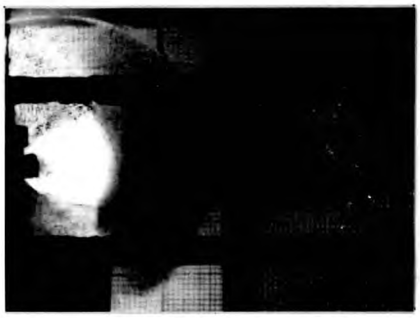

c

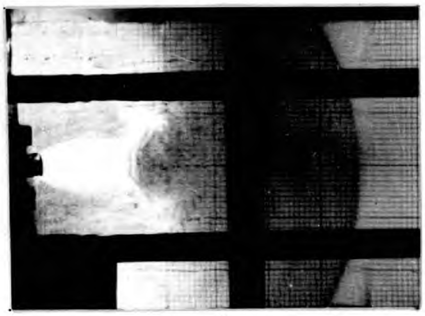

d

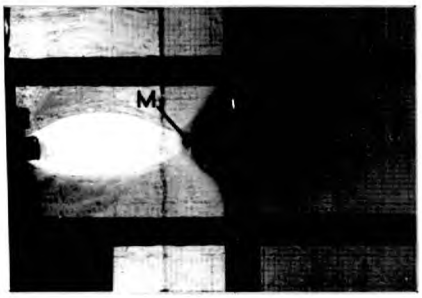

e

f

g

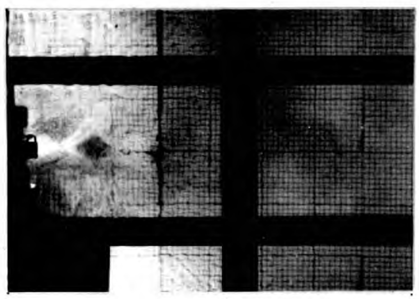

h

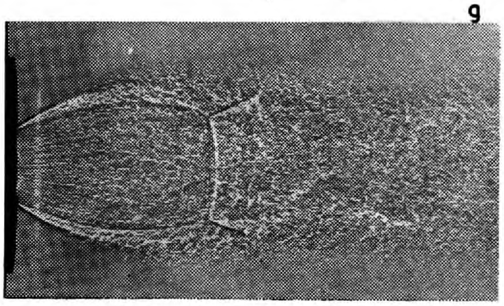

II REAR DIFFUSE ILLUMINATION

FOR DEMONSTRATING DEPTH VARIATION

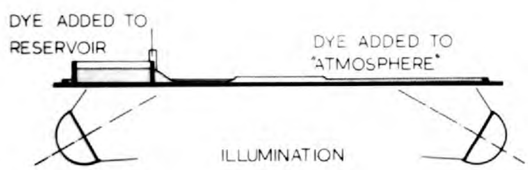

PLATE X Hydraulic Analogue

RUN No. 20/125/1 INITIAL DEPTH 1·25 ins ORIFICE WIDTH 1 in.

C.III.4 The formation of the jet and the expanding shock wave.

In Plate X a series of cine photographs have been reproduced showing the main phases in the jet formation outside the vessel. In these experiments a die was added to both the water in the vessel and the surrounding layer and the water table was lit from below as shown in the diagram. The light transmitted through the water is a function of its depth so that light areas in the photograph represent shallow water which is analagous to low density (i.e. low pressure) regions. Since the simplified energy equation is

$$gh + \frac{1}{2} q^2 = \text{constant}$$

these areas also represent regions of high velocity.

The first photograph shows the formation of a circular region of liquid expanding into the atmosphere and the second and third show how this region expands in a uniform manner throughout the field. The third photograph in the sequence also shows the formation of a jet and its subsequent expansion to full size is illustrated in (d) and (e). The jet shown in (e) can be compared with the photograph of a gas jet under similar conditions taken by Fraser et al (1957). The last three photographs show the contraction of the jet

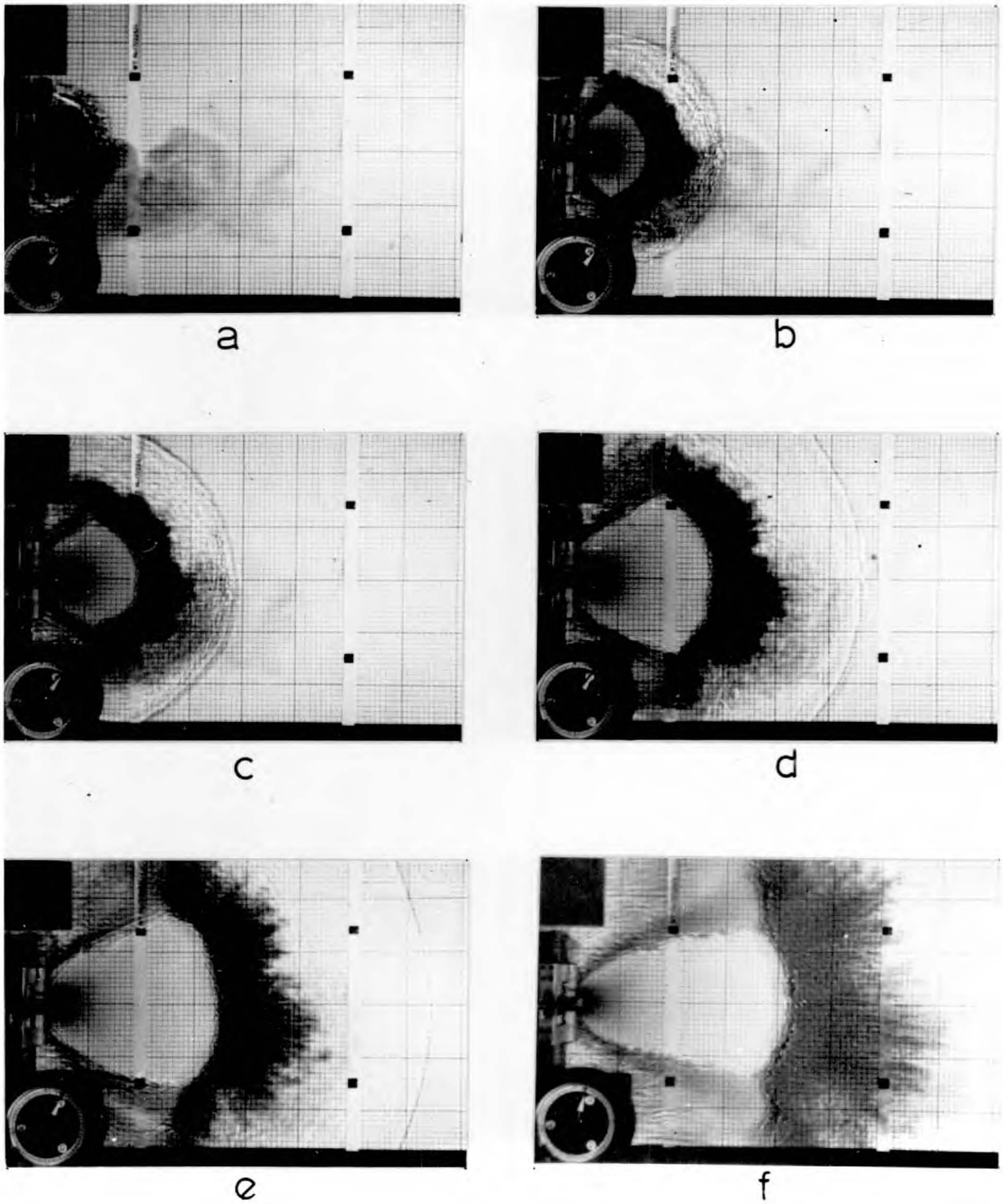

PLATE XI

Hydraulic Analogue

RUN No. 17/225/1
INITIAL DEPTH 2·25 ins
ORIFICE WIDTH 1 in

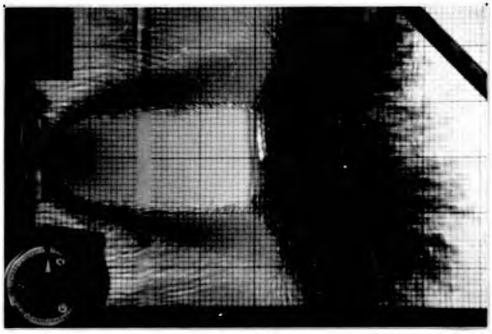

g

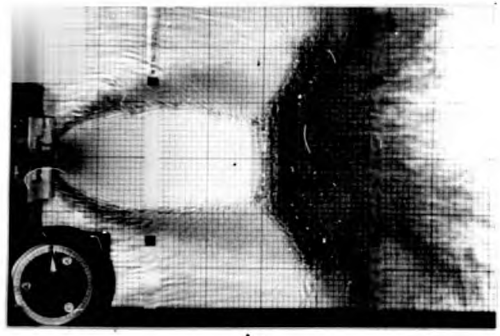

h

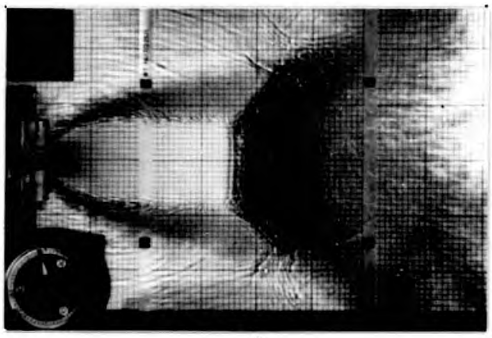

i

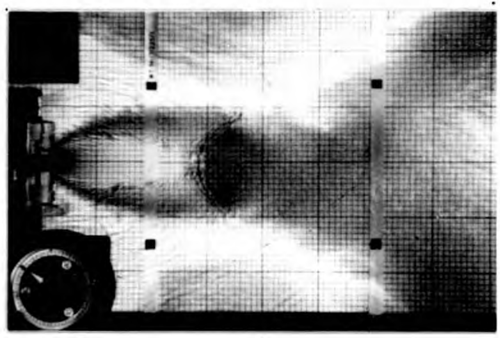

j

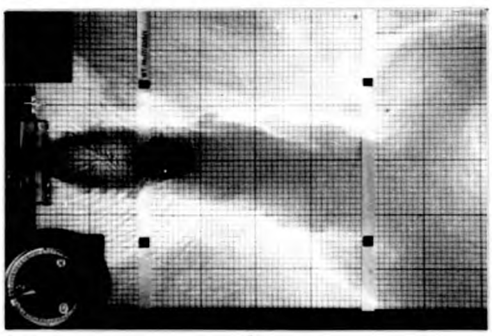

k

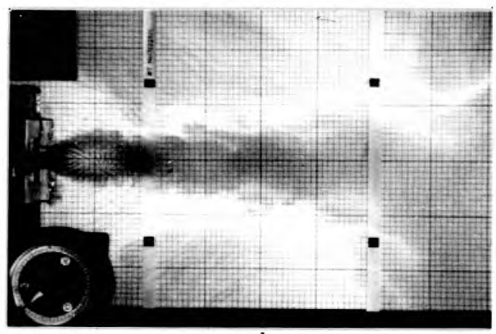

l

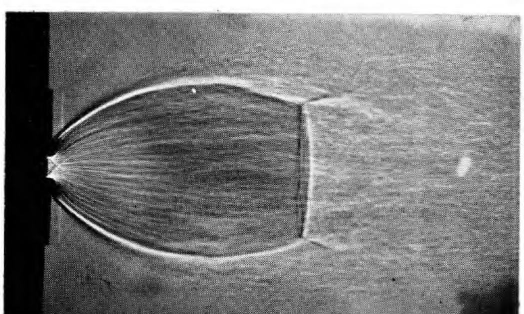

III OBLIQUE DIFFUSE ILLUMINATION

FOR DEMONSTRATING JET DIFFUSION

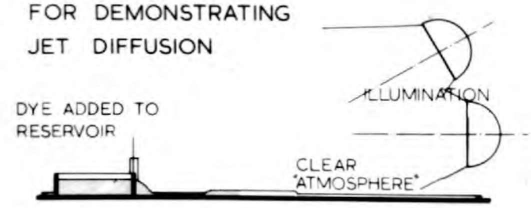

as the pressure in the vessel falls.

A number of important points are illustrated in this sequence. Firstly, the uniformity of the high pressure region behind the shock can clearly be seen especially in the later stages of the expansion. Also, the initial formation of the jet as depicted in (c) shows a wide fan not met with in steady-state gas flow. However, the analagous phenomenon of the formation of a gas jet has not been obtained experimentally and it is possible, in view of the closeness of the analogue in other phases, that a rapidly expanding jet is formed originally.

The discontinuity in the jet equivalent to the Mach Bridge is clearly visible at M in (e) and demonstrates the change from low pressure high velocity flow up stream to the relatively high pressure low velocity flow down stream.

These recordings do not show the boundary dividing the fluid that was originally in the vessel from the fluid originally forming the atmosphere. Hence, the jet boundary cannot be determined and the expanding sheet of fluid coming from the vessel cannot be differentiated from the atmospheric fluid between the expanding discontinuity and the jet. These boundaries have been marked by filling the vessel with water to which a die has been added and leaving the atmosphere clear. With lighting from above both the boundaries and the presence of waves on the surface are defined. The contact surface (boundary) between the expanding air from the vessel and the compressed atmosphere is well defined and it can be seen that there is a distortion of this boundary due to the instability inherent in an accelerating wall of fluid as discussed by Taylor and Lewis (1950). This distortion can also be seen in the photographs of the expanding gases when a disc bursts as described in Section A and shown in Plate VI.

These photographs also show the position of the jet boundary throughout the discharge. The results again agree with those for gas jets as a comparison with the photograph taken from a paper by Fraser et al shows.

It can be concluded from these results that the analogue represents two-dimensional gas flow in most respects and that it can be used qualitatively to demonstrate phenomena connected with the discharge of gases from a vessel. Further information on the expansion of the jet may be of importance to determine the analagous gaseous expansion but it was felt that this has little bearing on the present problem and information on wave formation within the vessel is of more use.

FIG. C.III.7.

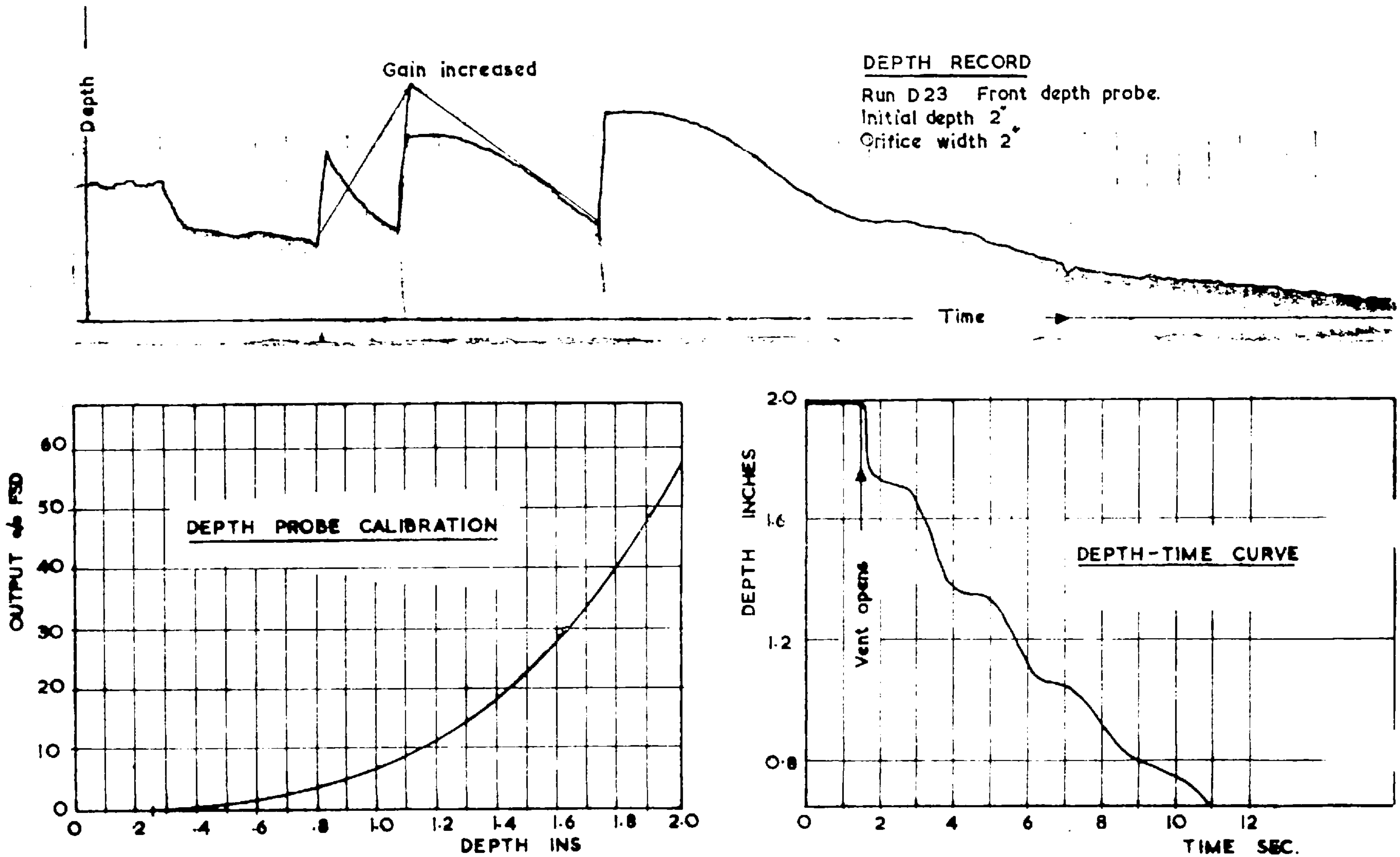

Gain increased
Depth
Time
DEPTH RECORD
Run D23 Front depth probe.
Initial depth 2"
Orifice width 2"
DEPTH PROBE CALIBRATION
OUTPUT % FSD
DEPTH INS
DEPTH-TIME CURVE
DEPTH INCHES
Vent opens
TIME SEC.

C.III.5 Wave formation within the vessel.

The pressure variation in the vessel is shown in the recording in Fig. C.III.7. The wave motion is quite clear and as with the case of the gas the frequency changes as the efflux continues. The length of the wave also increases with time and this would be expected from the expanding rarefaction wave. An attempt has been made to interpret, on the basis of observations made during the experiments, the wave motion in the vessel. Fig. C.III.8 depicts this result in terms of the depth-time and position-time diagrams discussed earlier. The velocity of the wave, represented by the slope of the lines in the x-t diagram, has been derived from the depth-time curve and the resulting wave pattern appears to correspond with the depth variation. However, due to the three dimensional effects, no exact representation is possible using this simple analysis. For this reason these experiments were discontinued and an investigation into the reflection of waves within the vessel commenced. The expansion waves in the vessel could not be photographed because of the small changes in depth. Instead, the reflection of a compression wave in a vessel was examined and the series of photographs shown in Plates XII, XIII and XIV obtained.

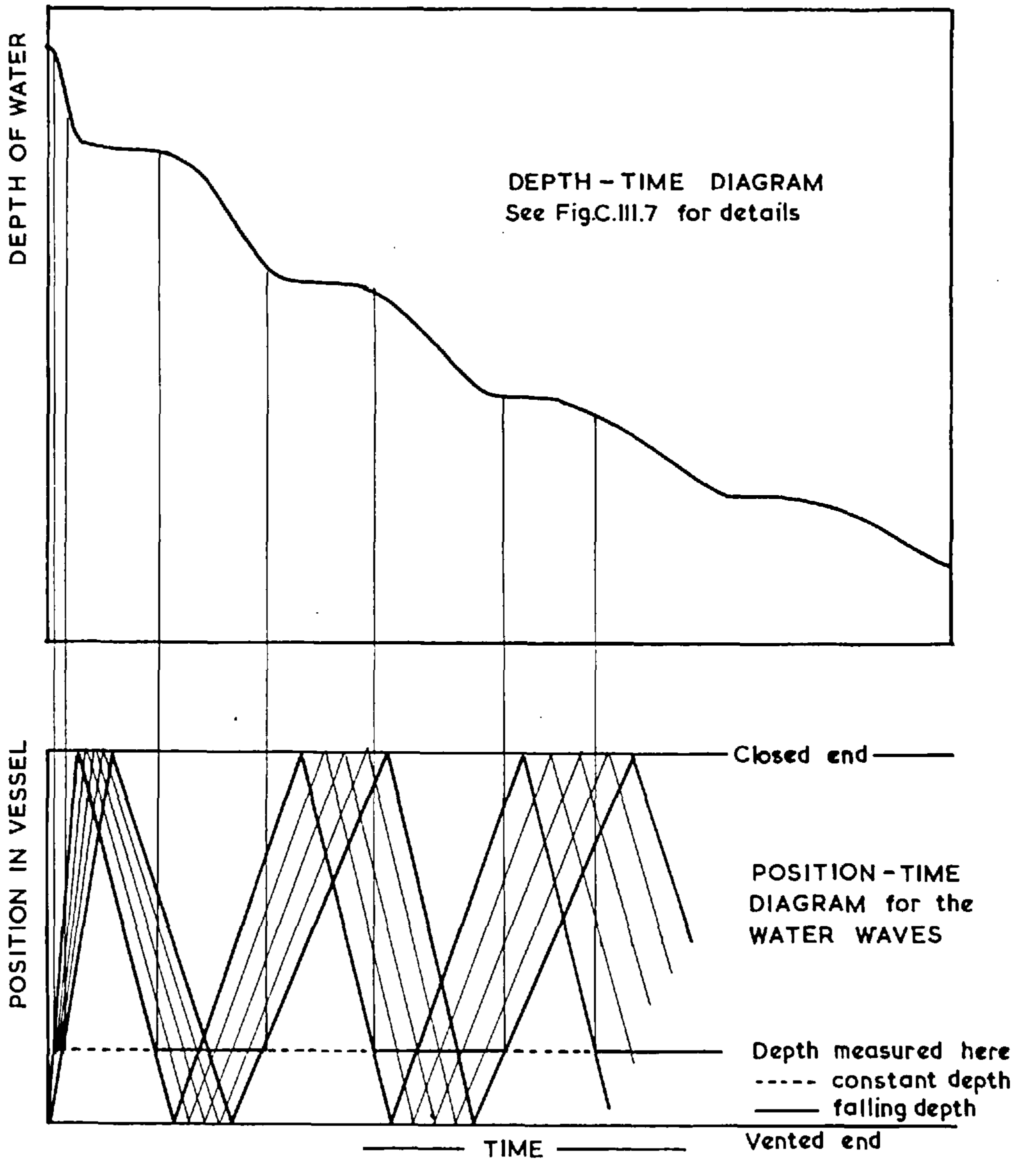

DEPTH OF WATER
DEPTH - TIME DIAGRAM
See Fig.C.III.7 for details
POSITION IN VESSEL
Closed end
POSITION - TIME
DIAGRAM for the
WATER WAVES
Depth measured here
----- constant depth
—— falling depth
Vented end
TIME

FIG.C.III.8.

Plate XII shows the simple reflection of a curved wave from a wall in which the reflected wave is the same shape as the incident wave.

Plate XIII shows the reflection within a semi-infinite vessel and the formation of a plane wave travelling between the parallel walls. It also shows the secondary waves which are reflected from the walls. These waves have been discussed by Glass (1950) and it is of interest to see them produced so exactly in the analogue.

Finally, in Plate XIV a more complicated system has been examined and the reflection and re-reflection of waves in a triangular vessel photographed. The complicated interaction leads to a system of multiple waves and it is clearly demonstrated how difficult any analysis must be.

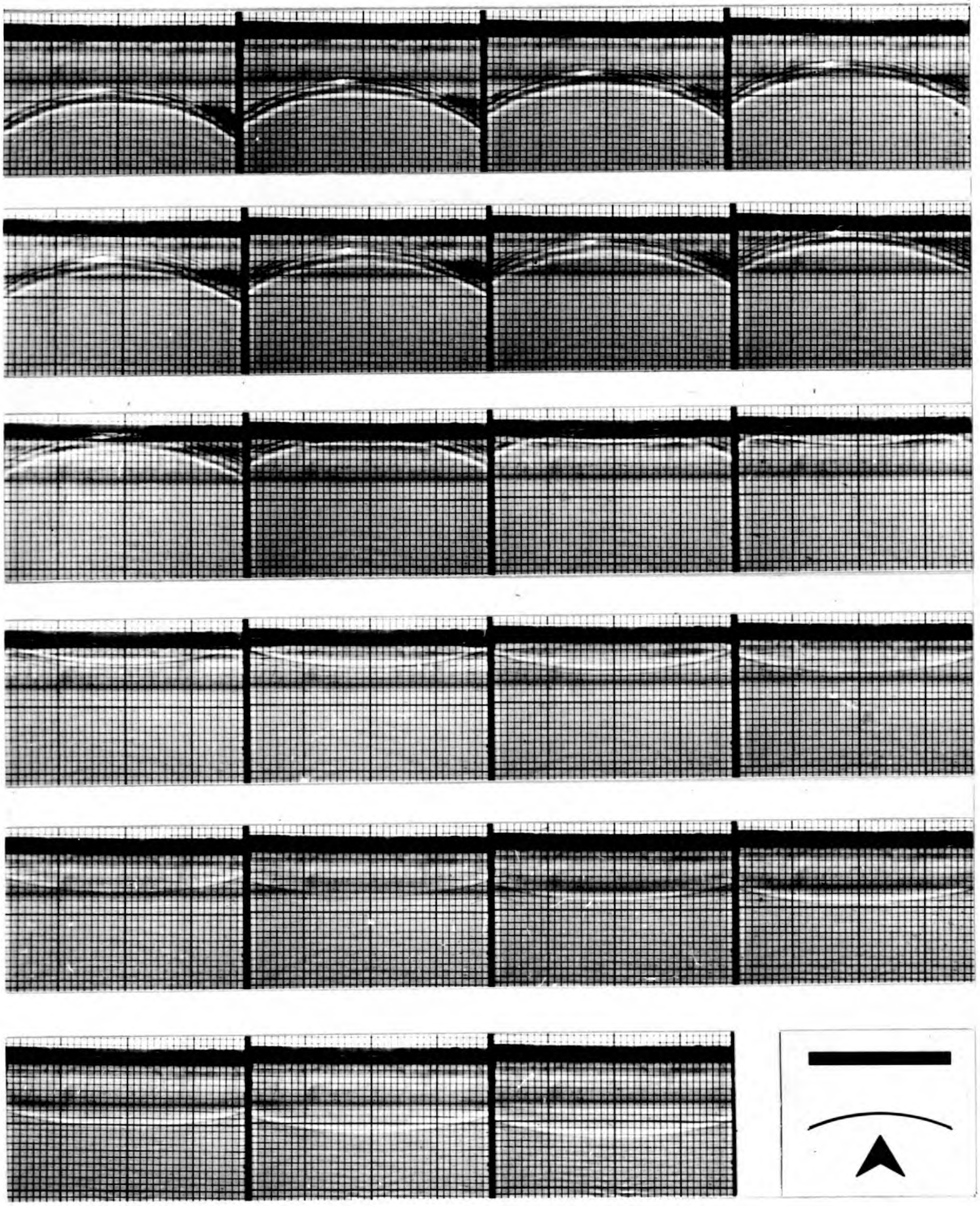

PLATE XII. Wave reflection 1.

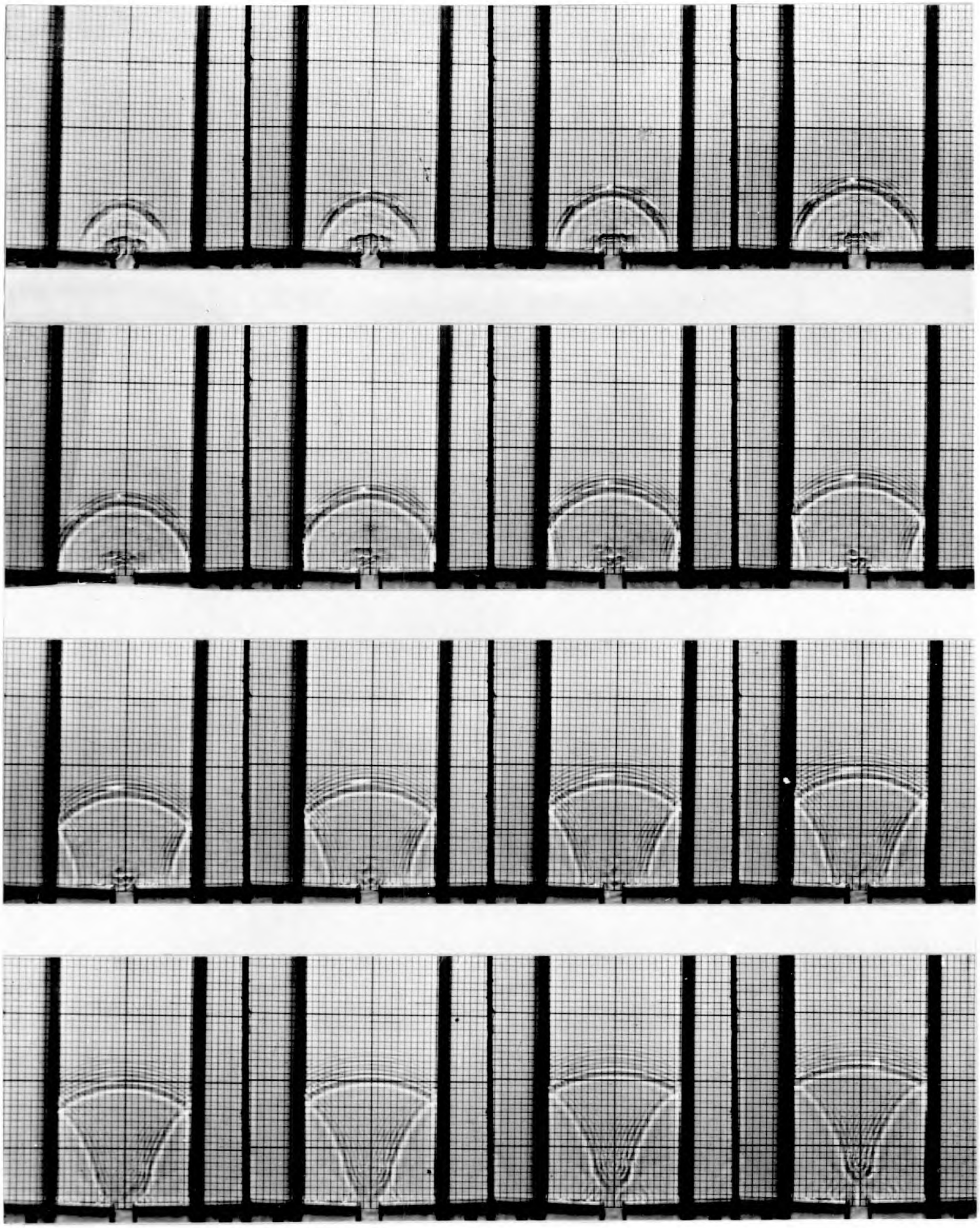

PLATE XIII. Wave reflection 2

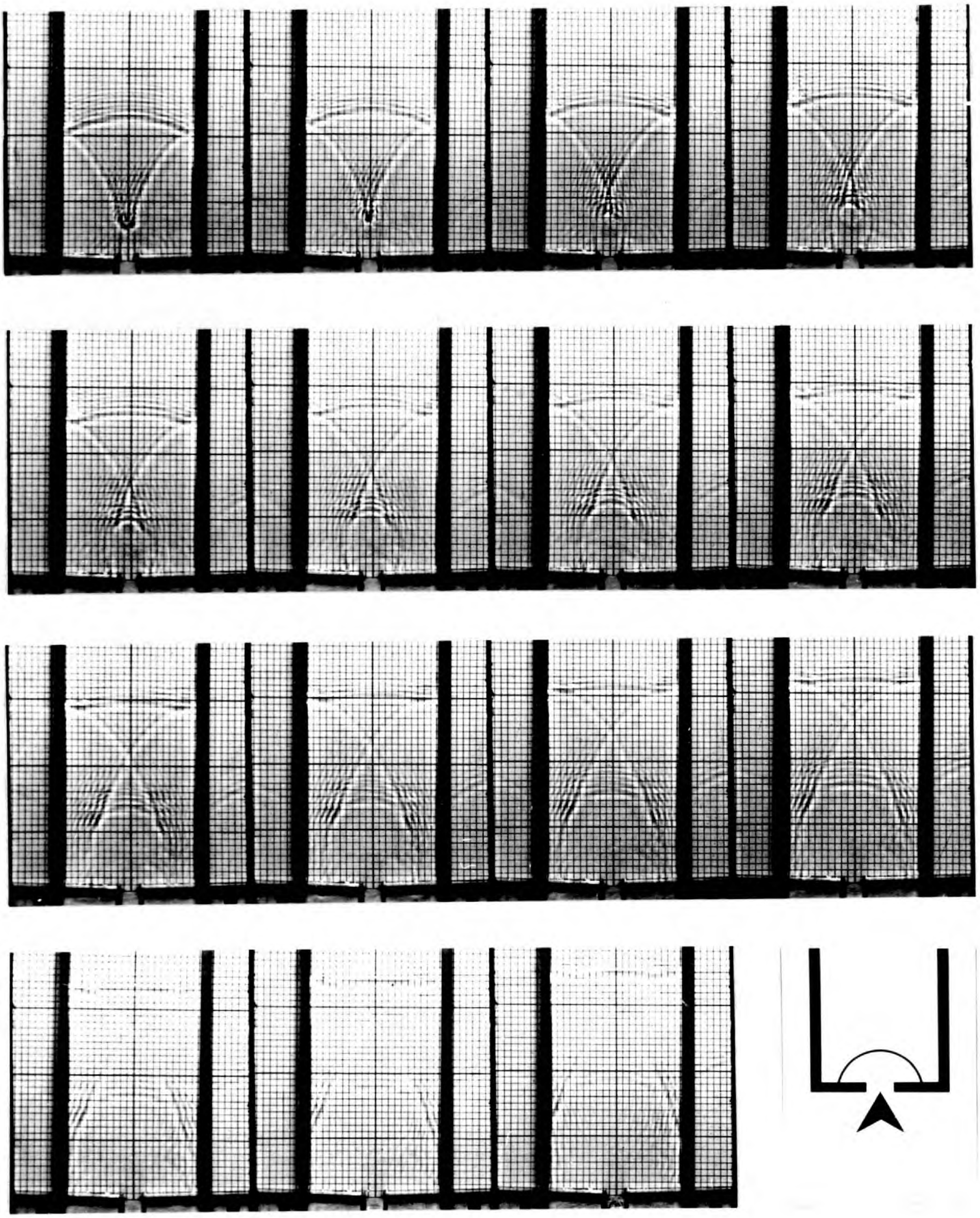

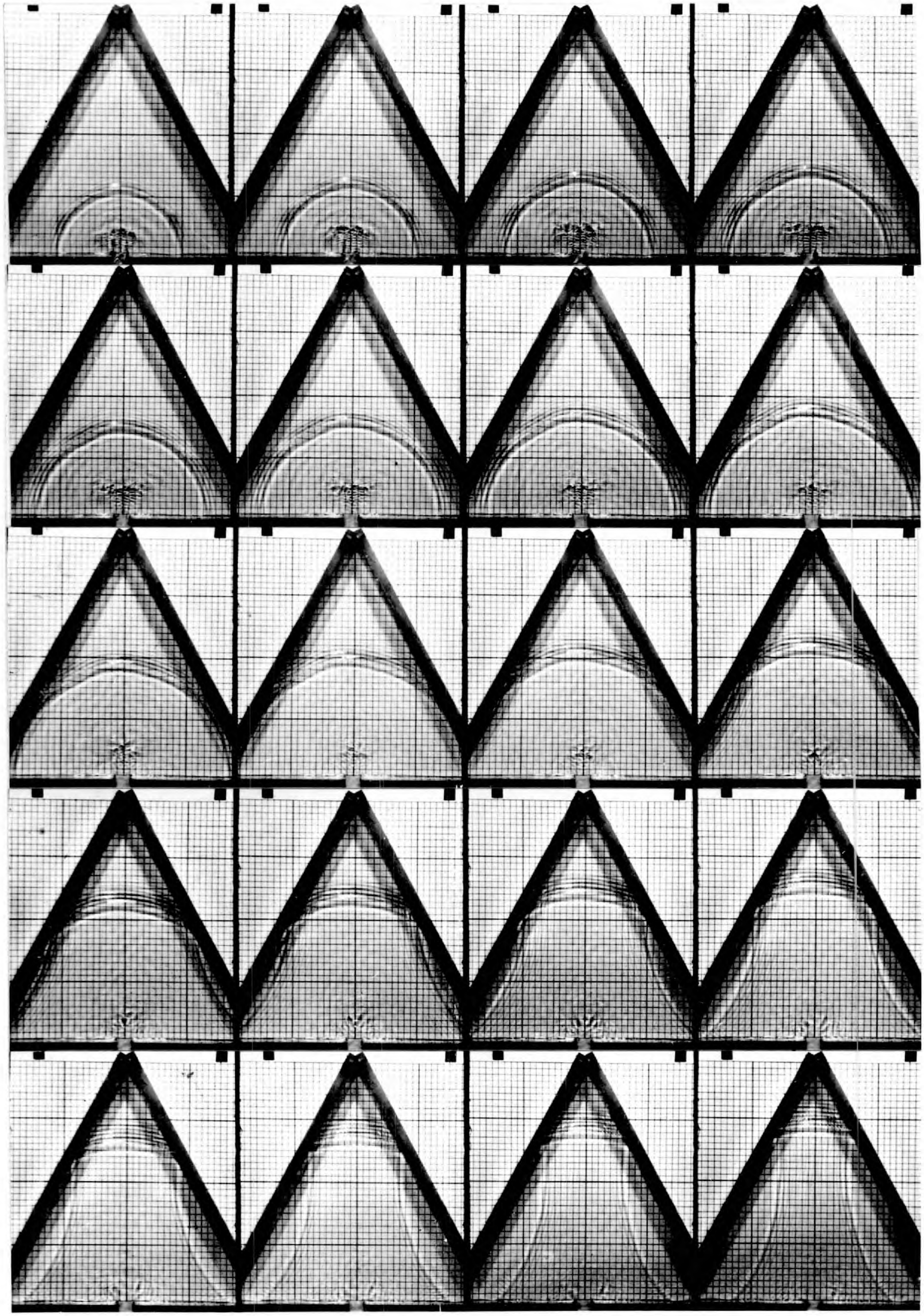

PLATE XIV. Wave reflection 3.

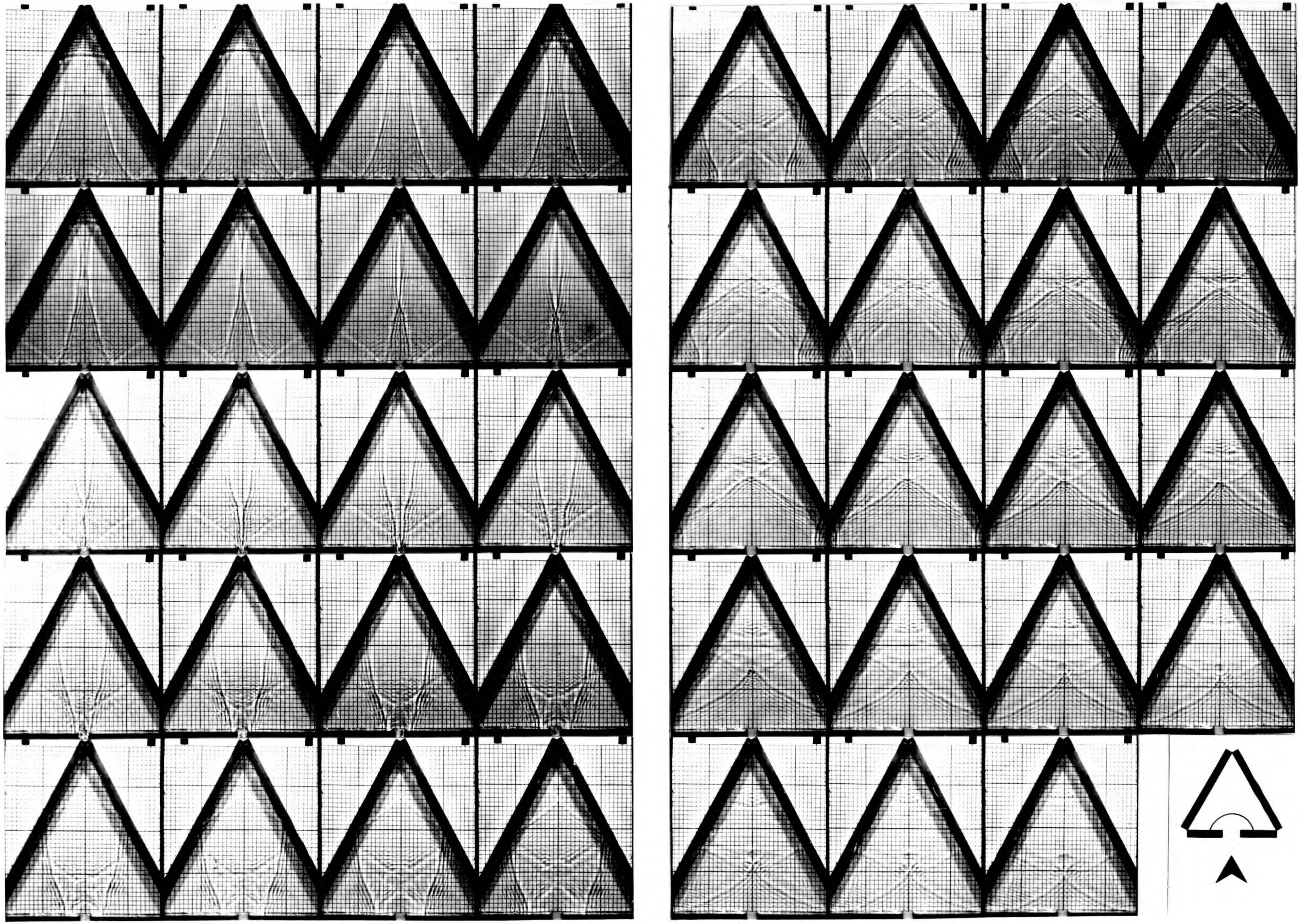

CHAPTER C.IV CONCLUSIONS

In this section an attempt has been made to calculate the optimum size for the vents. A simple analysis has proved successful provided the effect of turbulence is accounted for and an empirical relation between a correction factor for turbulence and the vent size is suggested. The more complicated analysis including the effects of waves has not been attempted although a possible method has been discussed. The difficulties involved in such an analysis are illustrated using an hydraulic analogue.

Hence, predictions of explosion pressures must at present be made using the simple theory and the method is outlined below.

Information is required concerning the nature of the explosive mixture and this is best obtained using a spherical vessel with central ignition. The final pressure and the maximum rate of pressure increase can be obtained from experiments on the spherical vessel and used to determine:

$$b = p_e - 1$$

where $p_e = \dfrac{P_e}{P_i}$,

P_e = final pressure and

P_i = initial pressure; and

β = the exponent in the pressure-burning-rate equation and given by

$$\left(\frac{d\,p_e}{dt}\right)_{max} = \frac{3.b.Su.}{R} \cdot p_e^{\beta}$$

where R = radius of the vessel and

Su = fundamental burning velocity

These results can be used for any vessel if the following dimensionless terms are used

$$p = \frac{P}{P_i} = \frac{\text{Pressure at given instant}}{\text{Initial pressure}} ;$$

$$\tau = C.\frac{Av}{V}.t ;$$

$$H = k\frac{Su}{C} ; \quad k = \text{correction factor for turbulance;}$$

and $$\alpha = \frac{A}{Av} ;$$

where

$$C = \left(\frac{2}{\gamma + 1}\right)^{\frac{\gamma + 1}{2(\gamma - 1)}} . \times (\text{Initial velocity of sound}),$$

Su = Fundamental burning velocity,

V = Volume of the vessel

Av = Surface area available for fixing vents and

A = corrected discharge area of the vent.

The term $\frac{Av}{V}$ has a special significance as it is a measure of the extent the vessel deviates from being spherical. Thus for vessels which have an aspect ratio less than three this term has a value

$$\frac{V}{Av} = \left(\frac{1}{z + 2}\right) . R$$

where $z = \frac{\text{Vessel diameter}}{\text{Vessel length}}$

$= \text{aspect ratio.}$

In vessels with aspect ratios greater than three the conditions approach one-dimensional and the available area, Av, is equal to the area of the ends on which vents operate. i.e. Av equals the cross-sectional area of the vessel when one end is vented and Av is twice the cross-sectional area when both the ends are vented.

The correction factor, k, is determined empirically and since experimental evidence is not yet available it is suggested that the relation between k and a Reynolds number shown in Fig. C.II.6c is used. The Reynolds number, Re^{*} is that for the flow through the vent under sonic conditions at the initial pressure in the vessel.

$$\text{i.e.} \quad Re^{*} = \frac{u\,D\,\rho_i}{\mu_i}$$

where u = velocity in vent

$= C,$

μ_i = the viscosity,

D = vent diameter,

ρ_i = density in vessel at $P = P_i$

The diagram in Fig. C.II.6c has been obtained from results for propane-air mixtures in a particular vessel and may not be applicable in all cases and this is one of the points of the theory which will have to be tested.

The most important equation derived in the analysis is that determining the safe venting area ratio, α_c.

$$\text{i.e. } \alpha_c = H.b.\ p_o^{\left(\beta - \frac{3\gamma-1}{2\gamma}\right)} \quad \text{for } z \leqslant 3$$

$$\text{and } \alpha_c = \frac{Af}{3Av} . H.\ b.\ p_o^{\left(\beta - \frac{3\gamma-1}{2\gamma}\right)} \quad \text{for } z > 3$$

where p_o = pressure ratio at which the vent opens,

Af = area of flame

= 2 or 4 times the vessel cross-section for one and two flames respectively and

S is a coefficient which depends upon the position of the vent and the point of ignition.

S/Af is therefore a criterion for the placing of the vent. Fig. C.II.2b gives the values of S/Af for a number of ignition positions and vent locations and it can be seen that:

(a) If the source of ignition is known the vent should be placed near it

(b) If the source is not known a number of vents should be distributed over the vessel.

The other equations can be used to predict the pressure variations and flame position but, if the equations for the area of the vent under safe venting conditions can be verified the others become unnecessary for the practical design of pressure relief vents.

CONCLUSIONS

The investigations described in this thesis were carried out with a view to obtaining data for the design of valves required in the protection of pressure vessels. A generalised form of the equations of motion has been established and the individual sections of the thesis deal with the determination of the functions in these equations under different conditions of valve operation. The equation of motion is:

$$\phi\,(P,T).f(X_i) - R(X_i) = \sum_j \left(\frac{\partial^2 X_i}{\partial t^2}\right)_j w_j$$

for the principal directions i = x, y, z.

where $\phi\,(P,T).f(X_i)$ represents the resultant force on the obstruction due to the passage of gas through the valve,

$R(X_i)$ represents the resultant of the system of forces retaining the obstruction in the vent,

$\sum_j \left(\frac{\partial^2 X_i}{\partial t^2}\right)_j w_j$ represents the resultant of the acceleration forces;

The following discussion is divided into two sections dealing with slowly changing pressures (equilibrium conditions) and rapidly changing pressures (dynamic conditions).

I Equilibrium conditions.

When the pressure changes slowly the rate of change of momentum of the moving parts of the valve is small and the equations of motion are:

$$\phi\,(P,T).f(X_i) = R(X_i)$$

The function $\phi\,(P,T)$ represents the relation between the thrust and the pressure and temperature in the vessel and these will depend upon the rate at which the gas is discharged from the vessel and the rate of increase in pressure. For slowly changing pressures a steady-state material balance supplies the necessary information for calculating these properties if the discharge characteristic of the particular valve is known. The characteristics have been determined experimentally for bursting disc valves and a simplified model of the spring loaded diaphragm valve.

In the former case it has been shown that the shape of the bursting disc holder plays an important part in the discharge process and that the rate of discharge is a maximum when the entry to the valve has a radius of curvature equal to half the valve diameter. Under these conditions the flow rate is about 95% of the maximum flow rate obtainable.

Theoretical considerations have been introduced to show that this result is to be expected although a quantitative analysis is not possible.

The discharge rates through spring loaded valves have also been determined experimentally. Theoretical estimates of the flow rate through the vent area have been made for one design of valve to show the deviation from one-dimensional inviscid flow but only measured values of effective flow area are quoted as a function of valve head displacement.

The movement of the valve depends upon the functions $f(X_i)$ and $R(X_i)$ and the two types of valve represent the complementary facets of two similar problems. The bursting disc valve remains closed during deflection and the function $f(X_i)$ is the area in the term representing the force exerted by the gas pressure and can easily be calculated. The term $R(X_i)$, however, depends upon the stress in the disc and hence on the degree of deformation and is computed only with considerable difficulty. By making certain simplifications a solution to the equation is possible but, since a knowledge of the deformation process is not required, a full analysis of the equilibrium deformation has not been attempted. The analysis has been restricted to the point of rupture at the pole of the deformed disc and the static bursting pressure has been calculated from the mechanical properties of the disc material. Using a graphical method, suitable when the physical data is in the form of an experimental curve, the instability strain, and hence the bursting pressure, has been determined for copper, aluminium and brass and these results compare well with both experimental and theoretical values reported by other workers.

In the case of the spring loaded valve the function $R(X_i)$ depends upon the valve head displacement and is computed from the spring strength and the design of the loading mechanism. The unknown function is $\phi\,(P,T).f(X_i)$ which will depend upon the shape of the valve head and the vent as well as on the displacement of the valve head. No attempt has been made to calculate this function but the thrust on several different valve heads has been measured and the functions $\phi\,(P,T)$ and $f(X_i)$ are expressed as a single curve for each of them.

By combining these results with the discharge rates past the valve head the performance of the spring loaded valve has been analysed and a graphical method is used to illustrate the function of three different types of loading mechanism. It is concluded that the direct loaded valve is the most inefficient of the three and that an indirect loading system is required which will give a load which decreases with displacement.

II Dynamic conditions.

The rate of change of momentum must now be included in the equations of motion. In addition all the other functions may take another form and each will be considered separately.

The first term, $\phi(P,T).f(X_i)$, will alter on two counts. Firstly because the gas and valve parts are moving at considerable speeds and a correction has to be applied to account for their relative motions. Analyses on the basis of gas dynamics are possible but require a knowledge of the valve motion. This means that the equations of motion must be solved without considering these effects and a subsequent correction made once the magnitude of the rate of valve opening is known. Secondly the properties, P and T, of the gas in the vessel are continually changing and will be effected by the valve performance. As a first step to the solution of the problem the pressure change has been stipulated as an instantaneous rise from ambient to some fixed proportion of the valve operation pressure. But, since these valves are to be considered in relation to explosion relief, a detailed survey has been made of possible analyses of the pressure changes involved in vented explosions. A simple theoretical analysis has been established and it is suggested that this should be the first step to a more rational approach to the subject. The theory has been used to compute pressure changes for explosions on which experimental data is available and agreement is good. The effect of venting these explosions has been examined and the problem tackled on the basis of wave phenomena. However, it can be concluded that a solution on this basis is impracticable and it has been shown, using an hydraulic analogue, that the analysis involved would be both lengthy and complicated. Instead a semi-empirical method is suggested and, on the results examined in this thesis, it can be stated that there is at least some possibility of a correlation on this basis for explosion data to be used in the design of pressure relief by venting.

The term $R(X_1)$ is fixed by the restraining system and in the case of the spring loaded valve can be assumed to remain unchanged. But, in the case of the disc it will depend upon stresses and hence on the deformation. Thus, this term cannot be considered separately and will form an implicit part of the solution.

Similarly, the term representing the rate of change of momentum can be determined in one case as an explicit relation involving the velocity of the moving parts of the valve whereas, for the disc, only an implicit solution is available since the mass of individual elements depend upon their thickness (state of strain).

Thus, for the spring loaded valve the equations of motion have been solved on the assumption that the thrust-displacement relation is not affected by the velocity of the valve head. The response of such a valve to the application of a shock load has been calculated and it is shown that the valve opening rate depends on the type of loading and the relative mass of the moving parts.

The more complicated equations obtained in the case of a disc do not yield an analytical solution except when the equations are simplified by assuming the material to be perfectly plastic. This stipulation leads to a differential equation representing the traverse of an "inertia" wave across the disc. The inclusion of strain hardening effects cannot be accounted for in the simple solution and the experimental investigation of shock loaded discs was carried out in an attempt to elucidate the true mechanism of deformation. It has been shown that the presence of strain hardening modifies the "inertia" wave in certain definite ways. These can best be accounted for by postulating the presence of a strain wave which travels through the disc at a velocity dependent on the magnitude of the strain. Since the velocity of the inertia wave also depends upon the strain intensity the interaction of these two waves will control the deformation process. Information on the propagation of strain waves is limited to the one-dimensional case and therefore the problem has been reduced to the consideration of the dynamic deformation of a wire under the influence of a suddenly applied magnetic field. A qualitative analysis indicates the possible mode of deformation and this appears to agree with the experimental measurements.

The results have been correlated in terms of the initial acceleration of the disc centre and the maximum dynamic deflection so that knowing these two quantities the phenomenon can be described as a single function, in this case an experimental curve. It has been shown that the initial acceleration depends on the radius and thickness of the disc and on the magnitude of the pressure loading. However, only an order of magnitude can be quoted and it is suggested that the initial acceleration is approximately half that of a free plate under the same loading conditions. The maximum dynamic deflection is proportional to the radius of the disc over the range of pressures used. In this way the deformation of any copper disc can be predicted.

The dynamic deflections have been obtained using a shock tube and this tool has shown remarkable flexibility. Discs of diameter 2", 4" or 6" can be loaded with pressure pulses of up to 300 p.s.i. and it has been designed to produce a pressure pulse of sufficient duration to allow as near constant pressure loads as possible. These experiments should be extended to a more detailed study of the deformation of discs and materials having different mechanical properties should be used.

Probably the most important design calculation for bursting discs concerns the determination of the bursting pressure. Under slow load conditions the experimental values are used but if the disc is to rupture under dynamic pressure loading the bursting pressure will be different. A suggested mechanism of rupture has lead to the prediction of dynamic bursting pressures and the results have been tested using the shock tube, with reasonable success. However, it is essential to extend these tests to other materials before accepting these results as conclusive.

When the rate of pressure increase is finite but insufficiently rapid to influence the mode of deformation the results described above cannot be used. To overcome this difficulty, the strain energy, the kinetic energy and the work done by the loading medium have been calculated from the equilibrium equations and, by applying the principle of conservation of energy, the rate of deflection for any pressure application has been determined. These results are of more importance than those for shock loadings but as yet they have not been tested experimentally.

To summarise, an attempt has been made to determine all the factors influencing the performance of bursting disc valves and spring loaded valves, particularly under dynamic conditions. The experimental work has been restricted to the use of gas in these valves and only supersonic conditions have been considered. Information has been presented for designing the most efficient relief valve and a method has been suggested whereby the positioning and size of the valve can be calculated.

LIST OF REFERENCES in alphabetical order

Bennet, G.E., Richards, G.R. & Voss, E.C. (1947) Aero. Res. Ctee. R & M No.2627.

Benson, R.S. (1955) Engineer 199, 546, 582, & 619.

Binnie, A.M. & Hooker, S.G. (1937) Proc. Roy. Soc. A.159, 592.

Black, J. & Mediratta, O.P. (1950) Aero. Res. Quart. 2, 227

Burgoyne, J.H. & Newitt, D.M. (1960) Symposium at the N.W. Branch of the Institute of Chemical Engineers.

British Standards 1123(1950), Part 2 ; 759(1955), Section 3A; & 2591(1956), Part 2.

Coulson, C.A. (1955) "Waves" (Oliver & Boyde)

Cousins, F.W. & Cotton, P.E. (1951) Chem. Eng, 58, 133.

Dugger, G.L. (1951) J. Amer. Chem. Soc. 73, 2398.

Elonka, S. (1954) Power 98, (1), 112.

Fraser, R.P., Rowe, P.N. & Coulter, M.O. (1957) Proc. I. Mech. E. 171, (16)

Flindt, C.B. (1956) Engineer 202, 193.

Gerstein, M., Carlson, E.R. & Hill, F.U. (1951) Ind. Eng. Chem. 46, 2558.

Giffen, E. (1940) Engineering 150, 134, 154 & 181.

Gilmore, F.R., Plesset, M.S. & Crossley, H.L. (1950) J. Appl. Phys. 21, 243.

Glass, I.I. (1950)+ See Glass, Martin & Patterson (1953) Institute of Aerophysics of Toronto UTIA Report No.2, p63.

Glass, I.I. & Patterson, G.N. (1955) J. Aero. Sci. 22, 73.

Glick, H.S., Squire, W. & Hertzberg, A. (1954) 5th Symp. on Comb. p.393.

Goldsworthy, F.A. (1953) Proc. Roy. Soc. A218,

Haringx, J.A. (1957) T.A.S.M.E. 79, 55.

Harlemann (1956) Bul. Amer. Phys. Soc. (Jan-Feb) (Abstract)

Harlemann & Ippen (1955) "Memoires sur la Mecanique des Fluides" Riaboushinski Memorial Volume.

Hartman,J. & Lazarus,F. (1941) Phil. Mag. 31, 35.

Kestin,J. & Glass,J.S. (1951) Aircraft Eng. 23, 30C

Laitone,E.V. (1952) J. Aero. Sci. 19, 265.

Laitone,E.V. (1954) "Memoire sur la Mecanique des Fluides"

Lamb,J. (1952) Proc. I. Mech. E. 166(3), 327.

Lewis,B. & von Elbe,G. (1934) J. Chem. Phys. 2, 283.

Lewis,B. & von Elbe,G. (1935) "Combustion, Flames & Explosions" (Interscience)

Manabe,D. & Ohira,H. (1955) J. Japan Soc. Aero. Eng. 3, 113.

Manson,N. (1953) Fuel 32, 186.

Oppenheim,A.K. (1953) J. Appl. Mech. 20(1), 115

Prieswerk (1938) Translation N.A.C.A. TN 934 & 935 (1940)

Rasbash,D.J. & Rogowski,Z,W. (1956) Fire Res. Estab. F.R. Note 298

Rasbash,D.J. (1959) Fire. Res. Estab. F.R. Note No.416.

Riaboushinski,M.D.P. (1934) Comptes Rend. 199(14), 632

Sammons. (1949) Proc. I. Mech. E. 161, 233.

Taylor,G.I. & Lewis,D.J. (1950) Proc. Roy. Soc. A201 & A202.

Wilcox,D.E., Weir,A. & Nicholls,J.A. (1957) J. Aero. Sci. 24(2), 150.

Wilson,M.J.G. (1954) PhD Thesis (University of London)

+ Error in text corrected in reference.

NOTATION FOR SECTIONS B AND C

Chapters referred to in parenthesis.

A		Gas flow area
Av		Maximum vent area
Af_{*}		Flame area
A_f^{*}		Critical flame area
A	(B.IV)	Constant in dynamic valve operation = $1 - n$
a		Speed of sound in gas
B	(B.IV)	Constant in valve operation = $n + \dfrac{m}{P_{oo}\ Av}$
b		$\left\{\dfrac{m_i \triangle H_i}{m_e\ (Cv)u}\right\}$
C		$(R.\ \gamma.\ T_i.\ B/m_i)$
Cd		Absolute discharge coefficient
Cv		Heat capacity at constant volume
D		Diameter of vent
E		Internal energy of the gas
F	(B.IV)	"Absolute" thrust
Fg		"Gauge" thrust
F	(C.III)	Froude number
F	(C.II)	Adiabatic function
F_p		F_b/F_u
F_{po}		$\dfrac{n_a}{m_i} \cdot \dfrac{F_b}{F_u}$ (at $x = 1$; $t = t$)
G		Mass flow rate
H		$\left\{\dfrac{m_i V}{A_f^{*} C\ .\ w_i}\right\}$
$\triangle H_i$		Heat of reaction
h		Depth of water
K		("Absolute" thrust)/(Absolute vessel pressure)
k		Flame velocity correction - a function of Re
L		Length of one dimensional vessel
M	(B.IV)	Constant in discharge equation B.IV.7
M	(C.III)	Mach number
m	(B.IV)	Slope of mechanism relation
m	(C.I.II)	Average molecular weight
n	(B.IV)	Pressure loading ratio
n	(C.II)	Fraction of gas burnt
n_a		Fraction of gas burnt when relief valve opens
P		Pressure (in absolute units)
P_o	(B.IV)	Pressure

P_o	(C.II)	Valve operation pressure
P_{og}		Gauge pressure
P_b		Blow off pressure
p		(Instantaneous pressure)/(Initial pressure)
R	(B.III)	Radius of flat plate
R	(C.II)	Radius of spherical vessel
$\mathcal{R}$		Universal gas constant
r		Radial position
Re^*		Venting Reynolds number
$R(X_i)$		Restraining force function
S		Coefficients in venting equation (Table C.II.1)
Su		Fundamental burning velocity
T		Absolute temperature
u		Velocity of gas
$\bar{u}$		Velocity vector
V		Volume of vessel
dV		Volume of gas element
$\bar{V}$		External force vector
w	(B.IV)	Mass of valve head
Δw		Mass correction for links etc.
dw		Mass of gas element
x	(B.III.IV)	Displacement of valve head
x	(C.II)	Position in one-dimensional vessel
X	(B.III)	x/R
X	(C.II)	x/L
z		Aspect ratio
$\phi(P,T)f(X_i)$		Gas thrust function
α	(B.III)	Dimensionless vent area $(A)/(A^*)$
α	(C.II)	Dimensionless vent area $(Cd.A)/(V)$
β		Exponent in combustion pressure law
γ		Ratio of specific heats
ϵ		Volume occupied by one mole of gas
η		r/R
ρ		Density of gas
θ		(Instantaneous Temperature)/(Initial temperature)
ϕ		Potential function
μ		Viscosity
τ	(B.IV)	Dimensionless time term
τ	(C.II)	Dimensionless time term

Subscripts

b	Burnt gas
u	Unburnt gas
pb	Burnt element at pressure P
i	Initial conditions
oo	Initial conditions
e	Final conditions
f	Flame

APPENDIX. C.II.1. Simple theory of combustion.

(i) Spherical case.

(a) Mass balance at time t

Mass element of unburnt gas $= dw_u$

$$= 4\pi\rho_u r^2 dr. \text{ for } r_f \leq r \leq R$$

Substituting for P and ρ_u

$$dw_u = m_i \cdot \frac{P}{F_u}^{1/\gamma_u} \cdot 4\pi r^2 dr.$$

at time $t = t_0$ the vent opens and the element of unburnt gas vented is

$$dw_v = A\sqrt{\gamma_u\left(\frac{2}{\gamma_u+1}\right)^{\frac{\gamma_u+1}{\gamma_u-1}} \cdot m_i g \cdot \frac{P}{(RT_u)^{1/2}}} \cdot dt$$

which, by substitutions of P and T_u, gives

$$w_v = \sqrt{g\gamma_u m_i (2/\gamma_u+1)^{\frac{\gamma_u+1}{\gamma_u-1}}} \int_{t_0}^{t} \frac{AP}{F_u^{1/2} \cdot P^{\frac{\gamma_u-1}{2\gamma_u}}} \cdot dt.$$

F_u is constant with respect to time and position and P is constant with prospect to position.

$\therefore$ mass unburnt gas $= w_u = (1-n)\, w_i$

$$= \frac{4}{3}\pi m_i \frac{P^{1/\gamma_u}}{F_u}(R^3 - r_f^3) + \frac{1}{F_u^{1/2}} \cdot \sqrt{g\gamma_u m_i B}\int_{t_0}^{t} A P^{\frac{\gamma_u+1}{2\gamma_u}} dt$$

and $w_i = \frac{m_i P_i V}{\mathcal{R} T_i} = \frac{4}{3}\pi R^3 \cdot \frac{m_i P_i}{\mathcal{R} T_i}.$

Mass element of burnt gas $= dw_b$

$$= \rho_b \cdot 4\pi r^2 dr. \quad \text{for } 0 \leq r \leq r_f.$$

$$\therefore w_b = n \cdot w_i = 4\pi m_e \cdot P^{1/\gamma_b}\int_0^{r_f} \frac{r^2}{F_b} \cdot dr.$$

F_b is a function of position and time

P is a function of time only.

Substituting $\eta = \frac{r}{R}$, $\phi = \frac{P}{P_i}$, $\theta = \frac{T}{T_i}$, $F_p = \frac{F_b}{F_u}$ and rearranging, these equations can be rewritten

$$1-n = (1-\eta_f^3)\,\phi^{1/\gamma_u} + \frac{c}{V}\int_{t_0}^{t} A \cdot P^{\frac{1+\gamma_u}{2\gamma_u}} dt. \quad \ldots\ldots\ldots \ (1)$$

$$n = \frac{m_e}{m_i}\,\phi^{1/\gamma_b}\int_0^{\eta_f} \frac{\eta^2}{F_p} \cdot d\eta \quad \ldots\ldots\ldots \ (2)$$

where $c = a_i\left(\frac{2}{\gamma_u+1}\right)^{\frac{\gamma_u+1}{2(\gamma_u-1)}}$

(b) Energy balance.

Energy in unburnt gas element $= dE_u$

$$= \frac{\mathcal{R}}{\gamma_u - 1} \cdot \frac{T_u}{m_i} \cdot dw_u = \frac{1}{\gamma_u - 1} P \cdot 4\pi r^2 dr.$$

Energy in vented gas from time $(t = t_0) = dE_v$

$$= \frac{1}{m_i} \frac{A}{\gamma_u - 1} \sqrt{m_i g \gamma_u \left(\frac{2}{\gamma_u + 1}\right)^{\frac{\gamma_u+1}{\gamma_u-1}}} \cdot P (\mathcal{R} T_u)^{\frac{1}{2}} dt$$

Energy in burnt gas element $= dE_b$

$$= \frac{1}{\gamma_b - 1} \cdot 4\pi r^2 dr.$$

Initial energy in combustibles $= \frac{W_i}{\gamma_u - 1} \cdot \frac{T_i}{m_i}$

Energy produced in reaction of element $dw_b = \Delta H_i \cdot dw_b$.

$\therefore$ Energy balance is:

$$3 \frac{m_e}{m_i} \cdot b \cdot p^{1/\gamma_b} \int_0^{\eta_f} \frac{\eta^2}{F_p} \cdot d\eta = (1 - \eta_f^3)\left(\frac{\gamma_b - \gamma_u}{\gamma_b - 1}\right) p + \left(\frac{\gamma_u - 1}{\gamma_b - 1}\right) p - 1 + \frac{c}{V} \int_{t_0}^{t} A \cdot p^{\frac{3\gamma_u - 1}{2\gamma_u}} \cdot dt \quad \ldots\ldots (3)$$

where $b = \frac{m_i}{m_e} \cdot \frac{\Delta H_i}{T_i (c) w_u}$

(c) Rate of combustion.

It has been postulated that the rate of combustion is given by the power law.

$$\frac{dn}{dt} = \frac{M_i}{W_i} \cdot \frac{A_v}{A^*} \cdot \eta_f^2 \cdot p^{\beta} \quad \ldots\ldots (4)$$

(d) The solution of equations (1), (2) and (3).

Eliminating $\int_0^{\eta_f} \frac{\eta^2}{F_p} d\eta$ between equations (2) and (3) and converting the time integral for vented gas into a fraction burnt (n) integral by using equation (4):

$$1 - n = (1 - \eta_f^3) p^{1/\gamma_u} + \frac{1}{H} \int_{n_0}^{n} \alpha \, p^{\frac{\gamma_u+1}{2\gamma_u} - \beta} \frac{1}{\eta_f^2} \cdot dn \quad \ldots\ldots (5)$$

and

$$bn = \left\{ \frac{\gamma_b - \gamma_u}{\gamma_b - 1} \cdot (1 - \eta_f^3) + 1 \right\} p - 1 + \frac{1}{H} \int_{n_0}^{n} \alpha p^{\frac{3\gamma_u - 1}{2\gamma_u} - \beta} \cdot \frac{1}{\eta_f^2} \cdot dn \quad \ldots\ldots (6)$$

where $H = \frac{M_i V}{A^* \cdot c \cdot W_i}$ and $\alpha = \frac{A}{A_v}$.

Eliminating $(1 - \eta_f^3)$.

$$bn = \frac{\gamma_b - \gamma_u}{\gamma_b - 1} \left\{ 1 - n - \frac{1}{H} \int_{n_0}^{n} \alpha p^{\frac{\gamma_u+1}{2\gamma_u} - \beta} \frac{1}{\eta_f^2} \cdot dn \right\} p^{1 - 1/\gamma_u} + \left(\frac{\gamma_u - 1}{\gamma_b - 1}\right) p - 1 + \frac{1}{H} \int_{n_0}^{n} \alpha p^{\frac{3\gamma_u - 1}{2\gamma_u} - \beta} \frac{1}{\eta_f^2} \cdot dn \ldots (7)$$

To simplify the calculation a step is taken which cannot be justified on purely mathematical grounds. However, the following explanations show that the error is small. By taking the factor $p^{1 - 1/\gamma_u}$ into the integrand in the first term on the right hand side of the equation, the equation can be differentiated to give a first order differential equation.

Since the index $1-1/\gamma_u$ is small a change in p would have to be large before p^{1-1/γ_u} differs to any extent from a constant. Also, before venting this term is zero and after venting the pressure is to be maintained constant. Hence, the error involved in bringing the pressure term into the integrand is small and, for the ideal venting case in which the pressure remains constant, zero. Further the integral concerned is multiplied by the factor $\frac{\gamma_b-\gamma_u}{\gamma_b-1}$ which is usually small and when $\gamma_b=\gamma_u$ is zero so that under the particular case in which there is no change in γ the following differential equation is without any error.

$$b.n = \frac{\gamma_b-\gamma_u}{\gamma_b-1}.(1-n)p^{1-1/\gamma_u} + \frac{\gamma_u-1}{\gamma_b-1}.p - 1 + \frac{1}{H}.\left(1-\frac{\gamma_b-\gamma_u}{\gamma_b-1}\right)\int_{n_0}^{n}\alpha\, p^{\frac{3\gamma_u-1}{2\gamma_u}-\beta}.\frac{1}{\eta_f^2}.dn$$

which, on being differentiated w.r.t. n. yields.

$$\left(p^{1/\gamma_u}+(1-n)\frac{\gamma_b-\gamma_u}{\gamma_u}\right)\frac{dp}{dn} = b.\frac{\gamma_b-1}{\gamma_a-1}.p^{1/\gamma_u} + \frac{\gamma_b-\gamma_u}{\gamma_u-1}.p - \frac{\alpha}{H}.p^{\frac{3\gamma_u-1}{2\gamma_u}-\beta}.\frac{1}{\eta_f^2} \quad \ldots\ldots (8)$$

η_f is obtained by eliminating the integral in equations (5) and (6)

$$\eta_f^3 = \frac{1+nb-\frac{\gamma_b-\gamma_u}{\gamma_b-1}.p-(1-n)p^{1-1/\gamma_u}}{\frac{\gamma_u-1}{\gamma_b-1}.p} \quad \ldots\ldots\ldots (9)$$

The solution is exact when $\gamma_b=\gamma_u$ or when $\alpha=0$ and in this latter case an explicit relation can be obtained for the solution of the differential equation.

(ii) One-dimensional combustion.

(a). Mass balance at time t.

mass element of unburnt gas in vessel $= m_i\frac{p^{1/\gamma_u}}{F_u}.A_0.dx.$

mass element of unburnt gas vented (if any) $= A\sqrt{m_i\gamma_u.g\left(\frac{2}{\gamma_u+1}\right)^{\frac{\gamma_u+1}{\gamma_u-1}}.\frac{p}{(RT_u)^{1/2}}}.dt$

To introduce the case of no unburnt gas vented through a particular vent a coefficient S_u has been used which is to be 1 when gas is vented and zero when gas is not vented. The two ends of the vessel are distinguished by the superscripts + and −.

Thus, mass of unburnt gas vented in "positive direction" is

$$m_i\; S_u^+\sqrt{m_i.\gamma_u.g.\left(\frac{2}{\gamma_u+1}\right)^{\frac{\gamma_u+1}{\gamma_u-1}}}.\int_{t_0}^{t}\frac{A.p^{\frac{1+\gamma_u}{2\gamma_u}}}{F_u^{1/2}}.dt$$

Similarly in the negative direction so that total mass of unburnt gas is:

$$(1-n) = \frac{\omega_u}{\omega_i} = [1-(X_f^- - X_f^+)]\,p^{1/\gamma_u} + \frac{c}{L}(S_u^+ + S_u^-)\int_{t_0}^{t} \alpha\, p^{\frac{1+\gamma_u}{2\gamma_u}}\,dt \quad \ldots \quad (10)$$

The coefficients S_b are introduced when burnt gas is vented and in order to allow for the state of the gas when venting occurs under the burnt condition the adiabatic function defined by the position $x=L$ and the time $t=t$ must be included. If we define $f_{p_0} = \frac{m_e}{m_i}\left(\frac{f_b}{f_u}\right)_{x=L,\,t=t}$ the mass of burnt gas is given by

$$n = \frac{\omega_b}{\omega_i} = \frac{m_e}{m_i}\cdot p^{1/\gamma_b}\int_{X_f^-}^{X_f^+}\frac{dX}{f_p} + \frac{m_e}{m_i}\cdot\frac{c}{L}\cdot(S_b^+ + S_b^-)\int_{t_0}^{t}\frac{\alpha\, p^{\frac{\gamma_b+1}{2\gamma_b}}}{f_{p_0}^{1/2}}\,dt \quad \ldots \quad (11)$$

(b). Energy balance.

This is identical to the spherical case with the inclusion of the coefficients S to account for venting at either or both ends.

$$\frac{\text{Energy in unburnt gas}}{\text{Energy in combustibles}} = \gamma_u - 1\, p\,[1-(X_f^+ - X_f^-)] + \frac{c}{L}(S_u^+ + S_u^-)\int_{t_0}^{t}\alpha\, p^{\frac{3\gamma_u-1}{2\gamma_u}}\,dt. \quad (12)$$

$$\frac{\text{Energy in burnt gas}}{\text{Energy in combustibles}} = \frac{\gamma_u-1}{\gamma_b-1}(X_f^+ - X_f^-)\cdot p + \frac{m_e}{m_i}\cdot\frac{c}{L}\cdot(S_b^+ + S_b^-)\int_{t_0}^{t}\alpha\, p^{\frac{3\gamma_b-1}{2\gamma_b}}\, {}^{1}/{f_{p_0}^{1/2}}\cdot dt \quad (13)$$

$$\frac{\text{Energy in combustibles}}{\text{Energy in combustibles}} = 1 \quad (14)$$

$$\frac{\text{Energy of reaction}}{\text{Energy in combustibles}} = \frac{\Delta H}{T_i(C_v)_u}\left\{p^{1/\gamma_b}\int_{X_f^-}^{X_f^+}\frac{dX}{f_p} + \frac{c}{L}\cdot(S_b^+ + S_b^-)\int_{t_0}^{t}\frac{\alpha\, p^{\frac{1+\gamma_b}{2\gamma_b}}}{f_{p_0}^{1/2}}\cdot dt\right\} \quad (15)$$

By adding (12) and (13) and equating to the sum of (14) and (15) an energy equation is obtained. This is somewhat more complicated than that for the spherical case and is immediately simplified by putting $\gamma_u = \gamma_b$ when

$$p + \frac{c}{L}\left\{S_u^+ + S_u^- + \frac{m_e}{m_i}\cdot(S_b^+ + S_b^-)\frac{1}{f_{p_0}^{1/2}}\right\}\int_{t_0}^{t}\alpha\, p^{\frac{3\gamma-1}{2\gamma}}\,dt$$

$$= 1 + b\cdot\frac{m_e}{m_i}\left\{p^{1/\gamma}\int_{X_f^-}^{X_f^+}\frac{dX}{f_p} + \frac{c}{L}\left(\frac{S_b^+ + S_u^-}{f_{p_0}^{1/2}}\right)\int_{t_0}^{t}\alpha\cdot p^{\frac{1+\gamma}{2\gamma}}\,dt. \quad \ldots \quad (16)\right.$$

This assumes that once venting has commenced f_{p_0} does not alter with time. This is not true but again the error introduced is small and for constant pressure venting is negligible.

(c) Rate of combustion.

The rate of combustion is given by $\frac{dn}{dt} = \frac{M_i A_0}{A^* \cdot \omega_i}\cdot\frac{A_f}{A_0}\cdot p^{\beta}$

(d) Solution on the same lines as the spherical case yields equations very similar in form as quoted in Section C. of the thesis.

APPENDIX C.II.2. Pentane-air explosion - Wilson.

(i) To calculate the exponent β from the experimental results.

$$\frac{dp}{d\tau} = H.b.\eta_f^2.p^\beta \quad \text{for a closed vessel.}$$

The maximum rate of pressure rise occurs when the flame just touches the walls and $\eta_{f_{max}}$ can be determined as can the pressure at which this occurs. Using Wilson's results.

$$\eta_f \max = \frac{2.1}{R} \quad \text{and } R \text{ is such that } \tfrac{4}{3}\pi R^3 = 60.6 \text{ ft}^3.$$

$$\therefore R = 2.438 \text{ ft}.$$

and $\eta_f \max = 0.862 \quad \therefore \eta_{f\,max}^2 = 0.743$

also $\left(\frac{dp}{dt}\right)_{max} = 78 \text{ sec}^{-1}$ and $b = 7.55$

and since $H\tau = S_u \frac{A}{V}.t$ where $\frac{A}{V} = \frac{3}{R}$ for a sphere

$H\tau = 1.478\, t$ for a burning velocity $S_u = 1.2$ ft/sec.

$$\therefore \frac{dp}{dH\tau} = \frac{1}{1.478}\frac{dp}{dt} = \frac{78}{1.478} = 52.7$$

Substituting these values in the equation.

$$52.7 = 7.55 \times 0.7430 \times (5.5)^\beta$$

$$\therefore \beta = 1.315.$$

This value of β can be compared with the expected change in burning velocity computed from the equations given by Dugger & Manson. Their results are related by the equations:

$$S_u = 10 + 0.00342T^2 \quad \text{cm/sec.}$$

and $$\frac{S_u}{S_o} = \left(\frac{P}{P_i}\right)^n$$

Since the temperature rise is adiabatic $\frac{T}{T_i} = \left(\frac{P}{P_i}\right)^{\frac{\gamma-1}{\gamma}} = (p)^{0.73}$

now $(S_u)_i = 37$ cm/sec $\quad \therefore \left(\frac{S_u}{S_{ui}}\right) = 0.25 + 0.75\left(\frac{T}{T_i}\right)^2$ for a constant pressure

$$\therefore \left(\frac{S_u}{S_{ui}}\right) = \left[0.25 + 0.75\,p^{1.46}\right] p^n \quad \text{when pressure \& temperature change adiabatically}$$

For most hydrocarbons $n = -0.25$ and these are the values Wilson uses.

$$\therefore \left(\frac{S_u}{S_{ui}}\right) = \left[0.25 + 0.75\,p^{1.46}\right] p^{-0.25} \quad \text{according to Dugger \& Manson.}$$

and $$\left(\frac{S_u}{S_{ui}}\right) = \left(\frac{P}{P_i}\right)^\beta \cdot \left(\frac{\rho_i}{\rho}\right) = \left(\frac{P}{P_i}\right)^\beta \left(\frac{P_i}{P}\right)^{\frac{1}{\gamma}} = p^{\beta - 1/\gamma} = p^{1.03} \quad \text{from the present theory.}$$

These two results are compared in chapter C.II.

(ii) Comparison of closed vessel results.

For a spherical vessel
$$b.\frac{dHT}{dp} = \frac{1}{\eta_H^2 . p^{\beta}}$$
and
$$\eta_H^2 = \left[1-(1+1/b)p^{-1/\gamma} + \frac{1}{b}.p^{\frac{1-\gamma}{\gamma}}\right]^{2/3}$$

numerical integration using Simpson's rule allows the evaluation of b.H.T for a series of values of p and these are plotted to give the dimensionless pressure rise.

$(\gamma_u = 1.401$ and $\gamma_b \simeq 1.336$ $\therefore \gamma$ is taken as $\gamma = 1.368)$

In plotting Wilson's results on the same graph the time axis is converted by $H.T.b. = Su.b.\frac{Av}{V}$ and the pressure by dividing by the initial pressure: for the unstrired explosion.

$$Su = 1.2, \quad \frac{Av}{V} = 1.231, \quad b = 7.55$$
$$\therefore \quad HTb = 11.15.t \quad \text{where } t \text{ is in seconds.}$$

APPENDIX. C.II.3. Pentane-air explosions in ducts – Rasbash & Rogowski.

Three phases of combustion.

① Spherical flame starting at the centre of ignition and drifting towards the remote end. This is calculated as for a spherical explosion with an equivalent radius given by
$$R = \frac{3V}{A} = \left(\frac{3/2 D}{D/L + 2}\right) = 0.360 \text{ ft.}$$
This radius is used because, for long ducts, the radial expansion depends upon the duct diameter only and as the vessel decreases in length the effect of the ends increases whereas the radius giving the same volume will increase indefinitely with length.

The spherical flame will drift away from the centre of ignition because of the difference in volume of the two portions of unburnt gas. If a mass balance on either side of the centre of the spherical flame is considered;
mass of unburnt gas on side (1) = initial mass of gas on side (1) – $\frac{\text{total burnt gas}}{2}$
similarly for side (2). The mass on either side of the centre of the burnt sphere will remain constant so that the position of this centre can be determined as a function of the total amount of gas burnt and the density of the unburnt gas.

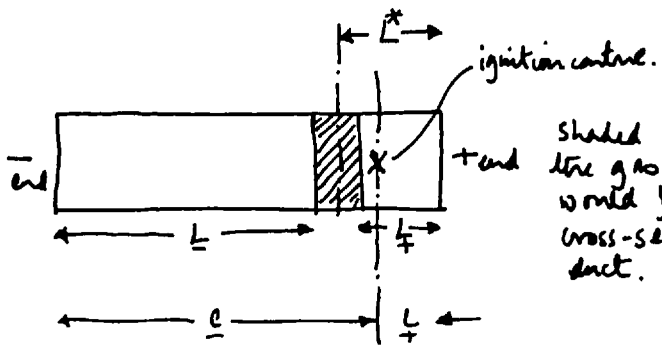

Shaded area represents the gas burnt as it would fill the whole cross-section of the duct.

The mass balance at the + end is

$$p\pi\frac{D^2}{4}\cdot L_+ = l_+\cdot\pi\cdot\frac{D^2}{4}\cdot p_i - \frac{n}{2}p_i\cdot\pi\cdot\frac{D^2}{4}(l_+ + l_-)$$

$$\therefore\ L_+ = \left[(1-\tfrac{n}{2})l_+ - \tfrac{n}{2}l_-\right]\frac{p_i}{p} \quad \text{since} \quad L_- = \left[(1-\tfrac{n}{2})l_- - \tfrac{n}{2}l_+\right]\frac{p_i}{p}$$

$\therefore\ 2L^* = (l_+ + l_-) - L_- + L_+ = (l_+ + l_-) - (l_- - l_+)\frac{p_i}{p}$ depending on p and the centre of ignition only. Substituting $l_+ = 6''$ and $l_- = 5'6''$

$$\frac{2L^*}{\text{total length}} = 1 - \frac{5}{6}p^{-1/\gamma}$$

This phase ends when $r = 3''$ $\therefore\ \eta_f = \frac{0.25}{0.360} = 0.694$

$\therefore\ p = 1.56$ and $HTb = 2.06$ (Results obtained from Appendix. C.II.2 since the gas used is still pentane.) and $n = 0.0742$

$\therefore$ Displacement of sphere $0.199 \times$(length of duct) from the R.H. end.

(2) Two flames travelling in opposite directions.

These flames, together, will have approximately 4 times the surface area of the hypothetical flat flame

$$\therefore\ \frac{dp}{d\,HTb} = \frac{A_f}{A_v}\cdot\frac{1}{b}\cdot p^{\beta} \quad \text{where} \quad \frac{A_f}{A_v} = 4\,\frac{\text{X-sect. area}}{A_v}.$$

This phase ends when one flame is extinguished against the nearer end wall. The distance between the flames has already been derived as:

$$\Delta X_f = 1 - (1+\tfrac{1}{b})p^{-1/\gamma} + \tfrac{1}{b}p^{1-1/\gamma}$$

and half this value – the distance between the centre of the burnt gas and the wall – has already been calculated for phase (1) as

$$\frac{L^*}{\text{total length}} = \frac{1}{2}\left(1 - \frac{5}{6}p^{-1/\gamma}\right)$$

$\therefore\ 1 - \frac{5}{6}p^{-1/\gamma} = 1 - (1+\tfrac{1}{b})p^{-1/\gamma} + \tfrac{1}{b}p^{1-1/\gamma}$ when the flame touches the wall.

$\therefore\ p_2 = (\frac{b}{6}+1)$ for this particular duct and ignition centre.

$= 2.26$, $\frac{L^*}{6} = 0.270$ or $\Delta X_f = 0.540$

This gives n as 0.167

(3) A single flame travelling along the duct.

The simplest of the three stages which ends when $\Delta X_f = 1.0$

$$\frac{dp}{d\,HTb} = \frac{A_f}{A_v} \cdot p^{\beta} \quad \text{from } p = 2.26 \text{ to } p = 8.55.$$

(4) If the combustion is considered as a single flame throughout the explosion

$$\frac{dp}{d\,HTb} = \frac{A_f}{A_v} \cdot p^{\beta} \quad \text{and} \quad \frac{A_f}{A_v} = 2 \quad (\text{hemispherical flame})$$

$$\therefore\ bHT = \frac{1}{2(\beta - 1)} \cdot \left\{ 1 - \left(\frac{1}{p}\right)^{\beta - 1} \right\} \quad \text{and for } \beta = 1.3$$

$$bHT = 1.667 \left[1 - p^{-0.3} \right]$$

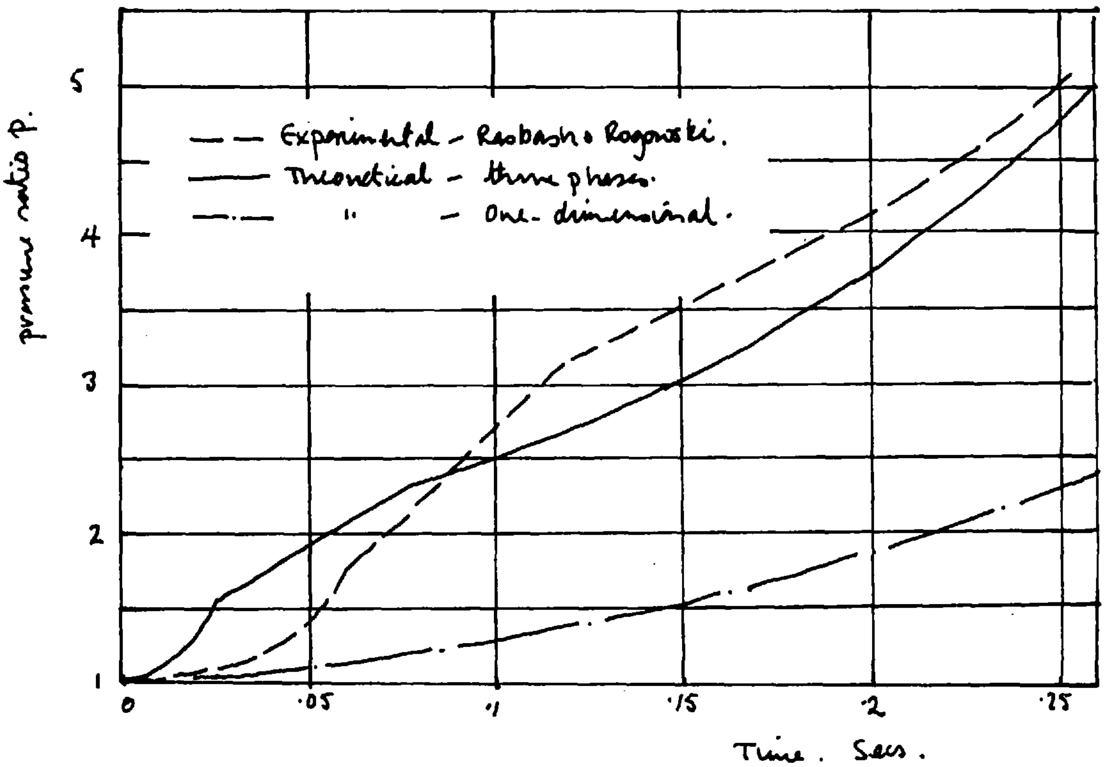

APPENDIX. C.II.3 . Propane-air explosion – Cousins & Cotton.

Since many hydrocarbons have similar combustion properties it will be assumed that the exponent β still has the value 1.3 and that the curves derived for spherical explosions in pentane are still valid. It will be assumed that the venting occurs over the entire surface area of the vessel so that the effects of directional flame propagation are not included.

For vented explosions the equations are:

$$\frac{dp}{dH\tau b} = \left\{ \eta_f^2 \cdot p^\beta - \frac{\alpha}{Hb} \cdot p^{\frac{3\gamma-1}{2\gamma}} \right\}$$

$$\frac{dn}{dH\tau b} = \frac{\eta_f^2 p^\beta}{b}$$

$$\eta_f^3 = \frac{1 + bn - (1-n) p^{1-1/\gamma}}{p}$$

The unvented explosion gives a pressure rise from $p = 1$ to $p = p_0$ when the vent opens and the flame continues to expand from η_{f0} to $\eta_f = 1$. The unvented explosion has been calculated for pentane air and these results are used here to find the initial values of η_{f0}, p_0 and $(H\tau b)_0$ when venting starts. Then, by taking small incremental steps in p the increase in $H\tau b$ and η_f are calculated from

$$\delta(H\tau b) = \left\{ \eta_f^2 \cdot p^\beta - \frac{\alpha}{Hb} \cdot p^{\frac{3\gamma-1}{2\gamma}} \right\}^{-1} \delta p$$

$$\delta n = \frac{1}{b} \cdot \eta_f^2 \cdot p^\beta \cdot \delta(H\tau b)$$

$$\text{and } \eta_f^3 = \frac{1 + bn - (1-n) p^{1-1/\gamma}}{p}$$

and the process repeated until $\eta_f = 1$ and $p = p_{max}$.

In this way the maximum pressures for a series of bursting pressures and for several vent area functions, $\frac{\alpha}{Hb}$, were calculated. Since, the factor H is contained in $\frac{\alpha}{Hb}$ as an independent variable the effect of initial burning velocity could be expressed as a function of $\frac{\alpha}{Hb}$.

Since Cousins & Cotton's results were presented in this form the correlation between vent Reynold's number & burning velocity could be obtained by matching the calculated curves to the experimental ones by a correction factor on the burning velocity.

i.e. $(Re^x)_{apr.}$ was associated with a certain curve, $\left(\frac{\alpha}{Hb}\right)_{calc}$ gives a curve which fits and $\frac{\alpha}{Hb} \propto \frac{A}{kS_u}$ so that S_u can be corrected to kS_u to give the required vent area, A.

APPENDIX E.I The response of the measuring equipment to static and dynamic changes in the measured variables.

The static response of the equipment can be calculated and measured comparatively easily and the methods are discussed in the individual sections below. However, the dynamic responses of a mechanism not only require a knowledge of the natural frequency but also the extent to which the mechanisms are damped. For this reason a preliminary description of the methods used to determine the errors introduced into the dynamic measurements is included here.

The perfect measuring device will respond exactly to the measured variable. If, however, the device has a natural frequency it will resonate when subjected to a change in variable of the same frequency so that there will be maximum magnification of the variable considerably greater than the static calibration suggests. If the impressed frequency does not equal the natural frequency but is of the same order of magnitude, an error is still introduced although it will be smaller than that described above.

If the variation of the measured property with time is to be recorded a further error is introduced. There will be

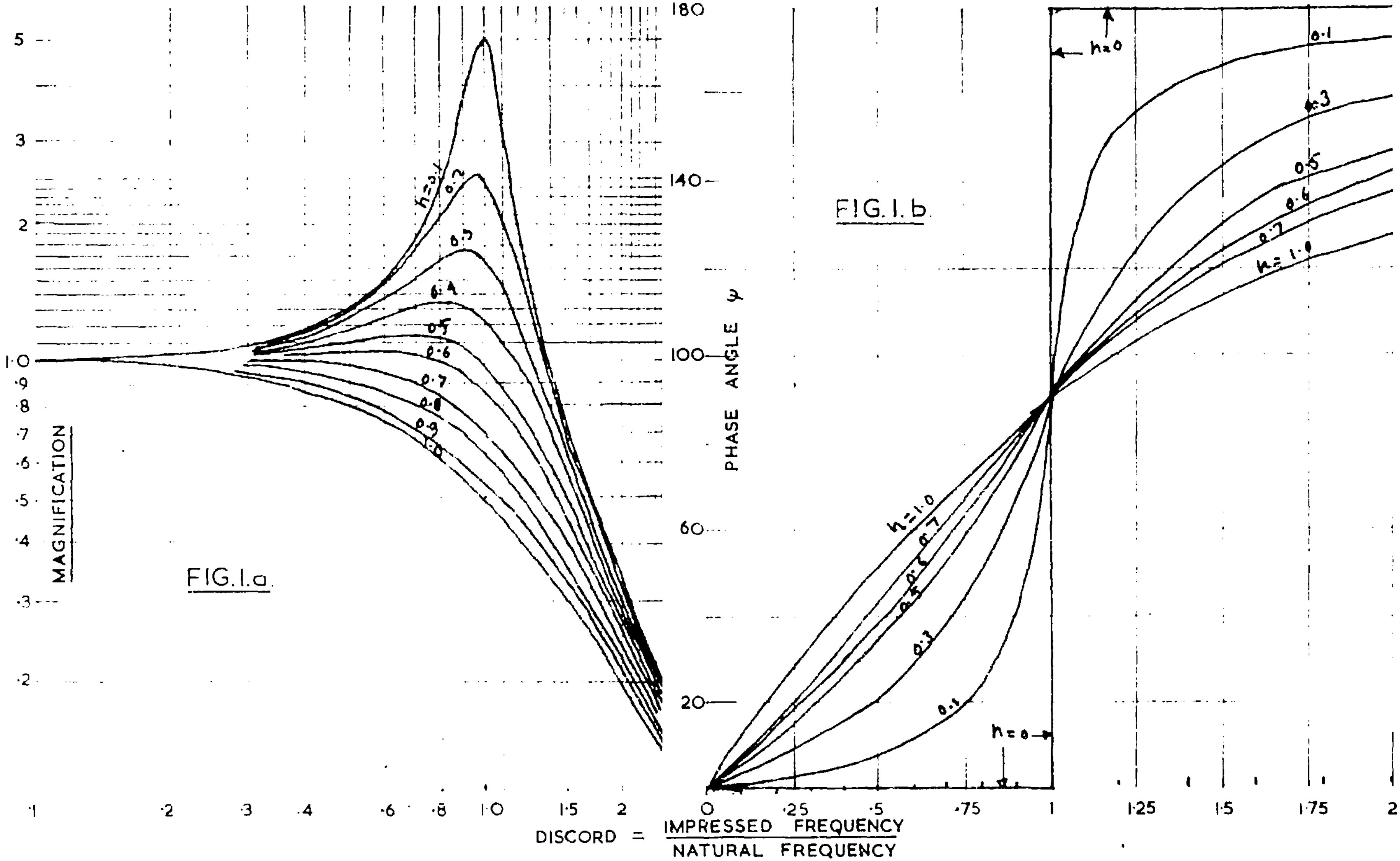

FIG.I.a.
FIG.I.b.
MAGNIFICATION
PHASE ANGLE ψ
h=0·1
0·2
0·3
0·4
0·5
0·6
0·7
0·8
0·9
1·0
h=0
h=1·0
DISCORD = IMPRESSED FREQUENCY / NATURAL FREQUENCY

a time lag between the change in property and the recorded change. This is of little consequence if it remains constant during the recording but, unfortunately, the lag depends upon the rate of change of the variable and since this is not constant the recorded time change of the property will be distorted. As with the magnification, both the natural frequency and the amount of damping effect the extend of this error.

The effect of discord (that is, the ratio of impressed frequency to natural frequency) and of damping factor can be expressed by the equations:

$$\frac{bk}{P} = \left\{ \left[1 - \left(\frac{f}{w}\right)^2 \right]^2 + 4h^2 \left(\frac{f}{w}\right)^2 \right\}^{-\frac{1}{2}}$$

$$\tan \Psi = \frac{2h \left(\frac{f}{w}\right)}{1 - \left(\frac{f}{w}\right)^2}$$

where $\frac{f}{w}$ = $\frac{2\pi \text{ Impressed frequency}}{2\pi \text{ Undamped natural frequency of system}}$

h = Damping factor

$\frac{bk}{P}$ = magnification factor

= $\frac{\text{dynamic recording}}{\text{static calibration}}$

Ψ = the phase angle by which the recorded frequency lags the impressed frequency.

These equations are quite simply solved and are plotted in Fig.1 for a series of values of the damping factor h. Both the natural frequency and the damping factor can be determined experimentally (as suggested by Bennet, Richards and Voss 1947) by shock exciting the mechanism and recording both the frequency of vibration, fd, and the rate at which the amplitude falls and calculating the required quantities from

$$h = \frac{\log_{10} \frac{Ao}{An}}{\left(1{\cdot}862n^2 + \log_{10} \frac{Ao}{An}\right)^{\frac{1}{2}}}$$

$$fn = \frac{fd}{(1 - h^2)^{\frac{1}{2}}} \qquad \text{if} \quad h < 0{\cdot}2$$

where Ao is the first considered amplitude measured from the rest position,

An is the amplitude of the n th succeeding swing past the rest position and

fn is the undamped natural frequency.

In this way the errors introduced by the dynamic requirements of the mechanism can be calculated for each instrument for the maximum impressed frequency to be expected.

The direct calculation of the natural frequency of a plane diaphragm is fairly simple when the movements are small but for the corrugated diaphragms used here which are subjected

RESPONSE TIMES

FIG.2

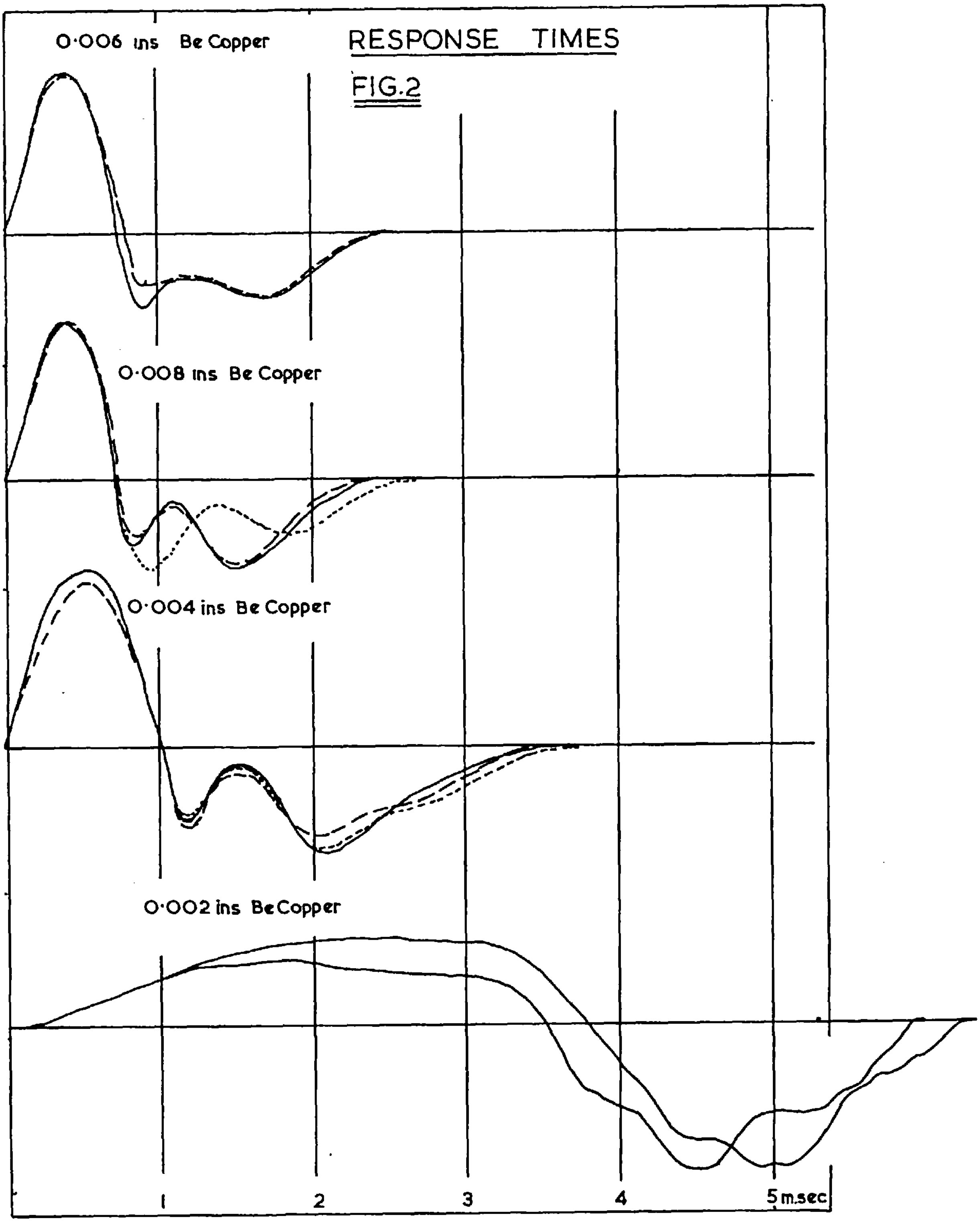

to comparatively large deflections the same equations do not apply and experimental methods are more reliable. Similarly in the case of more complicated mechanisms, the calculation of the natural frequency is difficult although on occasions the analysis can be reduced to that of part of the system which is most liable to low frequency vibrations.

(i) The static response of the pressure transducer.

The equations governing the deflection of corrugated diaphragms have been derived by Haringx (1957) and Flindt (1956) but when the present equipment was designed no such analysis was available. The design of the diaphragm was left to the manufacturers and a number tested under the specific conditions required in the experiments. The final choice of a 0·004" shim steel diaphragm was determined by the sensitivity requirements and by the response time.

(ii) Dynamic response of the pressure transducer.

The frequency and damping factor of the transducer was determined by tapping the diaphragm with a light rod. The rod was actuated by a small pendulum so that the same impact could be applied to all the diaphragms. The output from the transducer was recorded in the normal manner. The recordings for a series of Berillium-copper diaphragms, and for shim steel diaphragms in both designs of transducer are

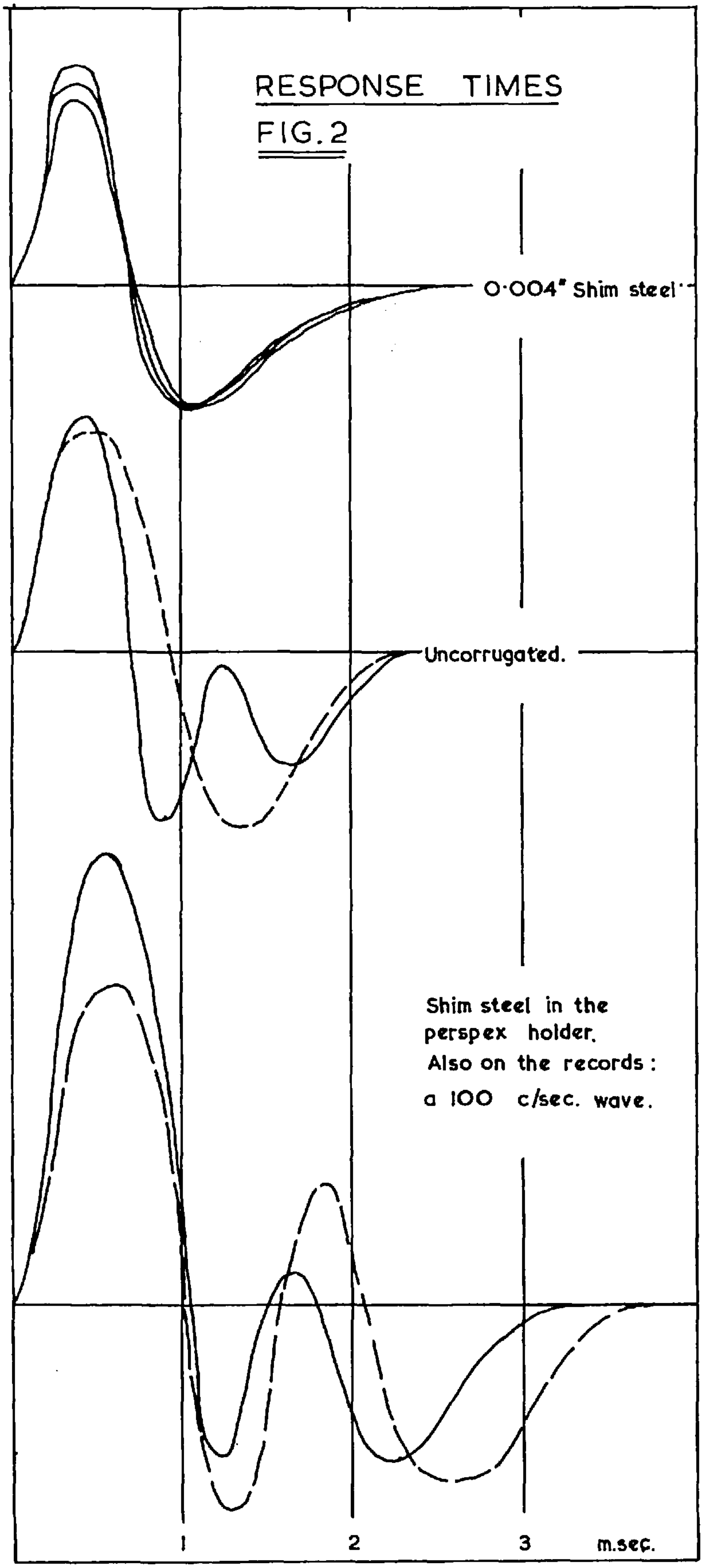

RESPONSE TIMES
FIG. 2
0·004" Shim steel
Uncorrugated.
Shim steel in the
perspex holder.
Also on the records :
a 100 c/sec. wave.
1
2
3
m.sec.

reproduced in Fig. 2. The thicker Be. Cu diaphragms and the shim steel diaphragms show about the same response frequency but the latter has the advantage of only one mode of vibration. The response of the shim steel diaphragm in the perspex holder was totally inadequate. A very low frequency disturbance is recorded some time after the initial impact and is probably due to the non-rigid nature of the holder.

The damping factor calculated from the equations given above is of the order of 0·06 so that the undamped frequency can be calculated and is about 500 c/sec. The maximum impressed frequency was always less than 150 c/sec so that the maximum discord was 0·3. and the magnification factor less than 1·1. Similarly the phase angle difference, which will effect time measurements, is at most 3° (equivalent to about 3% in the quarter cycle.) This means that for the greatest rate of change of pressure the errors may be in the order of a few percent but in all other cases they are negligible. This also accounts for the difficulties encountered in measuring the wave motion in the vessel since under these conditions the discord approached unity and the magnification and phase change are a maximum.

The natural frequency was checked by exciting the diaphragm at its resonant frequency using a loudspeaker driven from an audio-generator. The output from the transducer was fed to an osciliscope and the resonant frequency determined as being 500 c/sec. Since the damping factor, h, is nearly zero, this equals the natural frequency and agrees well with the value determined by the previous method.

(iii) The static response of the thrust transducer.

The transducer valve could be displaced by a maximum of $\frac{1}{2}^{\circ}$ of circular measure. The length of the extension arm is about 1" so that the maximum movement of the shaft is

$$y_{max} = \frac{1}{2} \times \frac{\pi}{180} \times 1$$

$$= 0{\cdot}009 \text{ inches.}$$

The thrust-displacement relation for the two diaphragms can be calculated from

$$\frac{yt^3}{R^4} = \frac{3}{4} \cdot \frac{P_1}{F} \left\{ 1 - \left(\frac{r_1}{R}\right)^2 \ln \frac{R}{r_1} - \frac{3}{4}\left(\frac{r_1}{R}\right)^2 \right\}$$

$$= \frac{3}{4} \frac{P_2}{F} \left\{ 1 - \left(\frac{r_2}{R}\right)^2 \ln \frac{R}{r_2} - \frac{3}{4}\left(\frac{r_2}{R}\right)^2 \right\}$$

where y = deflection of a disc of thickness t and radius R,

$P = \dfrac{W}{\pi R^2}$,

W = load concentrated over a rigid central area of radius r and

$$F = \frac{\text{Young's modulus}}{1 - (\text{Poison's ratio})^2}$$

and $W_1 + W_2$ = maximum load applied to the transducer

= 100 lb. wt.

Substituting the appropriate values for R, r_1 and r_2 and F of 0·25, 0·125, 0·0625 and 30×10^6 for a spring steel, the thickness of the two discs must be 0·019 ins. for a maximum deflection of 0·005 ins. The deflection in this range is linear with respect to the applied force.

(iv) The dynamic response of the thrust transducer.

Since the deflection of the diaphragms is less than their thickness the natural frequency was expected to be high. However, when tested it was found to vibrate and it was decided that the extension arm was causing the trouble (see Fig. B.III.2, Page 176). The natural frequency of such an arm can be calculated if it is assumed that the two ends are simply supported.

$$f = \frac{\pi}{2L^2}\sqrt{\frac{E.I}{m}}$$

where L = the length of the arm,

E = Young's modulus for the material,

I = the second moment of the cross-section and

m = mass per unit length of the arm.

For a circular section arm the ratio of the second moment and the mass per unit length is

$$\frac{I}{m} = \frac{R^2 + r^2}{4\rho}$$

where ρ = density of the material

R = outside radius of arm,

r = inside radius of arm when it consists of a tube.

$$\therefore \quad f = \frac{\pi}{4} \cdot \frac{R\sqrt{1 + \left(\frac{r}{R}\right)^2}}{L^2} \cdot c$$

where $c = \sqrt{\frac{E}{\rho}}$ = velocity of sound in the material

The frequency can be increased in three ways and each was tried in turn.

(a) Use a thin walled tube which will increase the frequency by a maximum of 1·4 times;

(b) Using a thicker arm to increase the frequency proportionally; and

(c) By decreasing the length to increase the frequency by the square of the length.

The final design of the transducer used an arm three times as thick and about half as long as the original design and the vibrations were reduced to negligible proportions. However, vibrations do occur and are produced by the initial sudden pressure application when the disc bursts and last for a very short period. They give some idea of the natural frequency of the transducer. This frequency is greater than 2000 c/sec. which means that the discord is considerably less than 0·1 and dynamic errors are negligible.

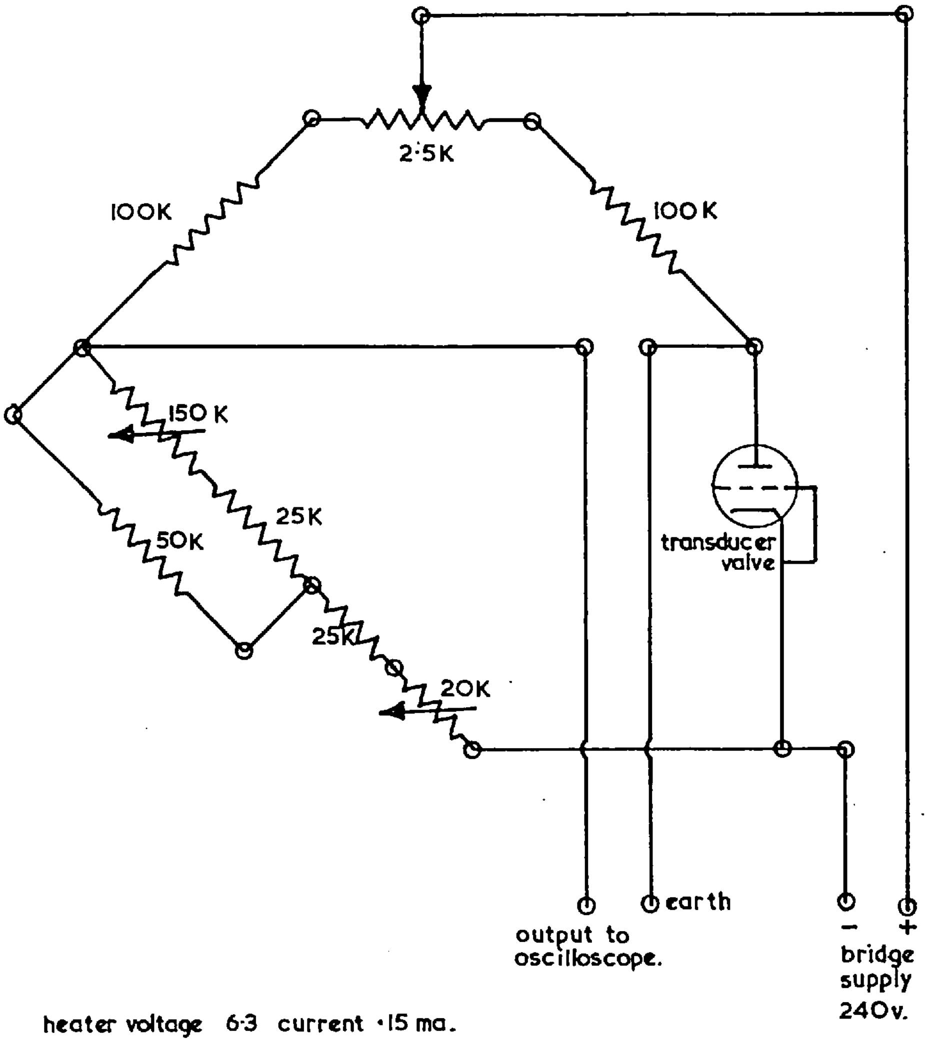

heater voltage 6·3 current ·15 ma.
amplification factor 20
plate resistance, undeflected 72000 ohms
DC plate current 1·5 ma.
moment of inertia of plate 3·4 mg.cm^2
max. angular deflection $\pm 0{\cdot}5^{\circ}$

FIG. 3 b.

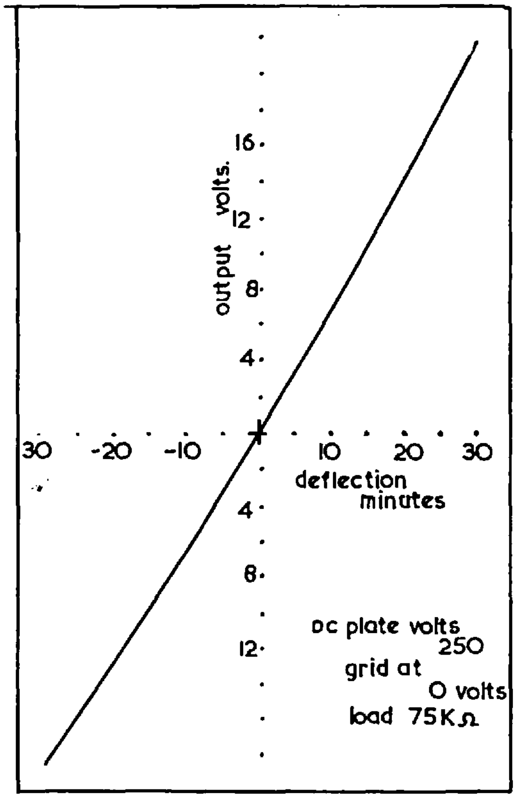

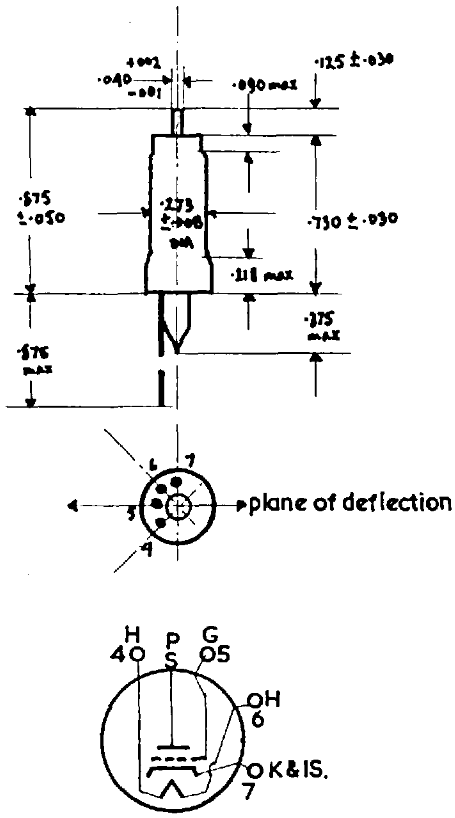

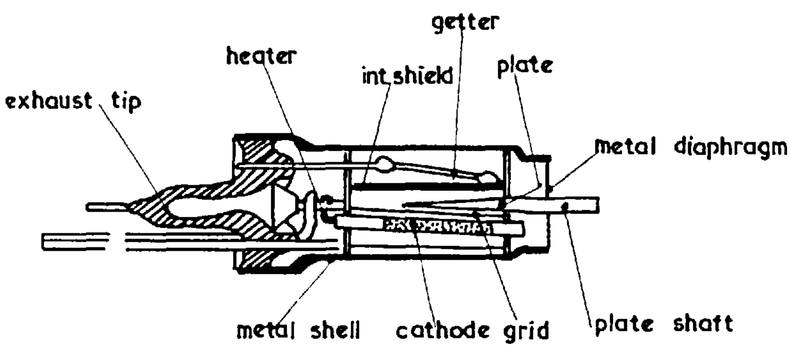

Heater	H. 4 & 6
Grid	G. 5
Cathode	K. 7
Internal shield	IS. 7
Metal shell	S

FIG. 3a.

APPENDIX E.II Electronic circuits.

(i) Pressure measurement.

The pressure was measured with a capacitance type pressure gauge using a proprietary capacitance bridge - the Fielden Proximity Meter P.M.2. The output was amplified in a Southern Instruments D.C. Amplifier and displayed on a Southern Instruments oscilloscope. The only other electronic circuitry used was the trigger device described in Chapter A.III and circuit diagrams will not be reproduced here.

(ii) Thrust measurement.

The electronic sensing element was an R.C.A. 5734 Mechano-electronic Transducer and important details from the data sheet are shown in Fig. 3a. The most suitable arrangement in the present application is to make the valve one arm of a resistance bridge as shown in Fig. 3b. The two variable resistances balance the bridge under zero deflection conditions so that when the transducer arm is moved the bridge becomes unbalanced and a potential is produced across the output terminals. This is fed to one beam of a Cossor 1049 double beam oscilliscope.

(iii) Flash initiation.

In order to obtain shadowgraphs of the gas streaming past the obstructions, a photomultiplier was fitted to the

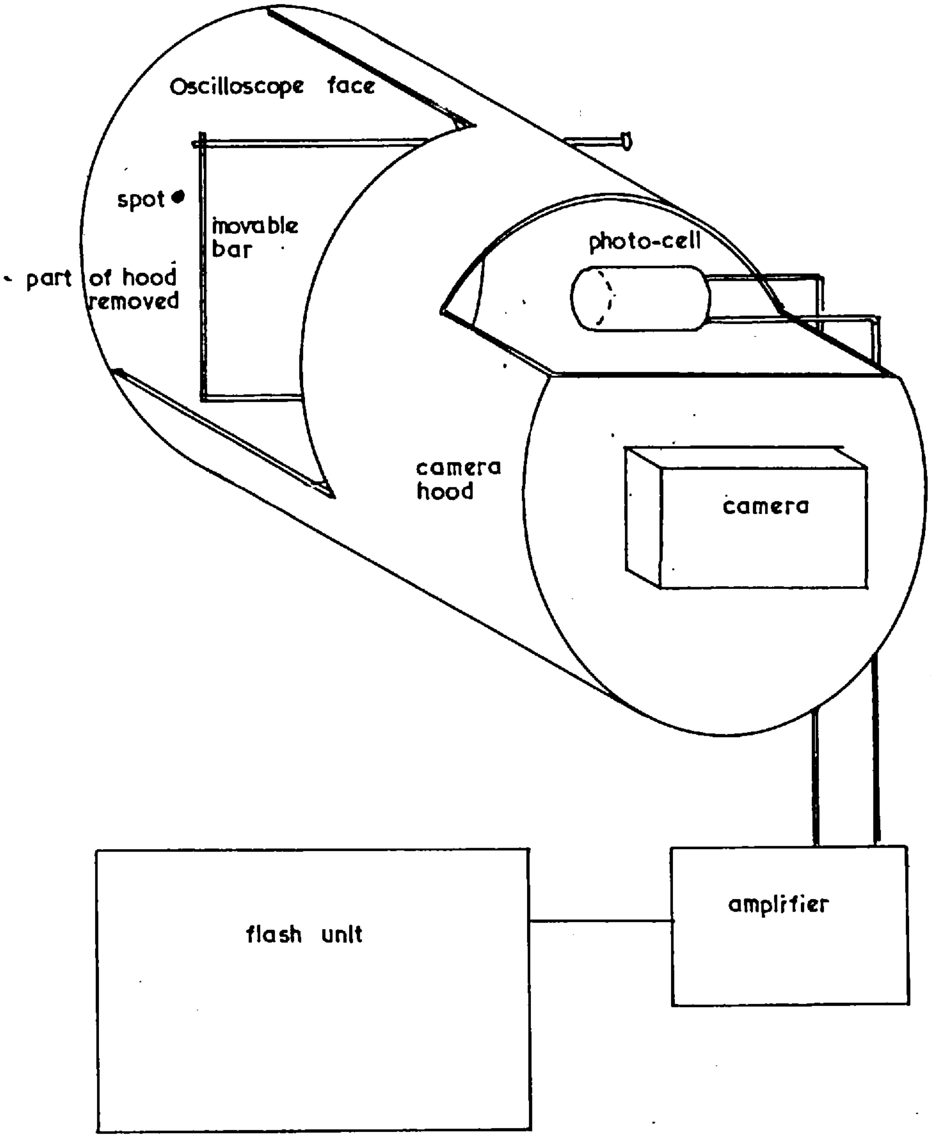
Oscilloscope face
spot
movable bar
part of hood removed
photo-cell
camera hood
camera
flash unit
amplifier

FIG.4

oscilliscope camera hood. When the oscilliscope beam passes behind a small obstruction on the CRT face the voltage across the photomultiplier load falls suddenly and this change is used to initiate the flash. The equipment is shown diagramatically in Fig. 4.

The signal from the photomultiplier is fed through a two stage amplifier to the trigger system of the flash unit. The second stage of the amplifier is a "long-tail-pair" to change the sign of the signal.

The flash unit is a Turner HS/5 capable of giving a 5 or 20 joules output in 4 μ. sec and initiated by a thyratron trigger.

(iv) Multiple flash equipment.

The requirement of this unit was the production of a series of fifteen one microsecond flashes at intervals of 100 microseconds to be triggered from the second of two pulses from the photomultiplier detector. These signals were produced by the light-screens when the shock wave passed them and gave negative signals of about 5v amplitude. In order to use the second of these pulses a "divide by two" circuit of the type used in nuclear counting equipment ensured that the second of the pulses was fed to a thyratron. The thyratron is a gas filled valve which is triggered to it's conducting state thus rejecting

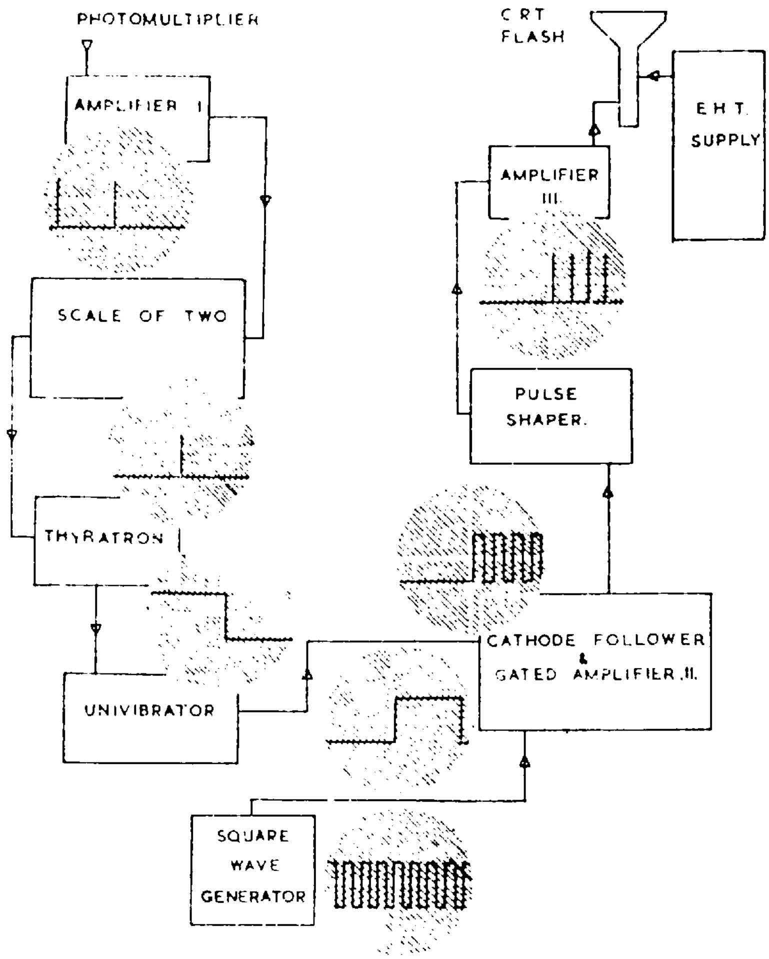
PHOTOMULTIPLIER
AMPLIFIER I
SCALE OF TWO
THYRATRON
UNIVIBRATOR
SQUARE WAVE GENERATOR
CATHODE FOLLOWER & GATED AMPLIFIER II.
PULSE SHAPER.
AMPLIFIER III.
C R T FLASH
E H T. SUPPLY

FIG.5.

any subsequeut pulses from the divide by two circuit. The signal from the thyratron operates a univibrator which generates a positive going square wave. This adjustable duration pulse is used as the screen voltage for a pentode amplifier, the pentode being normally cut off and being set to gain conditions for the duration of the pulse. The DC level and the impedance of the pulse source have been adjusted to match the input requirements of the pentode by a cathode follower. A square wave generator provides the grid signal to the pentode, and the output of this stage provides the trigger for a pulse generator. The pulses are then amplified to the level required to pulse the cathode ray tube light source to full brilliance.

This CRT is a Ferranti tube specially designed to be used as a light source. It requires a potential of 25,000 v between the cathode and anode and is held at cut-off by a bias voltage on the grid. The pulses oppose this bias and switch on the tube for the duration of each pulse when the whole of the CRT face is lit up. The high potential is supplied from a 25 kv r.f. unit and a 0·05 μf high voltage condenser.

Once the two signals have been received by the equipment only the required number of light pulses are

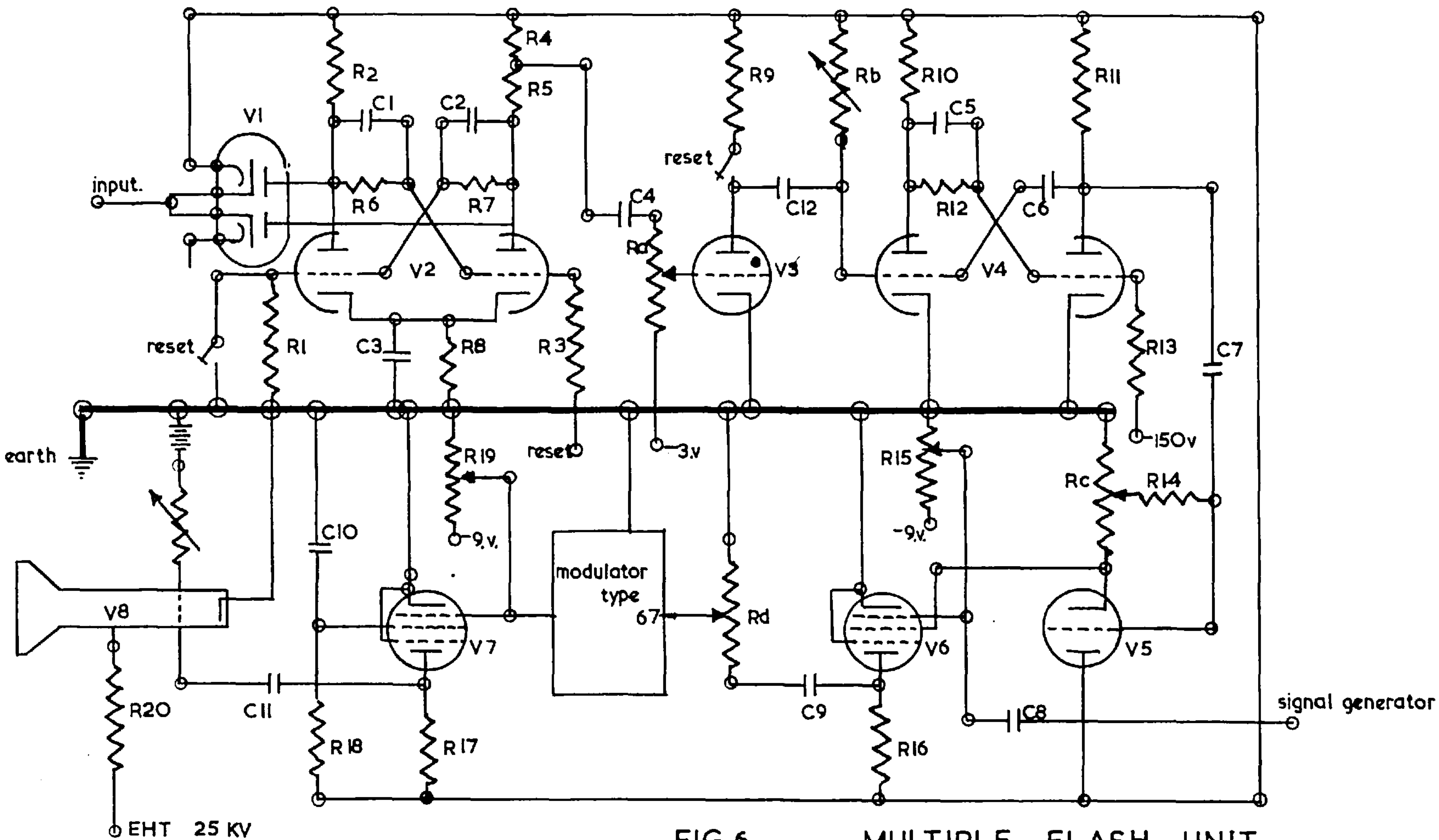

FIG.6. MULTIPLE FLASH UNIT

available. Hence, the thyratron and scale-of-two have to be reset before the operation can be repeated.

The circuit is broken down into its constituent parts in Fig. 5 which illustrates, by cathode ray tube displays, how the final microsecond pulse train, initiated by the photomultiplier, is processed through the system.

The circuit is detailed in Fig. 6 in which the circuit values are as follows:

V1	6 H 6		
V2	6 SN 7	Scale-of-two valve	
V3	EN.91	Thyratron	
V4	6 SN 7	Univibrator valve	
V5	6 CH 6	Cathode follower	
V6	6 CH 6	Gated amplifier	
V7	6 CH 6	Video-amplifier	
R1	100 K	Ra	1. M
R2	22 K	Rb	1. M
R3	100 K	Rc	50 K
R4	47	Rd	10 K
R5	15 K	Re	10 K
R6	220 K	C1	47 pf
R7	220 K	C2	47 pf
R8	10 K	C3	0·01 µf

R9	100 K	C4	0·002 μf
R10	22 K	C5	47 pf
R11	22 K	C6	0·01 μf
R12	220 K	C7	0·1 μf
R13	150 K	C8	0·1 μf
R14	1 M	C9	0·5 μf
R15	1 M	C10	0·1 μf
R16	10 K	C11	0·05 μf
R17	10 K	C12	37 pf
R18	68 K		
R19	330 K		
R20	current limiting resistor		